Spike-timing dependent plasticity and connectivity in primate sensorimotor cortex

Stephanie Seeman

A dissertation

submitted in partial fulfillment of the

requirements for the degree of

Doctor of Philosophy

University of Washington

2016

Reading Committee:

Steve Perlmutter, Chair

Eberhard Fetz

Marc Binder

Program Authorized to Offer Degree:

Graduate Program in Neuroscience

© Copyright 2016

Stephanie Seeman

University of Washington

Abstract

Spike-timing dependent plasticity and connectivity in primate sensorimotor cortex

Stephanie Seeman

Chair of the Supervisory Committee:
Prof. Steve Perlmutter
Physiology and Biophysics

Specific connectivity between populations of neurons gives rise to network function. The plasticity of these connections allows for network learning and adaptation. While much work has explored plasticity and underlying connectivity, there is still much to learn about why particular connections are susceptible to manipulation. Hebbian plasticity has been shown in a variety of neural circuits, yet there are subtle differences in the mechanisms driving these effects at each synapse. Similarly, functional connectivity has been described utilizing varying methods. Ultimately, these bodies of work tile a broad spatiotemporal view of cortical function. Here, we explore plasticity between sensorimotor populations and the underlying connections which serve targeted changes. The variability we observed in our results further highlights that one size does not fit all, and perhaps only by looking at the collective may we begin to understand the complexities of cortical processing.

I. Paired-stimulation for spike-timing dependent plasticity in primate sensorimotor cortex

Classic studies *in vitro* have described spike-timing dependent plasticity (STDP) at a synapse: the connection from neuron A to neuron B is strengthened (or weakened) when A fires

before (or after) B within an optimal time window. Accordingly, more recent *in vivo* works have demonstrated behavioral effects consistent with an STDP mechanism; however, many relied on invasive single-unit recordings. The ability to modify cortical connections becomes useful in the context of injury when connectivity, and associated behavior, is compromised. To avoid the need for long-term, stable isolation of single units, one could control timed activation of two cortical sites with paired, electrical stimulation. We tested the hypothesis that STDP could be induced via prolonged paired-stimulation as quantified by cortical evoked potentials (EPs) in sensorimotor cortex of awake, behaving monkeys. Paired-stimulation between two interconnected sites produced robust effects in EPs consistent with STDP; however, only at a subset of tested pairs (2/15). This protocol otherwise produced increases in global network excitability or depression of the conditioned pair. Taken together, these results suggest that paired-stimulation *in vivo* is a viable method to induce STDP between cortical populations, but that factors beyond activation timing must be kept in mind to produce a site-independent effect.

II. Intrinsic functional connectivity of neural populations in forelimb sensorimotor cortex

The structure of neocortex is defined by its anatomical and functional connections, from which processing and cognition arise. Functional connectivity exists and may be investigated along a wide spatiotemporal range utilizing a variety of electrophysiological techniques and analyses. Single- and multi-unit recordings can show connectivity of local micro-circuits whereas electrocorticography (ECoG) or functional imaging highlights macro-scale connections across the whole brain. Further, recordings of action potentials compared to local field potentials (LFPs) in ECoG are based in fundamentally different mechanisms generating neural activity and connectivity. We explored meso-scale connectivity in hand area of primate sensorimotor cortex via EPs and band-limited coherence in spontaneous LFP between cortical sites. The strength of both EPs and coherence showed an inverse relationship with inter-site distance as well as regionality between primary motor (M1) and somatosensory (S1) cortex. Despite these similarities, EP and coherence connectivity maps were not well correlated likely due to different underlying mechanisms driving the two signals. Taken together, these results show connectivity structure at a meso-scale, population level similar to that at other scales. Further exploration utilizing different recording techniques or functional connectivity metrics may elucidate additional network structure.

TABLE OF CONTENTS

LIST OF FIGURES

LIST OF TABLES

ACKNOWLEDGEMENTS

So many people contributed to this work and my ability to reach this point. A first thank you to my advisor, Steve Perlmutter, whose unwavering support and presence were second to none. Steve, you allowed and encouraged me to think independently and I am truly grateful for the space you gave me to make my own mistakes and discoveries; it has certainly shaped the scientist I have become. I am also honored to be your first graduate student, and hope I did you proud.

Being in Steve's lab meant being a part of the Perlmutter/Fetz super group! I enjoyed not only our yearly camping trips (guess someone else needs to plan those now) but also the broad expertise and viewpoints from everyone in the lab. I am hugely indebted to Brian Mogen who let me join in on this project and for teaching me so much about engineering, along with Tyler Libey. I thoroughly enjoyed our office discussions about the future of neuroscience and bioengineering. Bethany Kondiles, thank you for not making me an only child in Steve's lab and for being a sounding board not only in the office, but as a friend too. Becky Schaefer and Rob Robinson, I would probably have more exposures if not for you. Thank you for teaching me how to be a monkey wrangler and I cannot thank you enough for all of the support you provide for the animals and the lab to keep it running smoothly. When either of you are gone for even a short while it is painfully clear how much you contribute, and that science could not be done without you. Thank you to Larry Shupe, who is one of the most patient people I've ever known. I lost count of the number of times and the hours you spent helping me set up recording equipment, code, or getting my computer to recognize the printer; and what's more is you always just seemed to be there ready to help! A final thank you to Eb Fetz. It is a privilege to say that I've worked with you and I am continually humbled by the breadth of your experience and legacy. There are also so many more people that have come and gone from the lab during my time including Stavros Zanos, Guoji Wu, Matt Edwardson, Olivia Robinson, Samira Moorjani, Jacob McPherson, Ryan Miller, Ryan Eaton, Andrew Bogaard, and many more. Thank you all for creating a fun and intellectually stimulating atmosphere to call work.

Thank you to the members of my committee, Eb, Tom Daniel, Marc Binder, and Maureen Neitz. I appreciate the support, encouragement, and advice you have provided me during the course of my graduate career.

The friends I have made in Seattle truly enriched my life and have been supportive through this whole process. Thank you to my Calendar Dinner ladies, Leah Bakst, Florie D'Orazi, Sweta Agrawal, and Sarah Pickett for all of the great food, drinks, and laughter. My fasterer ladies, thank you for pushing me to be a better athlete and for making me feel like a smart, mad

scientist. There are many more people, especially in the Neuroscience Program with whom I have been lucky to share this journey.

A big, BIG thank you to my family. My parents, Ellen and Bill, you have supported me through all of my endeavors and I could not have done any of it without you. Thank you for setting the bar high and for pushing me to be the best person I can be. Thank you to my little sister, Sara, not only for your statistical input, but for always being there and being my best friend. I love you all more than words can say.

Last, but certainly not least, to Chloe, you are the weirdest little fur ball, but I always want to come home to you.

SS
Seattle, 2016

INTRODUCTION

Over the past decade there has been renewed interest in studying local field potentials (LFPs) in order to better understand function and communication within cortical networks (Einevoll et al., 2013). Traditional single-unit recording allows one to measure action potentials from an individual or a few principal neurons with high-impedance, intracortical electrodes. Alternatively, recording of LFPs may similarly be acquired intracortically or from the cortical surface using lower-impedance electrodes. LFPs incorporate extracellular currents throughout the cortical column from hundreds to thousands of neuronal and non-neuronal cells (Buzsáki et al., 2012). Use of LFP recording has gained popularity for control of brain-computer interfaces (BCIs) in patients suffering neurologic damage. There are a number of reasons for this, the first being that implantation of surface electrocorticography (ECoG) arrays is less invasive than intracortical micro-arrays. Secondly, stable and reliable recording of chronic LFP is less susceptible to signal degradation over time, which occurs with microelectrodes (Moran, 2010). Thirdly, distinct neural features can be reliably decoded from LFPs and used by humans and animals to control a BCI (Schalk and Leuthardt, 2011).

While recording of LFPs has attractive applications in translational research, there is still much to be learned concerning the intrinsic contribution that population activity has to cortical processing in the intact brain. This thesis approaches this question through recording of stimulation-evoked LFP (EPs) and spontaneous LFP at many sites in sensorimotor cortex of awake, behaving non-human primates. Cortical EPs have been described in humans as event-related potentials, such as the P300 response (Schalk and Leuthardt, 2011), but also may be evoked via electrical stimulation of a distant cortical site (Matsumoto et al., 2007). These latter

cortico-cortical EPs likely highlight specific and functionally-relevant connections between cortical populations. The first chapter of this thesis tests the susceptibility of these connections to spike-timing dependent plasticity utilizing paired-stimulation between two cortical sites and quantified via changes in EPs. A large body of literature has described modification of specific synaptic connections through Hebbian mechanisms typically utilizing electrical stimulation to activate pre- and post-synaptic elements (Caporale and Dan, 2008).

Spontaneous LFPs show periods of oscillatory activity in particular frequency bands which may be synchronized between cortical regions (Buzsáki and Draguhn, 2004). It has been proposed that coherent oscillatory activity is a mechanism to bind different neural ensembles in a flexible manner to promote functional connectivity (Engel et al., 2001; Akam and Kullmann, 2014). The second chapter explores the functional connectivity of sensorimotor cortex via coherence patterns of spontaneous LFPs between cortical sites in various, functionally relevant frequency bands. This view of connectivity is considered alongside that described by EPs. A brief comparison of functional connectivity described by coherence and EPs attempts to highlight common themes as well as illustrate that these are likely different measures of cortical communication.

Chapter 1. PAIRED-STIMULATION FOR SPIKE-TIMING DEPENDENT PLASTICITY IN PRIMATE SENSORIMOTOR CORTEX

1.1 Introduction

Neuroplasticity underlies many brain functions from learning and memory to recovery from injury (Sanes & Donoghue 2000; Stuchlik 2014). Even before there was empirical evidence, Hebb postulated that repeated association of pre- and post-synaptic spiking would specifically enhance neuronal connections and thus form the basis of learning (Hebb, 1949). This tenet of Hebbian plasticity has fueled an entire field of neuroscience research as the basic mechanism by which the brain learns and modifies itself (Bi & Poo 2001; Brown et al. 1990; Caporale & Dan 2008). Hebbian plasticity has been demonstrated in multiple model organisms, *in vitro* and *in vivo*, and in cortical and subcortical structures.

Seminal studies by Markram (1997) and Bi and Poo (1998) elucidated the activity-dependent nature by which a synapse is modified. If a post-synaptic neuron, B, consistently generates an action potential within a short time window after receiving input from pre-synaptic neuron A, the connection from A→B is strengthened. On the other hand, if B's action potential occurs before the arrival of A's, the connection from A→B is weakened (Bi and Poo, 1998). Further studies have demonstrated this spike timing-dependent plasticity (STDP) rule in many brain regions and model organisms, including humans (Arai et al., 2011; Koch et al., 2013). However, the intricacies of the precise temporal window and symmetry of the effect vary across synapse types, brain areas, and species (Caporale and Dan, 2008; Feldman, 2012).

Much of the work on STDP has been conducted in *in vitro* studies in which pre- and post-synaptic activity was controlled to probe deeper into the cellular mechanisms governing plasticity. The back-propagating action potential in the dendrites of the post-synaptic neuron

facilitates removal of the magnesium block from NMDA receptors such that depolarization from pre-synaptic transmitter release coincides with calcium influx resulting in synaptic potentiation (Markram et al., 1997). Additional studies have shown that while timing is an important factor, others such as dendritic location (Froemke et al., 2005) and convergence (Sjostrom et al., 2001) of inputs, the relative timing of spike trains (Froemke and Dan, 2002), and background firing rate (Sjostrom et al., 2001) all play a role on the effects of plasticity.

Many *in vivo* studies have demonstrated effects consistent with STDP, utilizing protocols such as pairing of sensory stimuli with electrical stimulation of central sensory neurons, or pairing of two different sensory stimuli (Feldman 2012). Pairing of recorded, pre-synaptic spikes with post-synaptic electrical stimulation in primary motor cortex has also produced STDP-like effects in studies of non-human primate (Jackson et al., 2006; Lucas and Fetz, 2013; Nishimura et al., 2013) and rodent (Rebesco et al., 2010). In these studies recorded spikes or muscle activity were used to repeatedly trigger stimulation at a distant but connected site. Varying the interval of this activity-dependent stimulation produced an STDP curve remarkably similar to *in vitro* results while also promoting long-lasting effects on behavior. Furthermore, Rebesco and Miller (2011) showed that paired-stimulation (pre→post pairing) in awake, behaving rats increased functional connectivity between sites at short but not long intervals, suggesting that discrimination of a neural signal for activity-dependent stimulation may not be necessary.

These findings, coupled with heightened interest in brain-computer interface technology, suggests that directed STDP may be used to produce lasting, functional recovery in neural injuries such as stroke or spinal cord injury (SCI). Employing STDP protocols, primarily in sensorimotor cortices, could preferentially strengthen or reorganize damaged or spared connections after injury. Functional motor recovery facilitated by STDP paradigms has been

demonstrated in animal models of stroke (Guggenmos et al., 2013) and SCI (McPherson et al., 2015) as well as in human stroke patients (Buetefisch et al., 2011), providing support for the use of STDP in rehabilitation. Towards the goal of clinical applications of neuroplasticity, great strides have been made in the understanding of more global neural signals, such as local field potentials (LFPs), which can be acquired less invasively and are stable over longer periods of time compared to traditional single unit recording (Moran, 2010).

With these applications in mind, we sought to investigate the efficacy of open-loop, paired-stimulation between sites in sensorimotor cortex of awake, behaving monkeys to induce STDP. While closed-loop stimulation has many advantages, one limitation is the need to record a strong and relevant trigger signal. This requirement is challenging for clinical applications that need to be effective over a patient's lifetime. Thus, we employed paired-stimulation at a fixed interval, which can be applied anywhere in the brain, at any time, to control the timing of pre- and post-synaptic activity. Additionally, previous findings have largely focused on changes in behavioral outputs in response to STDP protocols and the extent of cortical reorganization due to these protocols remains unclear. By recording LFPs from many sites in the hand area of sensorimotor cortex, we were able to measure fairly direct changes in connectivity. Finally, these experiments were conducted during free behavior or while the monkey was engaged in a trained motor task to further explore how activity induced by STDP stimulation protocols integrates with natural brain activity.

1.2 **Methods**

1.2.1 **Implant**

Dual Electrodes

Two monkeys (*macca nemestrina*), Q and U, were implanted with custom made dual electrodes (Figure 1.1) arranged in two 3x5 grids over bilateral sensorimotor cortex (Figure 1.1b). Dual electrodes were constructed using two 0.005" bare PtIr wire rods cut to 3 mm (surface) and 5 mm (intracortical) and each soldered to independent, 32 gauge, insulated lead wire (Figure 1.1a). The PtIr rod-lead wire connection was further insulated with 10 μm of parylene by the UW Microfabrication Facility to insulate the solder joint and PtIr rod. The tips of each rod were then de-insulated by hand using a scalpel to an impedance of 22-160 kΩ (monkey Q) and 4-60 kΩ (monkey U). For each dual electrode, a 3 mm and 5 mm PtIr rod were secured in a small piece of PTFE tubing with silicon glue. The tips of the 3 and 5 mm rods were placed approximately 0.5 and 2-2.5 mm from the edge of the PTFE tube (Figure 1.1b). In this way the 5 mm rod penetrated to layer 5, where output pyramidal cells reside, while the 3 mm rod rested on the surface of the brain. After each dual electrode was constructed, the back end of the lead wires were soldered to connectors, one per hemisphere.

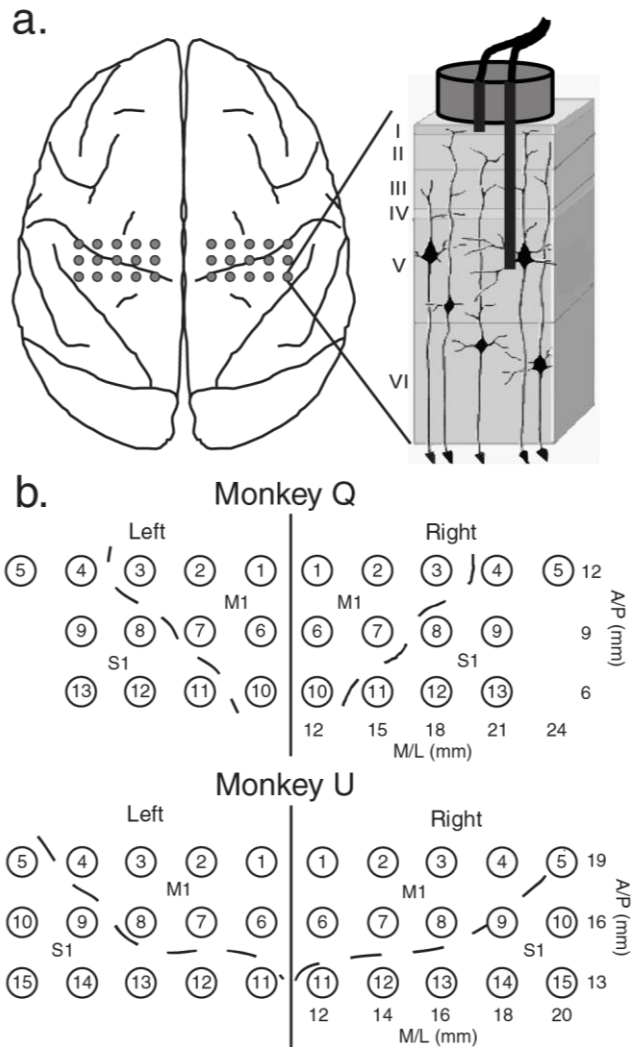

Figure 1.1 Cortical implant schematic. **a)** Top-down schematic of macaque brain. Grey circles indicate approximate position of each plug electrode with respect to midline and the central and arcuate sulci. Expansion shows side-view schematic of plug electrode leads with respect to cortical layers. **b)** Numbered electrode sites for each monkey relative to the central sulcus (dotted line) as determined by median nerve stimulation.

Surgery

All surgeries were performed under isoflurane anesthesia and aseptic conditions. An incision was made along the midline of the scalp, and muscle and connective tissue were resected to expose enough skull to place a 2.5 inch diameter titanium casing. Four to eight skull screws were placed around the edge of the exposure. At least four of the skull screws were T-screws used as grounds for the electrode implant. Holes were drilled with a 1.1 mm bit in a 3x5 grid with 2-3 mm center-to-center spacing using stereotaxic coordinates (Figure 1.1b). After all of the holes were drilled, one dual electrode was placed with forceps into each hole until

resistance was felt between the longer rod and the dura. The dual electrode was then pushed through the dura and into the brain until a second resistance was felt between the shorter rod and the dura. We use the term "surface," instead of epi- or subdural, to describe the location of the shorter rod because it was impossible to know whether it punctured the dura. Once all of the dual electrodes for one hemisphere were implanted, a thin coat of dental acrylic (methyl methacrylate) was used to seal the holes and hold the electrodes in place. This process was repeated for the other hemisphere. The casing was then placed over the implant and secured to the skull screws with acrylic. The connectors for the dual electrodes were cemented to the skull within the casing. Animals received a post-operative course of analgesics and antibiotics.

1.2.2 **Behavior**

Monkey U performed a center-out target acquisition wrist task in a sound-attenuating recording booth. Monkey U's right hand was restrained in a manipulandum measuring torque about the wrist in the radial/ulnar (RU) and flexion/extension (FE) axes. The torque produced in the FE-RU plane was displayed as the x-y coordinates of a tracking cursor on a video monitor in front of the animal. A trial began when a center target appeared on the monitor, representing the "zero force" or neutral position of the cursor. Monkey U was required to hold the cursor in the center target for 2 seconds before a peripheral target at one of eight cardinal positions was presented. Monkey U then moved the cursor by exerting isometric force on the manipulandum to the intended target and held it there for 2 seconds before returning to a second center target. The center-out-center sequence was considered one trial. Applesauce reward was dispensed on a variable 1:2 ratio for every peripheral target presented and at the end of each trial. Monkey Q merely sat quietly in the recording booth.

1.2.3 **Recordings**

General Acquisition

LFP recordings were obtained using amplifiers from Guger Technologies (Graz, Austria) in monkey Q (4,800 Hz sampling rate) and the Grapevine Neural Interface System from Ripple (Salt Lake City, UT) in monkey U (30,000 Hz downsampled to 5,000 Hz post-hoc). Single-ended recordings from the intracortical and surface electrodes of one hemisphere, referenced to a skull screw, were made simultaneously on up to 26 channels (13 dual electrodes) in monkey Q and up to 30 channels in monkey U (15 dual electrodes). Post-hoc, recordings were re-referenced as a bipolar signal for each dual electrode (intracortical – surface) to acquire a more localized recording, then high-pass filtered over 10 Hz. Wrist torques in the RU and FE axes were sampled for monkey U by the Grapevine system at 1,000 Hz. Post-hoc, torque was smoothed and bandpass filtered from 2-10 Hz.

Estimate of electrode location relative to the central sulcus

The stereotaxic coordinates at which the electrodes were implanted were determined prior to surgery using an atlas to target the hand area of sensorimotor cortex. As the atlas is only a rough guide, coordinates were sometimes amended in surgery such that the middle of the grid was ~18 mm lateral to Bregma, which is the approximate location of the hand motor area (Fetz and Cheney, 1980). To more accurately determine the location of each dual electrode relative to primary motor (M1) or sensory (S1) cortex, monopolar responses to stimulation of the contralateral median nerve were recorded with the monkey under ketamine sedation. The waveshape of the evoked potentials in stimulus triggered averages (StTA) of single-ended, surface recordings indicated the position of the recording site relative to the central sulcus (McCarthy et al., 1991). Evoked potentials with a positive phase followed by a negative phase

were generated in precentral cortex, while a negative phase followed by a positive phase occurred in postcentral cortex. Based on these recordings, a putative position of the central sulcus was drawn onto the grid (Figure 1.1b).

1.2.4 **Stimulation**

Assessment of cortico-cortical connectivity

To identify connectivity between recording sites, monkeys were seated in a primate chair in a recording booth while electrical stimulation was delivered to each dual electrode. Stimulation was biphasic, with the negative phase leading on the intracortical wire and the positive phase leading on the surface wire of a given dual electrode. Stimuli were delivered in a series of increasing current intensities, termed stimulus ramps, ranging from 0 mA to 2.25 mA with 7-10 increments in the ramp; each ramp was repeated 100 times (Figure 1.2b) . Stimulus-evoked potentials (EPs) were measured at all ipsilateral sites in response to stimulation at one

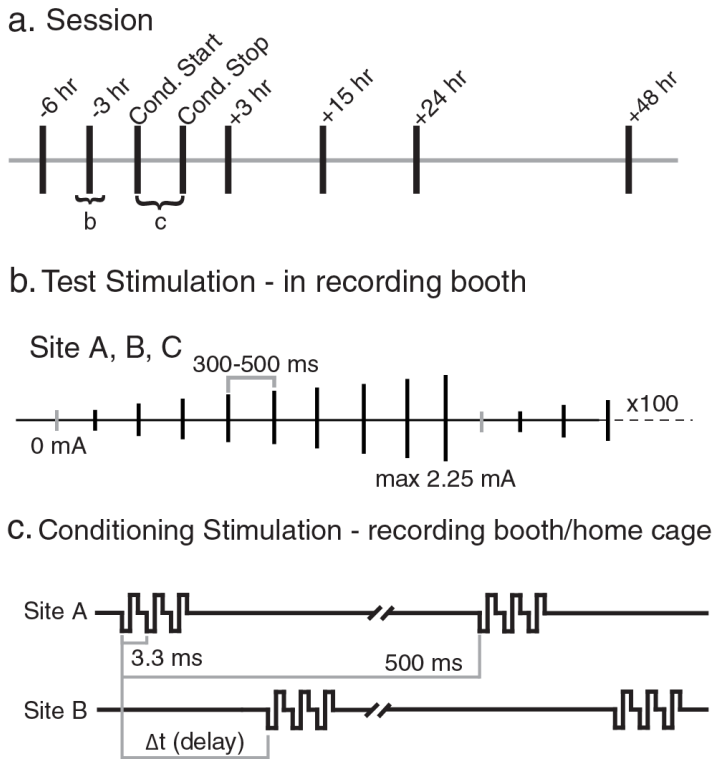

Figure 1.2 Experimental timeline and stimulation parameters.
a) Session timeline with all possible time points for testing and conditioning stimulation (note, not all time points were measured for every session). **b)** Schematic of test stimulation applied to sites A, B, and C during each testing time point ('b' in **a**). Exact number and magnitude of current steps varied across sessions, but were consistent within a session. **c)** Schematic of conditioning stimulation applied at sites A and B during conditioning period ('c' in **a**).

site during testing. A stimulus-response curve was produced for each site (Figure 1.4c), building a map of connectivity across the grid. Single-pulse stimulation of some sites elicited wrist and hand movement (see Stimulus Evoked Torques). For paired-stimulation conditioning experiments, ramp stimulation was performed in the booth for the two sites involved in conditioning (site A and B) as well as a third control site (C) not involved in conditioning. The order of test stimulation was randomized among the three sites. Test stimulation was delivered at various time-points relative to conditioning as shown in Figure 1.2a. However, not all time points were recorded for each session as a complete session spanned several days and thus we tried to minimize the amount of time an animal was handled.

Conditioning

Three reciprocally connected sites were identified via EPs and selected for paired-stimulation conditioning. The "pre-synaptic" site was termed A, the "post-synaptic site" B, and the third site, C, was used as a control. For monkey Q, conditioning stimulation was performed with the Neurochip2 (Zanos et al., 2011) in the home cage to assess the efficacy of STDP while the animal was freely behaving, similar to previous monkey and rodent studies (Jackson et al., 2006; Rebesco et al., 2010; Rebesco and Miller, 2011; Lucas and Fetz, 2013; Nishimura et al., 2013). Stimulation pulses were bipolar and biphasic as described during testing. Conditioning stimulation was delivered first to site A then site B with a fixed delay (Figure 1.2c). For monkey U, conditioning stimulation was performed in the recording booth, using rack-mounted equipment, allowing for measurement of behavioral changes after conditioning. Similar to monkey Q, site A received stimulation first followed by site B.

The paired-stimulation protocol during conditioning was as follows: 3 pulses at 330 Hz were delivered to site A and site B separated by the specified delay (Δt) as measured from the

first pulse in each train. This sequence was repeated at 2 Hz for 1 – 3 hours (Figure 1.2c). Other stimulation protocols were also tested, including 2 Hz single pulses, trains of 5 pulses at 1 kHz, trains of 10 pulses at 500 Hz, as well as longer duration conditioning sessions from 24 up to 72 hours. We saw no consistent effects under these protocols and thus utilized 3 pulses at 330 Hz for the remainder of the study. A previous study also showed that stimulus trains promote better plasticity *in vivo* than single pulses (Rebesco and Miller, 2011). The stimulus current selected for conditioning was one-third of the current in the middle of the dynamic range of the stimulus-response curve during testing (as conditioning stimulation was a 3-pulse train instead of a single pulse during testing). The selected amplitudes were sufficient to activate neurons at site A and B without adverse effects, such as disturbing the animal, causing cortical depression (due to prolonged stimulation with high currents (McCreery et al., 1986)), or causing seizures. The current was further adjusted to be just at or below motor threshold if the one-third criterion evoked clear movements.

1.2.5 **Analysis**

All analysis was conducted using MatLab (The Mathworks, Inc., Natick, MA)

Stimulus-Evoked Potentials (EPs)

The peak-trough amplitude of EPs was measured to document the strength of cortico-cortical connectivity. Trials were aligned on stimulus onset and grouped for a given current intensity. All trials were inspected by eye and those with movement artifacts were removed. From the remaining trials, StTAs were calculated from 50 ms before to 300 ms after the time of stimulation for each current intensity (Figure 1.4a). In order to separate a physiological response from electrical artifact, a biphasic stimulation pulse was delivered directly into the Guger Technologies amplifiers to visualize the artifact. The artifact returned to baseline by 1 ms after

stimulation and thus any response within the first millisecond was ignored. The Grapevine system has built-in artifact suppression, which grounded the recording channels for 1 ms at the time of stimulation. Each stimulus-aligned trial was also examined by eye for evidence of a clean separation between the stimulus artifact and the response. Trials in which there was possible contamination by the artifact were discarded. The amplitude of the average EP was quantified by subtracting the largest trough from the largest peak in a window 1.5 ms to 30 ms after stimulation for all current intensities (Figure 1.4a, arrowheads). This metric was chosen as a simple, unbiased way to capture the complicated, often multi-phase, shape of the EP. Conditioning effects were measured as the percent change in average EP amplitude from before to after conditioning, similar to other studies measuring changes in field potential recordings (Hess et al., 1996). For some conditioning experiments, testing was performed at various intervals before and after the conditioning window to assess trends and wash-out of the effect over time. Pre-conditioning EP amplitudes were then quantified as the mean of all testing sessions prior to the start of conditioning. We also quantified a subset of EPs in monkey U by the slope and amplitude of the first phase of the response as this was the most likely response component to be due to a monosynaptic connection between sites A and B. The timing of pre- and post-synaptic activation will be most preserved in the monosynaptic connections and thus may be more susceptible to effects of STDP (Diesmann et al., 1999). Only EPs from monkey U were analyzed in this way since the artifact suppression feature of the Ripple amplifiers, and their ability to record up to 30 kHz, allowed consistent identification of the rising edge of the first phase of the response. However, we saw no difference in the results of conditioning stimulation using the first phase metrics or the peak-trough amplitude (Figure 1.3, peak-trough

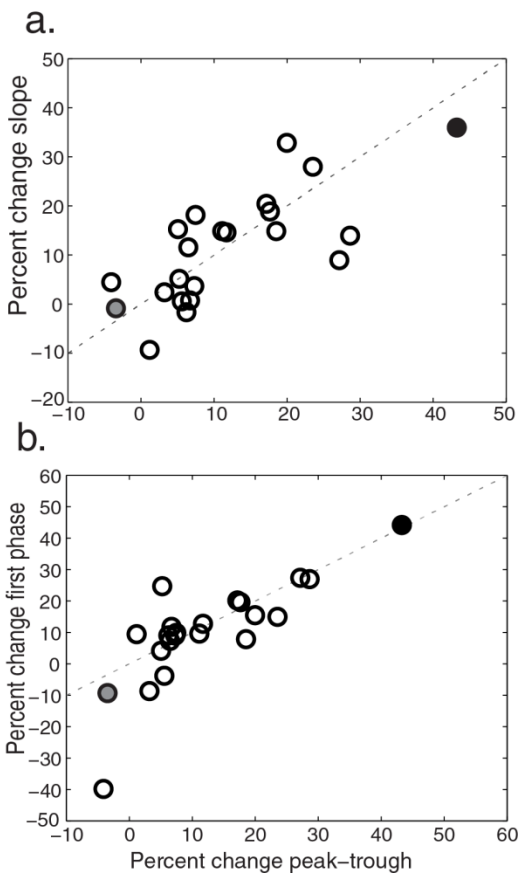

Figure 1.3 Comparison of EP measures.
a) Percent change in A→B EP amplitude after conditioning compared to percent change in slope of the first A→B EP phase. **b)** Percent change in A→B EP amplitude after conditioning compared to percent change in amplitude of first A→B EP phase. Dotted line denotes unity; filled black point shows result from a successful conditioning session (Figure 1.9) while filled grey point shows result from an unsuccessful conditioning session (Figure 1.15).

vs slope p = 0.66, peak-trough vs first phase p = 0.38, paired t-test) and therefore the peak-trough measure was used throughout Results to quantify EP amplitude.

Stimulus-Evoked Torques

Stimulus-evoked torques (ETs) about the right wrist were measured for monkey U in the RU and FE directions for sites that showed movement in response to the stimulation ramps (8/15 sites). Similar to EPs, torque was aligned on stimulus onset and grouped for a given current intensity. Since ETs were produced while monkey U was performing a wrist task, the torque at stimulation onset was variable (i.e., non-zero). In order to normalize all ETs, the torque amplitude immediately before stimulation was subtracted for each trial. Trials in which the ET was outside of 2.5 standard deviations of the StTA were eliminated. ET amplitude was measured from a torque trajectory in the FE-RU plane, and the direction of torque trajectory quantified as the angle at maximum amplitude (Figure 1.9e). The distributions of ET amplitudes and directions were non-Normal and thus the median was used for summary measures. The percent change in ET amplitude after conditioning was quantified, and separation of torque direction between the A, B, and/or C sites

was compared before and after conditioning (Jackson et al., 2006). A reduction in separation between sites would indicate that the ET direction from, for example, site A shifted towards that of site B, suggesting a strengthening in the neural connection between these sites.

Statistics

All EP amplitudes were quantified using mean ± SEM and p-values were calculated with a two-sample z-test, except where noted. Results from the z-test indicated that many connections outside of the A→B pair changed strength after conditioning stimulation. To quantify this network-wide change, and to determine if the A→B connection showed greater effects, we created cumulative distribution functions for the A, B, and C sites. A control distribution for the outputs of site A (A_{cont}) were compiled from the percent change after conditioning of the evoked responses at all sites except B and C. Similar distributions were calculated for sites B (B_{cont}) and C (C_{cont}). The Kolmogorov-Smirnov test was used to assess significant differences between the distributions for A, B, and C compared to that of the rest of the network. Cumulative distributions have been used in *in vitro* STDP studies to assess effects between different experimental conditions (Lu et al., 2007). Two-sided significance of $p < 0.05$ for EP changes was based on the lower 2.5^{th} and upper 97.5^{th} percentile of control distributions. ET amplitudes and directions were quantified using median ± standard error of the median. Recorded p-values were calculated using a one or two-sample Wilcoxon rank sum test.

1.3 **Results**

Paired-stimulation conditioning was delivered between pairs of sites in sensorimotor cortex of awake, behaving monkeys to induce STDP. Long-lasting STDP was observed, but only for a minority of pairs tested. Results were obtained from two male *M. nemestrina* for 15 different

pairs of sites, 2 of which showed delay-dependent effects consistent with STDP, as measured by the peak-trough amplitude of stimulus evoked potentials.

1.3.1 **Selection of conditioning pairs from stimulus-evoked potentials**

We used EPs to identify and quantify the connections between recording sites. Changes in EP amplitude due to paired-stimulation conditioning were interpreted as a change of connection strength. Stimulus ramps (see Methods) were delivered at each site individually while responses at all other sites on the electrode grid were recorded. StTAs of EPs revealed high connectivity across the grid as indicated by short-latency, multi-phase potentials. Figure 1.4a shows an example EP at site R11 in response to stimulation of 1.1 mA at site R07. Above threshold, EPs were present on every trial and the first phase usually began within 2 ms. Broad, longer latency phases usually returned to baseline by ~50 ms post stimulation. After distinguishing the physiological response from the stimulation artifact (see Methods), a peak-trough measure quantified the amplitude of EPs between 1.5-30 ms post stimulation (EP amp = largest peak – largest trough; Figure 1.4a, arrowheads). We found this measure best captured the overall shape of the response and the effects of conditioning. The stimulus ramps used a range of current amplitudes to describe the stimulus-response relationship (Figure 1.4b & c). We chose a current range and step resolution that identified a threshold, linear range, and saturation point for a wide range of connected sites (see Methods). As can be seen in Figure 1.4b, stimulation at a single site elicited responses at many other sites, though not all. EP latency, shape, number of phases, and amplitude varied greatly from site to site, likely due to multiple factors both technical (e.g., the relative positioning of the electrodes) and physiological (e.g., underlying mono and polysynaptic connectivity between sites). The polarity of EPs varied from site to site as well (Figure 1.4b), likely due to the location of the electrodes with respect to the current

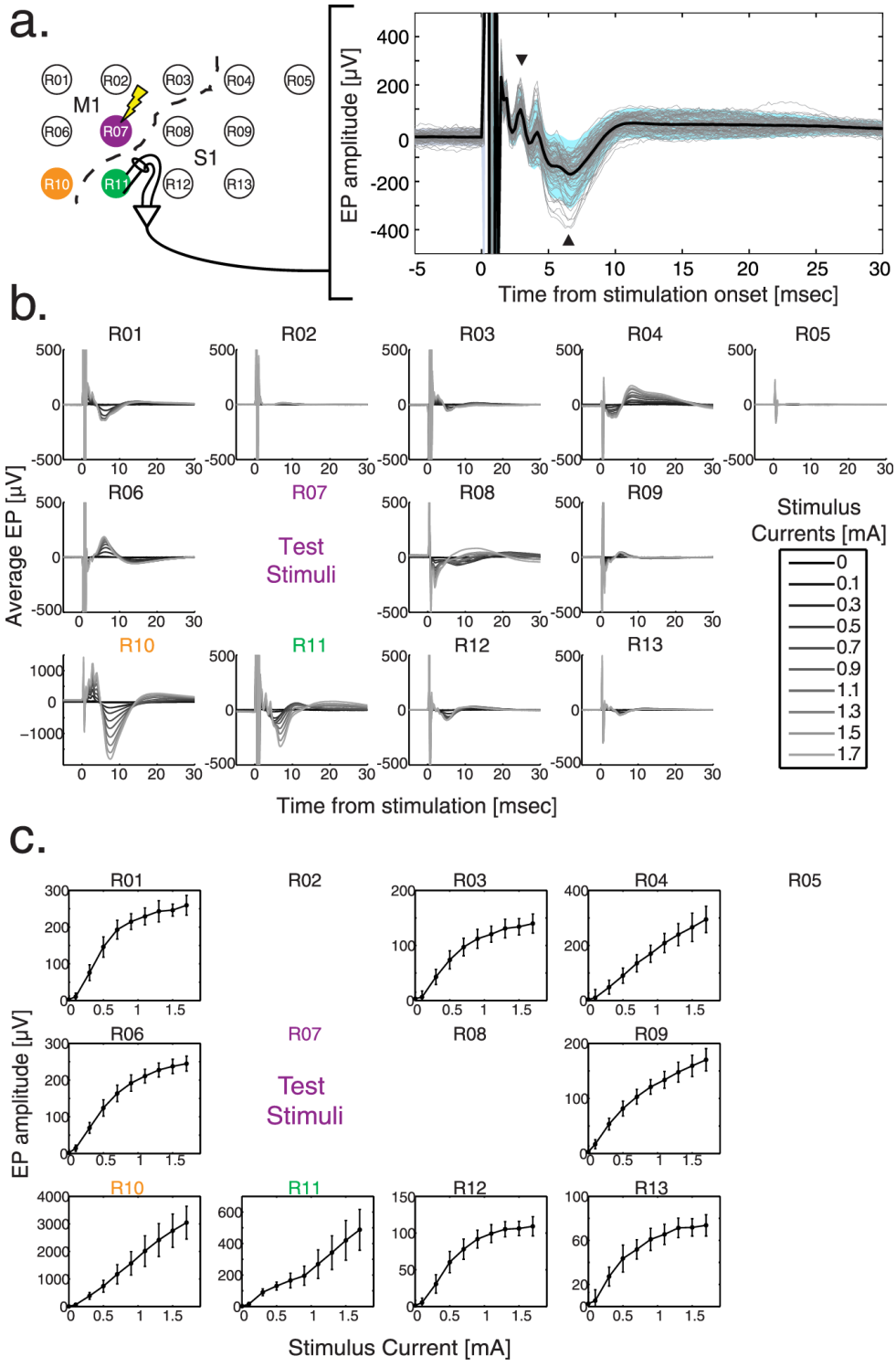

Figure 1.4 Cortical connectivity from stimulus-evoked potentials.
a) Example test stimulation (1.1 mA) applied to purple site and recorded at green site. StTA shown in black, individual trials (n = 97) are shown in grey, and the light-blue shadow is the 95% confidence interval. Black arrowheads denote the max peak and trough used to calculate EP amplitude. **b)** StTAs for all current intensities at all recording sites for test stimuli at R07. **c)** Stimulus-response curves for each recording site for stimulation at R07 (mean ± SEM). Blank panels indicate no response as judged from **b**.

dipoles both in cortical depth and across the central sulcus (Buzsáki et al., 2012). The median latency to the first EP phase was 2.7 ms, although the range was quite large (1.6 – 12.7 ms, n = 187 EPs, Figure 1.5a). The number of phases in a given EP ranged from one to eight with a median of three (Figure 1.5b). Because EPs were highly variable from site to site, coupled with the conflation of technical and physiological mechanisms underlying EP shape, we were hesitant to infer too much about the precise connectivity between sites solely based on EP characteristics (i.e. which EP phases correspond to monosynaptic versus polysynaptic connections). Therefore we used the peak-trough amplitude to quantify the strength of connections between sites and how this changed with paired-stimulation.

Sites were chosen for paired-stimulation conditioning based on EP connectivity. Three reciprocally connected sites were selected; a pre-synaptic site, A, a post-synaptic site, B, and a control site, C. During testing periods, ramp stimuli were delivered separately to the A, B, and C sites while during conditioning paired stimuli were delivered to A and B (see Methods,). It is important to note that while we selected a C site that was reciprocally connected to both A and B, many other sites on the grid showed EPs from A and/or B (Figure 1.4b) and could be used to detect changes in global excitability due to the stimulation.

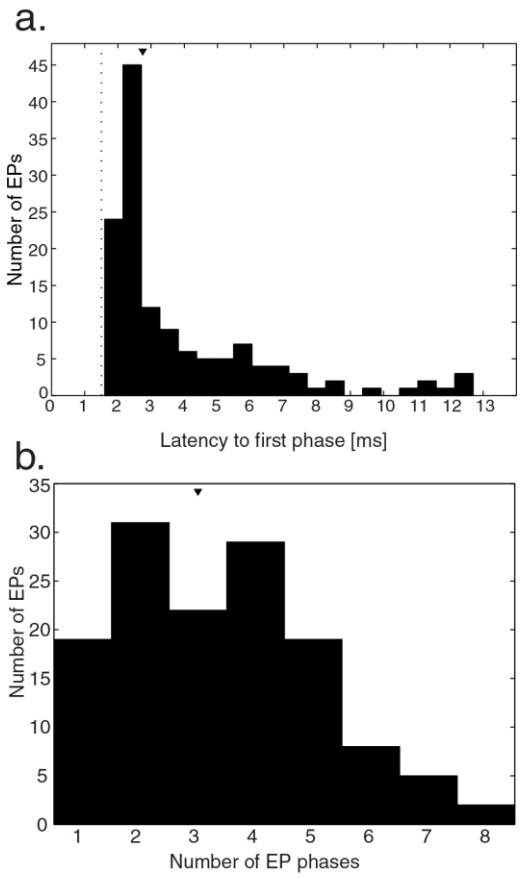

Figure 1.5 Characterization of EPs across sites.
a) Histogram of latency to first phase of EP. Dotted line denotes minimum cutoff due to electrical artifact and arrowhead denotes median (2.7 ms). **b)** Histogram of number of phases in each EP. Arrowhead denotes median (3.0).

1.3.2 **Paired-stimulation produces STDP in a subset of site pairs**

A paired-stimulation conditioning session (Table 1.1, session 20140917) with a 20 ms delay between stimuli is shown in Figure 1.6. Three hours of conditioning stimulation (3-pulse trains at 330 Hz every 500 ms, 330 μA) were delivered between sites R07 (A site) and R11 (B site) (Figure 1.4a) while monkey Q was in the home cage. While stimulus ramps were used to probe the connectivity between sites (Figure 1.4), a majority of the analysis focused on responses to 1.1 mA (outlined by the black box in Figure 1.6b), which was close to the cumulative current used during conditioning (i.e., 3 pulses of 330 μA) and was in the middle of the stimulus range. In addition to testing connection strengths immediately before and after conditioning, we tested at times relative to the three-hour conditioning window (Figure 1.6b-d). While EP amplitudes within a given testing period showed little variance (e.g., 0.34 CV, Figure 1.4a), there was more variability over the course of three hours before conditioning, consistent with previous observations (Richardson and Fetz, 2012). To account for this variability we used the mean of all pre-conditioning EPs as a baseline (Figure 1.6c & d). Immediately after conditioning, the EP amplitude from A→B increased 87.4% (from 219.3 μV ± 83.6 μV to 411.0 ± 9.0 μV, mean ±std, n = 295; p = 7.9 x 10^{-103}). This increase in connection strength from A→B was maintained three hours later (410.0 ± 9.0 μV, +86.9%, p = 1.23 x 10^{-110}). Twenty-four hours after conditioning ceased, the amplitude fell back within the standard deviation of the pre-conditioning baseline, but was still significantly elevated (297.0 ± 10.0 μV, +35.3%, p = 2.34 x 10^{-16}) and by 48 hours post conditioning had fully returned to baseline (224.0 ± 7.0 μV, +2.1%, p = 0.56, Figure 1.6d.). Changes in the slope of the stimulus-response curve, another measure of connection strength (Hess et al., 1996), follow those of the EP amplitude at the chosen current (Figure 1.7, p = 0.54,

paired *t*-test, n = 41 sessions) suggesting that these results are consistent over the range of stimulus currents tested.

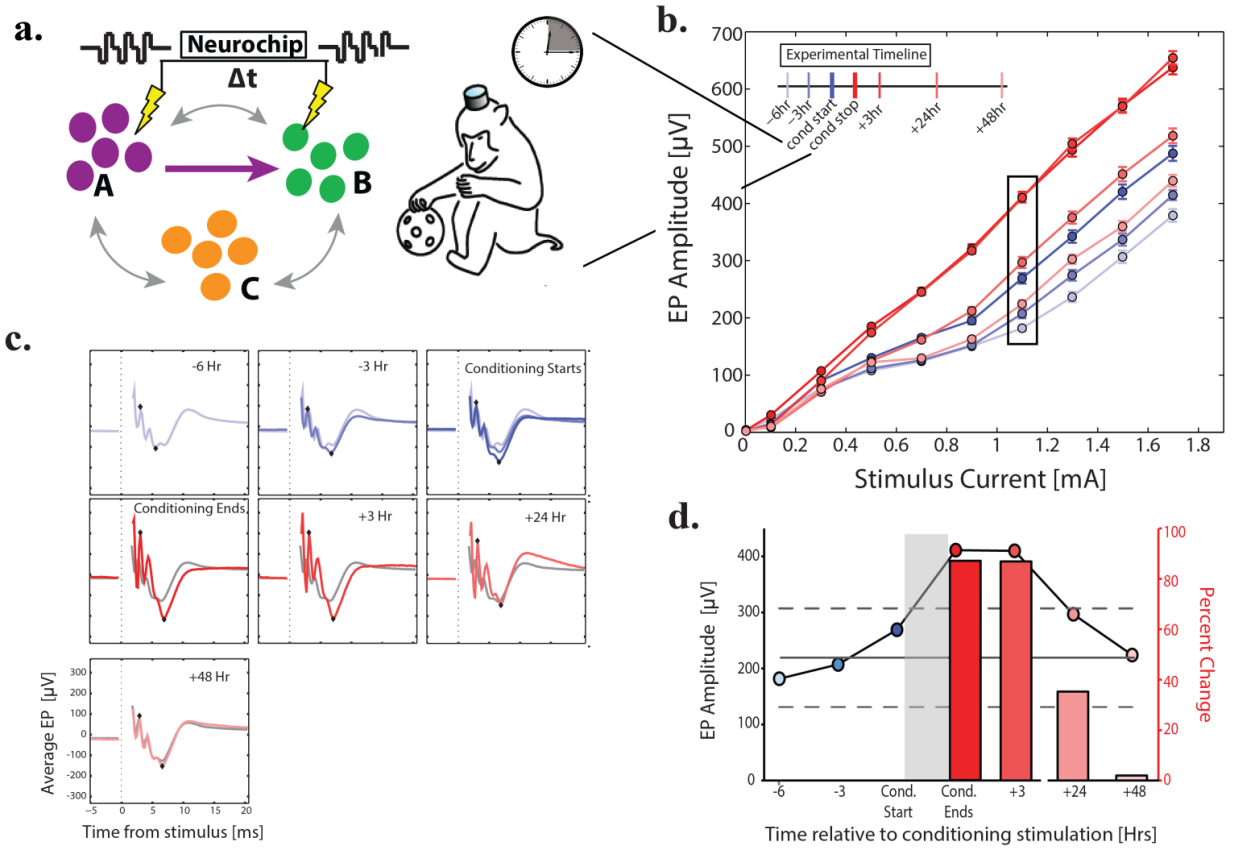

Figure 1.6 Paired-stimulation conditioning session at 20 ms delay.
a) Schematic of conditioning between site A and site B using the Neurochip while monkey Q was in the home cage for 3 hours. Sites A, B, and C were same as Figure 1.4a. **b)** Pre- (blue) and post- (red) conditioning stimulus-response curves at time points relative to conditioning as denoted by timeline. **c)** Average EP from A→B at current denoted by black box in **b**; diamonds denote peak and trough used to measure amplitude in **b**. Blue EPs in top 3 panels are averaged into a composite baseline (grey trace) in subsequent panels. **d)** Circles and left axis show EP amplitude at times relative to conditioning. Horizontal grey line is mean of 3 pre-conditioning points; dashed line is 95% confidence interval. Bars and right axis show percent increase in EP amplitude above mean baseline. Conditioning occurred during grey bar, delay between stimuli was 20 ms.

While paired-stimulation was delivered between specific A→B sites, the widespread connections across the electrode grid allowed us to see global effects of conditioning on the network. A summary of the post-conditioning responses at all sites to stimulation at A, B, or C during this session is shown in Figure 1.8 (white squares indicate no EP recorded). Two other

sites also showed a significant amplitude increase in EPs elicited from A (R06: +17.6%, $p = 3.22 \times 10^{-36}$; R12: +11.7%, $p = 5.23 \times 10^{-14}$) immediately after conditioning, suggesting network-wide changes in response to paired-stimulation, as has been previously reported (Rebesco and Miller, 2011). However, neither the recurrent B→A connection (+3.1%, p = 0.27), or the connection from A→C (R10; +3.9% p = 0.21) showed a significant change. The bottom 3 panels of Figure 1.8 show network-wide changes at testing periods +3, +24, and +48 hours after conditioning.

A second example conditioning session in monkey U (Table 1.2, 20150603) is shown in Figure 1.9. Since monkey U was engaged in a behavioral task, testing and conditioning periods were obtained in the booth during one session. Conditioning stimulation was delivered for 1 hour at a delay of 20 ms between site L03 (A site) and L07 (B site) with site L02 serving as the control (C site) (Figure 1.9a). Figure 1.9b shows the average EP before and after conditioning with the peak and trough denoted by the black diamonds, and the corresponding stimulus-response relationship in panel Figure 1.9c. The insets show similar results obtained using the rising slope of the first component of the evoked potential as the measured variable, as has been used in *in vitro* paired-stimulation plasticity experiments (Froemke and Dan, 2002). Both metrics show a similar effect of conditioning (Figure 1.3a, black filled circle). Again we saw the largest increase in EP amplitude from A→B (+43.3%, p << 0.0001) compared to B→A (+7.2%, $p = 8.43 \times 10^{-8}$) or A→C (-16%, $p = 1.23 \times 10^{-14}$), even though

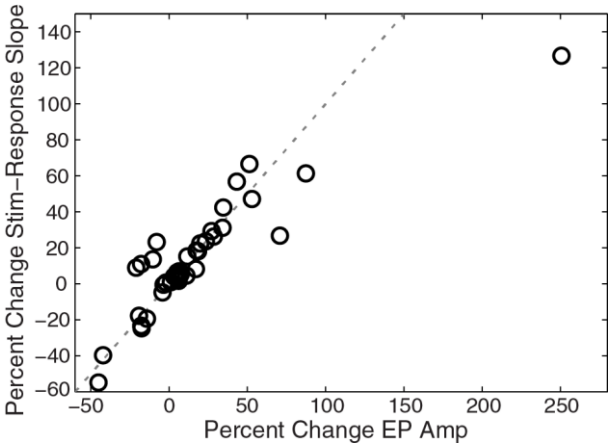

Figure 1.7 Comparison of conditioning effects with two different EP measures. Percent change in A→B EP amplitude after conditioning compared to percent change in A→B slope of stimulus-response curve after conditioning. The stimulus-response curve was fit with a linear function to a good approximation ($r^2 \geq 0.82$).

changes at other sites were also statistically significant (Figure 1.9d). In fact, 15 of 19 EPs showed significant changes after conditioning which could be due to global changes in excitability or to natural variability in EPs over time (discussed further below).

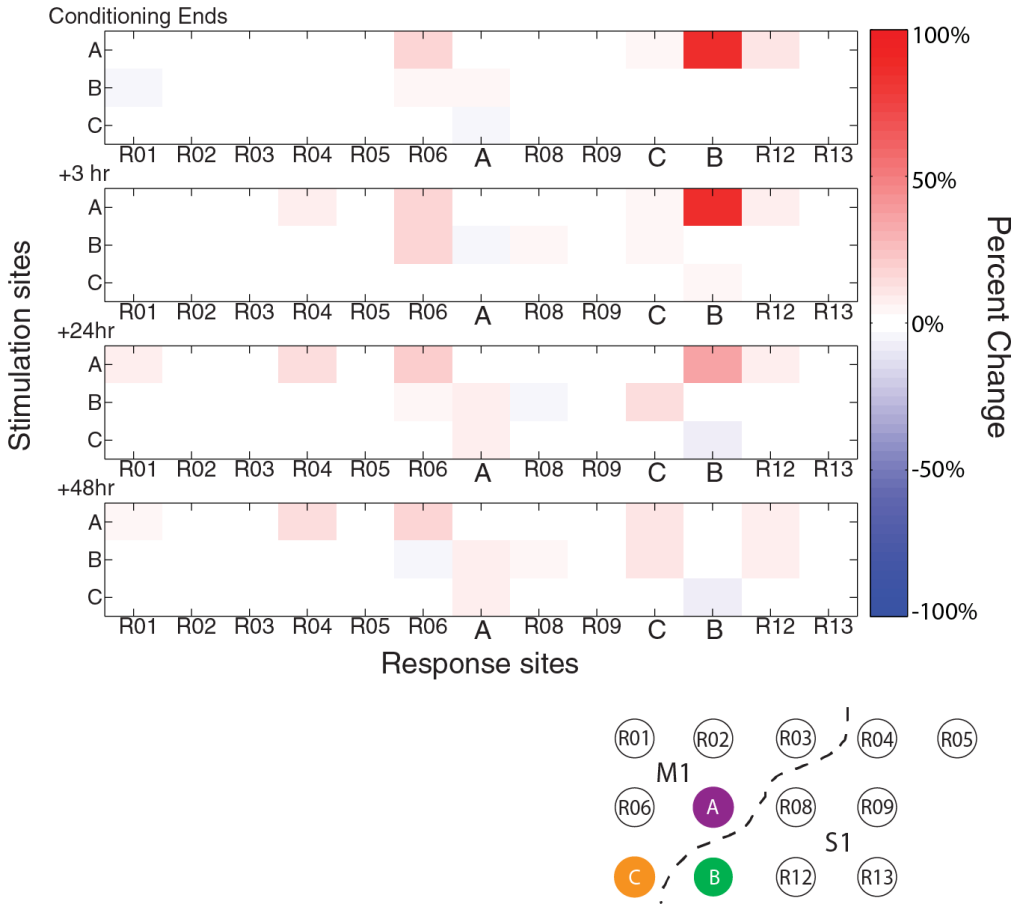

Figure 1.8 Network-wide effects of conditioning.
Percent change in EPs from A, B, and C to all other sites where there was a response. Panels show time points after conditioning (top to bottom). Data are from the same conditioning session shown in Figure 1.6

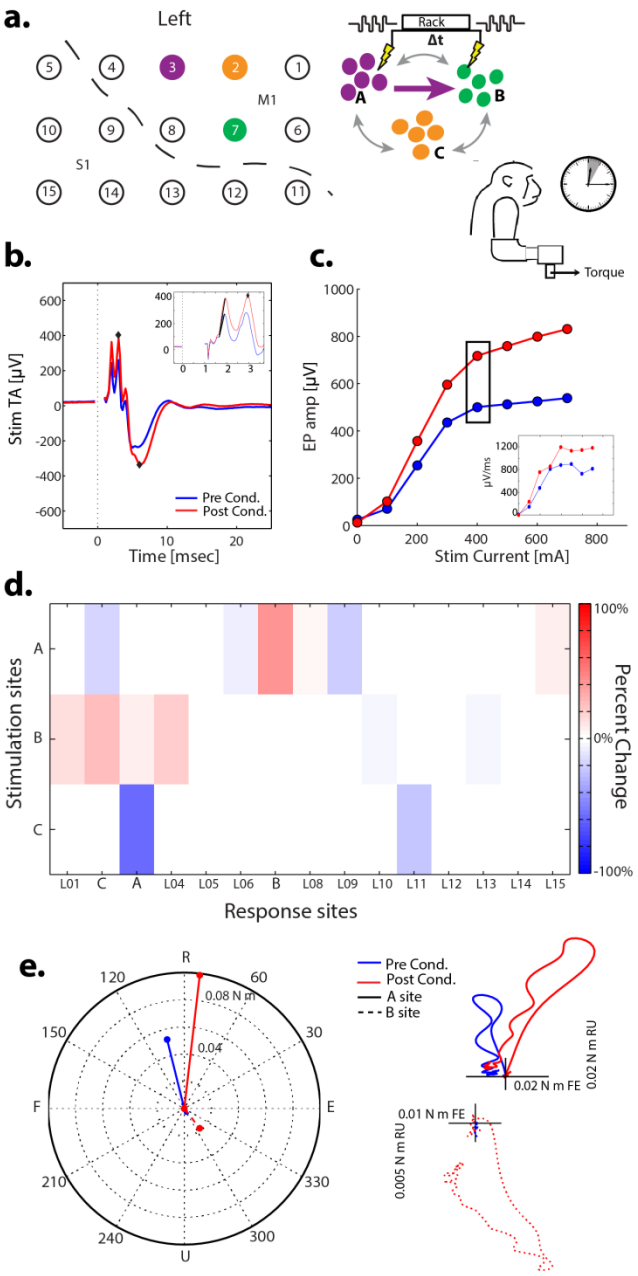

Figure 1.9 One hour long conditioning session at 20 ms delay.

a) Schematic of conditioning session with 20ms delay using rack-mounted equipment while monkey U was in the booth for 1 hour. Left panel shows cortical positions of A (purple), B (green), and C (orange) sites relative to the central sulcus (dotted line). **b)** StTA of A→B EP before (blue) and after (red) conditioning at current amplitude denoted by black box in **c**. Inset shows zoomed in view of the first response phase; black line indicates the slope. Diamonds indicate peak and trough used to calculate amplitude plotted in **c**. **c)** Stimulus-response curve of A→B EP before (blue) and after (red) conditioning. Black box is current amplitude depicted in **b**. Inset shows stimulus-response curve for slope of the first phase denoted by the inset in **b**, with the same color scheme. **d)** Percent change in EPs from A, B, and C to all other sites where there was a response, similar to Figure 1.8. **e)** *Left*, direction and magnitude of evoked torque (ET) from site A (solid lines) and site B (dotted lines) before (blue) and after (red) conditioning. *Right*, StTA ET trajectories from which magnitude and direction were calculated; same colorization and line-style apply.

The above examples used a paired-stimulation delay of 20 ms, which is in the optimal range for STDP (Bi and Poo, 1998). We tested a range of delays (6, 10, 20, 30, 50, 100 and 200 ms; Table 1.1 Table 1.2) for the two site pairs highlighted above to determine whether the paired-stimulation conditioning effects were consistent with STDP rules. Figure 1.10 shows that at delays of less than 50 ms, the A→B connection is preferentially potentiated in accordance with a pre-before-post rule (Bi and Poo, 1998). The reverse B→A connection serves as a proxy for post-before-pre conditioning; however, most B→A effects showed no change. As in the examples described above, we observed EP changes outside of the target A→B pair in all sessions.

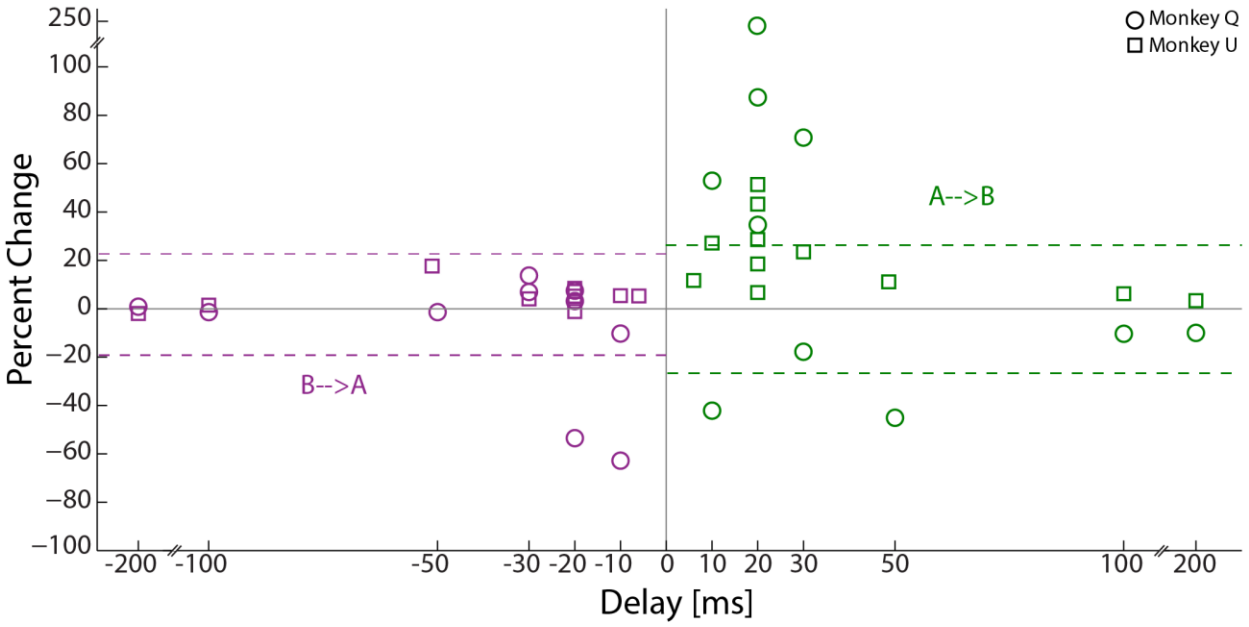

Figure 1.10 Conditioning effects as a function of paired-stimulation delay.
Conditioning delay versus percent change in EP amplitude. Positive delays indicate pre→post (A→B) stimulation while negative delays indicated post→pre (B→A) stimulation. Dotted lines indicate 2.5th and 97.5th percentiles for the A distribution (green, Figure 1.11a) or the B distribution (purple, Figure 1.11b). Data from monkey Q is in circles and data from monkey U in squares.

In order to separate global effects from targeted paired-stimulation effects on EP amplitude, we created a distribution of effects for all outputs from site A (except B and C) and site B (except A and C) for these two pairs across all delays (*n* = 23 sessions, Figure 1.11); these two distributions were termed A_{cont} and B_{cont} (see Methods). On average, A_{cont} EPs increased 4.0 ± 1.0% (*n* = 146 EPs, p = 0.0001, 1-sample *t*-test) while B_{cont} EPs increased 1.3 ± 1.0% (*n* = 143 EPs, p = 0.2, 1-sample t-test). The cumulative density function of the A_{cont} distribution compared to that of A→B effects highlights the significant separation between these distributions (p = 0.0003, K-S test)(Figure 1.11a), indicating that the increase in connectivity strength from A to B due to the targeted conditioning surpasses that of the global effects on the network. Conversely, changes in the B→A distribution were not different from the B_{cont} distribution (p = 0.27, K-S test)(Figure 1.11b).

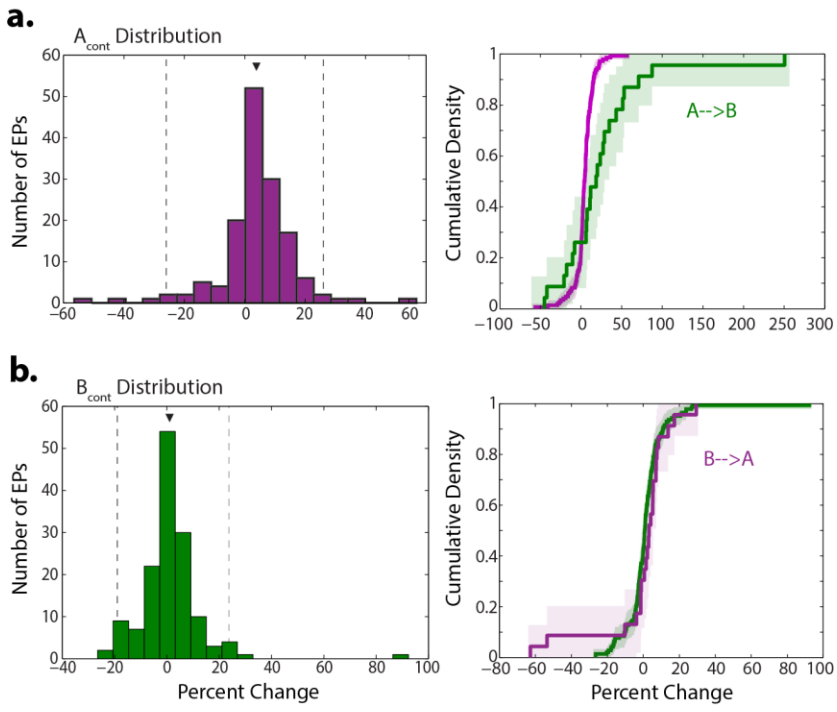

Figure 1.11 Cumulative density curves describe network-wide effects of conditioning.
a) *Left*, A_{cont} distribution of percent change in EP amplitudes from all sites except B and C in which site A evokes a response; arrowhead denotes mean (+4.0%) and dotted lines indicated the 2.5th and 97.5th percentiles recapitulated in Figure 1.10. *Right*, A_{cont} distribution depicted as a cumulative density (purple) superimposed with the cumulative density of percent change in A→B EPs (green) from all delays depicted in Figure 1.10. Light colored shadows indicate the 95% CI. **b)** *Left*, B_{cont} distribution (mean = +1.3%) similar to **a**. *Right*, B_{cont} distribution cumulative density (green) compared with cumulative density of percent change in B→A EPs (purple) similar to **a**. *Bottom right*, significance of effects; on-diagonal quadrants indicate *p*-value of self-control distributions calculated with a one-sample *t*-test, while off diagonal quadrants indicate comparison of the directed connection with the appropriate control distribution calculated with a two-sample Kolmogorov-Smirnov test.

Since potentiation of the A→B connection was maintained for at least three hours in the absence of continued paired-stimulation, we were curious whether a second conditioning block would potentiate A→B further. We tested this during one session (Table 1.1, session 20150403†) in which a three hour block of paired-stimulation occurred, followed by three hours of no stimulation, and then an additional three hours of paired-stimulation. During the first conditioning block the A→B EP increased from 123.1 ± 25.0 μV to 431.6 ± 56.2 μV (+250.7%, $p < 0.05$). After three hours of no stimulation the A→B amplitude fell to 261.6 ± 44.6 μV, still significantly larger than the pre-conditioning amplitude (+112.5%, $p < 0.05$). However, after a second, 3-hour block of paired-stimulation the A→B EP amplitude did not increase further and was maintained at 256.6 ± 36.0 μV (-3.45% compared to the previous testing period, $p > 0.05$).

1.3.3 **Paired-stimulation produces inconsistent effects at most site pairs**

We found that a delay of 20 ms produced the most robust and consistent effect (Figure 1.10) and thus used this delay to test 13 other site pairs in the hand area of primary motor and sensory cortex in both monkeys (Figure 1.12). Similar to the analysis above, Figure 1.13a summarizes the results of all 15 site pairs tested at a 20 ms delay using the A_{cont} distribution compared to the cumulative density of A→B and A→C. Similar distributions are shown for the B and C sites. The changes in the A→B distribution show significant separation from the changes in A_{cont} connections (Figure 1.13a, $p = 0.026$, K-S test) particularly at large percent increases, indicating an effect of targeted conditioning above that of global effects on the network. Upon closer inspection, only three of the 15 site pairs tested, including the two pairs described in Figure 1.6 and Figure 1.9 (monkey U: L03→L07 and monkey Q: R07→R11, L07→L11), drive this separation and lie outside of the 95th percentile of the A_{cont} distribution. Thus, a majority of site pairs tested did not show a significant conditioning effect. It should be

noted that while Q: L07→L11 did produce a significant effect in one session, we failed to repeat this effect in two other sessions (Figure 1.14). Changes in the A→C distribution were marginally significantly different from A_{cont} ($p = 0.045$). There were no significant differences in the distributions for the B→A connection ($p = 0.08$) or the B→C connection ($p = 0.31$) compared to B_{cont} (Figure 1.13b). Similarly, there was no difference in the distribution for the C→A connection ($p = 0.63$) compared to the C_{cont} distribution, or between the distribution for the C→B connection ($p = 0.36$) and C_{cont} (Figure 1.13c). We also saw a small but significant shift in the mean of A_{cont} (+2.5 ± 0.9%, 1-sample *t*-test, $p = 0.0064$, $n = 251$, Figure 1.13a *inset*) and B_{cont} (+2.7±1.0%, 1-sample *t*-test, $p = 0.0084$, $n = 237$, Figure 1.13b *inset*) away from zero after conditioning at a 20 ms delay indicating that there was some global change or variability in connection strengths across the network.

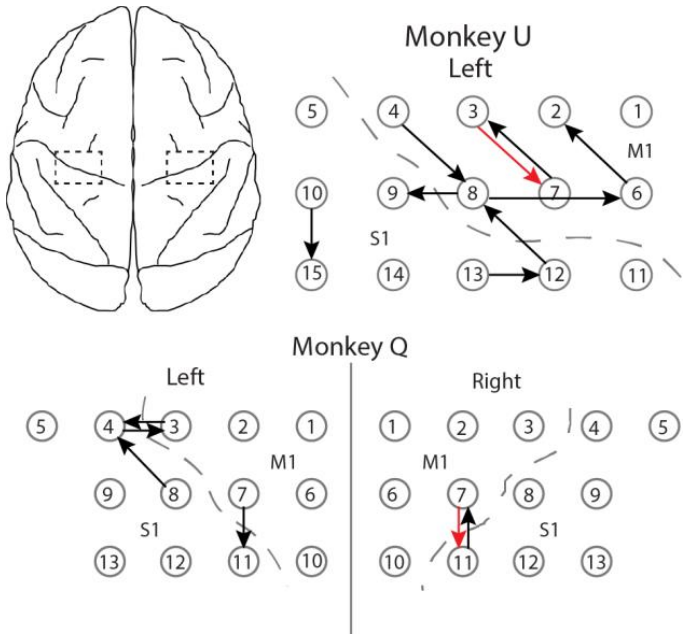

Figure 1.12 Schematic of all conditioning pairs.
Upper left, top-down view of macaque brain; dashed boxes outline positions of implant area bilaterally. *Upper right*, Left electrode grid in monkey U with A→B pairs used for conditioning sessions indicated by arrows; arrow points from A to B. Only the left hemisphere was used in monkey U, who performed a behavioral task using his right hand. *Bottom*, Bilateral electrode grids for monkey Q with A→B pairs used for conditioning sessions indicated. Dashed lines in monkey U and Q mark the central sulcus. Red arrows indicate site pairs with successful conditioning.

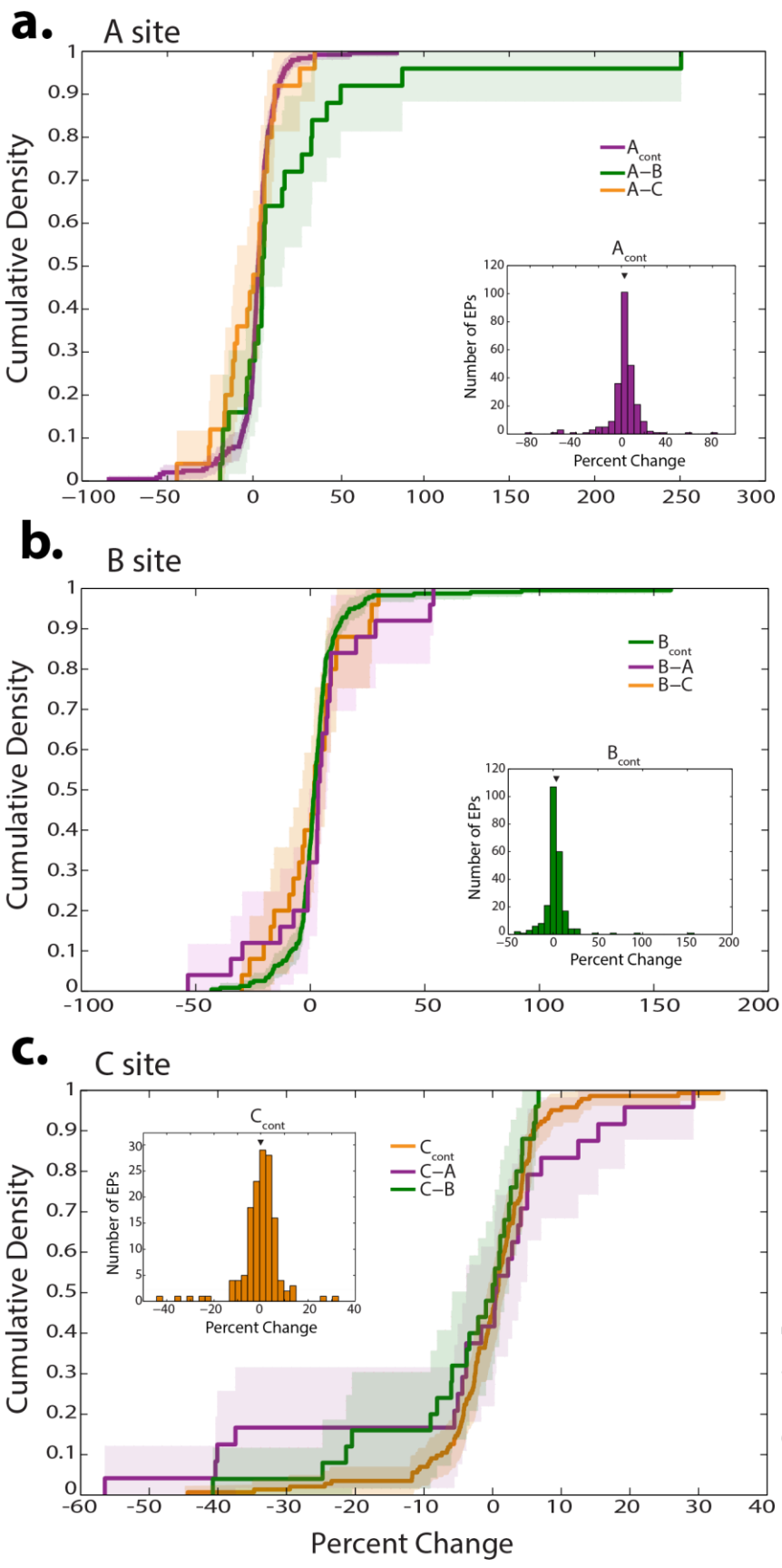

Figure 1.13 Network-wide effects of paired stimulation across all sessions.

a) Cumulative densities for A_{cont} distribution (purple) from all site pairs at a conditioning delay of 20 ms overlaid with the A→B (green) and A→C (orange) distributions. **b)** Cumulative densities for B_{cont} distribution (green curve), B→A (purple), and B→C (orange). **c)** Cumulative densities for C_{cont} distribution (orange curve), C→A (purple), and C→B (green). For all panels light colored shadow indicates 95% CI; *insets* show distribution for the appropriate control distribution, arrowhead marks the mean. Cumulative densities were calculated similarly to that in Figure 1.11. *Bottom right*, significance matrix for all combinations. Quadrants on the diagonal indicate *p*-value for the appropriate self-control distribution using a one-sample *t*-test. Off-diagonal quadrants indicate *p*-value for the directed connection compared to the control distribution on its row using a two-sample Kolmogorov-Smirnov test.

An example site pair that did not exhibit a significant conditioning effect (Table 1.2, session 20150708) is shown in Figure 1.15. The A→B EP amplitude was 722.6 ± 6.6 μV prior to conditioning and 697.6 ± 6.0 μV after conditioning (-3.5%, $p > 0.05$, Figure 1.15b-d). Again we measured the slope of the rising phase of the EP to confirm that the absence of an effect was not due to the peak-trough measure. As can be seen in the insets of Figure 1.15b & c, the changes in slope before and after conditioning follow closely those of the peak-trough amplitude (Figure 1.3a, grey filled circle). This was consistently seen across many experiments. There was no significant difference between the percent change seen in A→B after conditioning using the

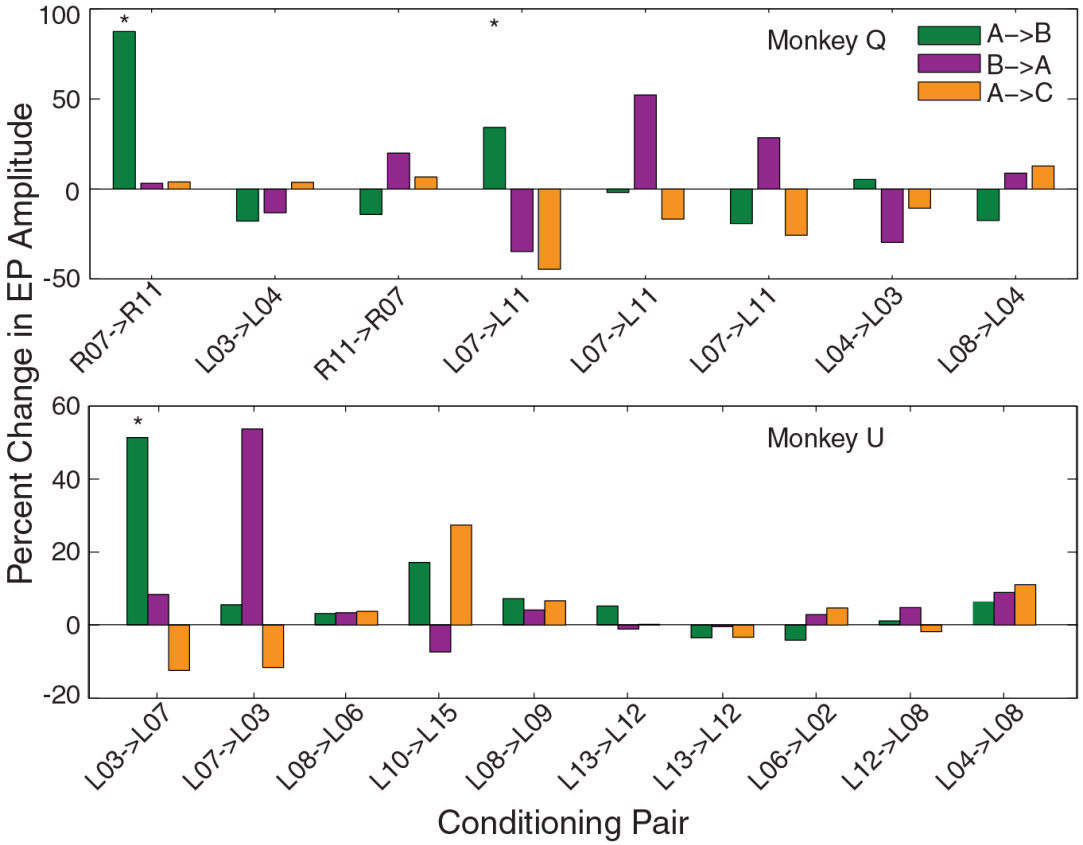

Figure 1.14 Summary of conditioning results across all conditioning sessions.
Percent change in A→B, B→A, and A→C connections after conditioning at 20 ms delay for all site pairs tested in monkey Q (top) and monkey U (bottom). For the far left pair in each panel (*top*, R07→R11; *bottom*, L03→L07) multiple sessions at a 20 ms delay were conducted and these data are representative examples as depicted in Figure 1.6 and Figure 1.9. Asterisks denote $p < 0.05$ as determined by control distributions in Figure 1.13.

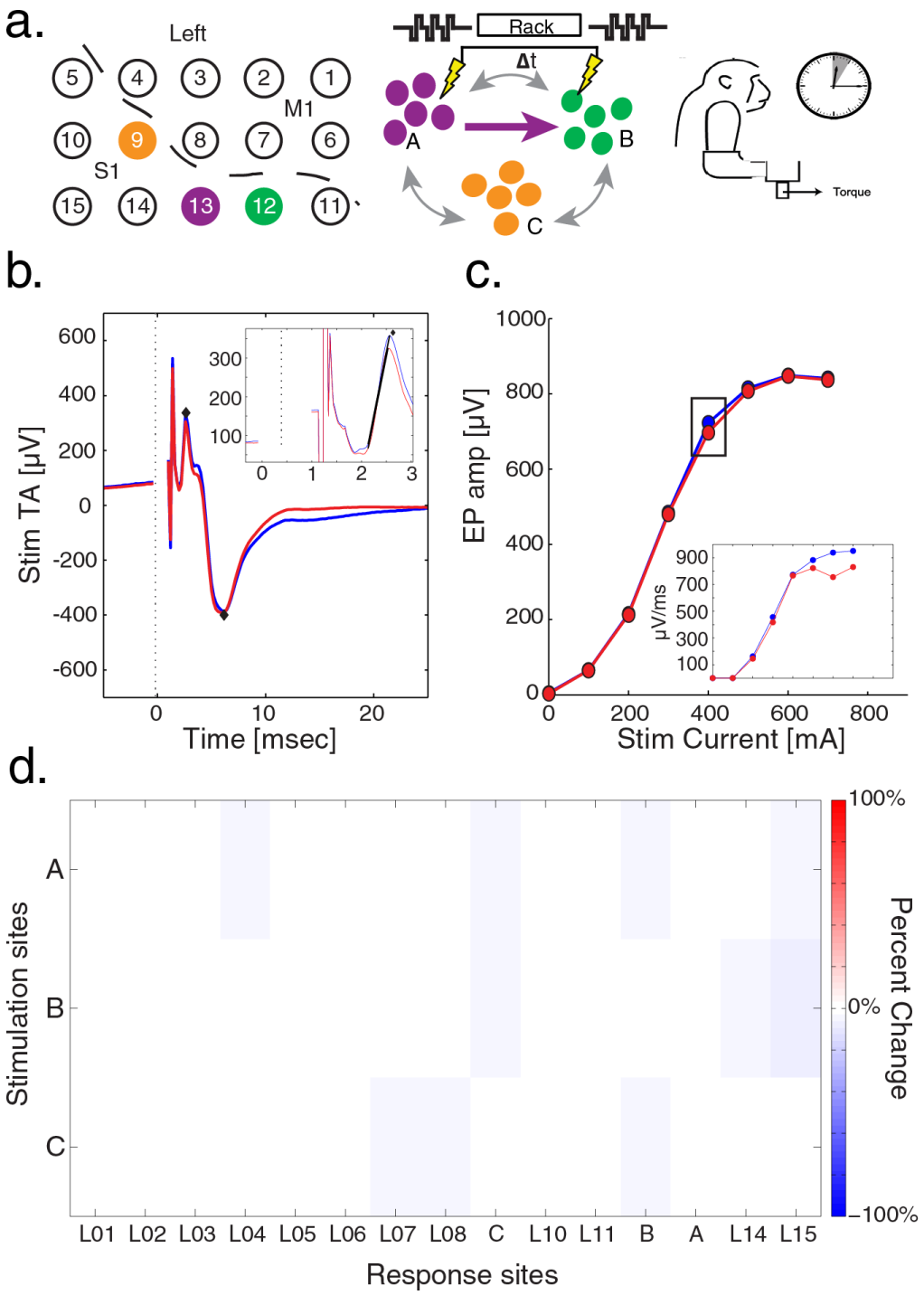

Figure 1.15 Paired-stimulation does not produce a conditioning effect at all sites.
a) Schematic of recording grid with A (purple), B (green), and C (orange) sites denoted for a conditioning session at a 20 ms delay in monkey U while in the recording booth for 1 hour. **b)** StTA of A→B EP before (blue) and after (red) conditioning. *Inset*, expansion of StTA showing the slope (black line) of the first EP phase. Black diamonds denote peak and trough used to calculate amplitude in **c**. **c)** A→B stimulus-response curve before (blue) and after (red) conditioning. Black box denotes current depicted in **b**. *Inset*, stimulus-response curve before and after conditioning for slope of first EP phase. **d)** Percent change in EP amplitude from A, B, and C to all other recording sites after conditioning.

peak-trough amplitude compared to the slope of the first rising phase ($p = 0.66$, paired *t*-test; Figure 1.3a) or the absolute amplitude of the first phase ($p = 0.38$, paired *t*-test; Figure 1.3b). A summary of changes seen in A→B, B→A, and A→C at 20 ms delay for all site pairs tested is shown in Figure 1.14 (asterisks denote significant pairs mentioned above) and Table 1.1Table 1.2 summarize all conditioning experiment parameters.

1.3.4 **State dependence on paired-stimulation effects**

The excitability of cortex is known to vary with attention, context, and other "brain state" variables (Gilbert and Sigman, 2007) which could underlie the varied results seen with paired-stimulation conditioning. In an attempt to control for brain state during conditioning, we delivered paired-stimulation to monkey U only while he was performing a particular movement as part of the behavioral task, hypothesizing that cortex would be in a similar state on each stimulation event. The subset of peripheral targets during which paired-stimulation was delivered was based on the torques evoked with stimulation at site A (see Methods). While the evoked torques (ETs) could be quite large, stimulation did not interfere with monkey U's ability to perform the task. Figure 1.16 shows results from a site pair (L04→L08) that did not produce a conditioning effect in A→B EPs (+6.5%, $p > 0.05$, Figure 1.16b-d solid lines). Since site A's ETs were largely in the radial direction, paired-stimulation was only delivered when monkey U was acquiring R-related targets (R, FR, and ER) in a second conditioning session. The paired-stimulation still did not produce a change in EP amplitude under this target-restricted paradigm. It is important to note that there was also an overall reduction in the total number of paired stimuli delivered during this protocol (3,324 target-restricted vs. 7,200 all targets), which may have reduced the effectiveness of the conditioning. We repeated this paradigm in a second site pair (L03→L07), restricting conditioning to targets in the directions of ET from sites A and B.

For both site pairs, paired-stimulation produced the largest effects in A→B EPs (Figure 1.17). Target-restricted conditioning did not enhance an effect already present in pair L03→L07, nor did it promote the appearance of an effect in L04→L08.

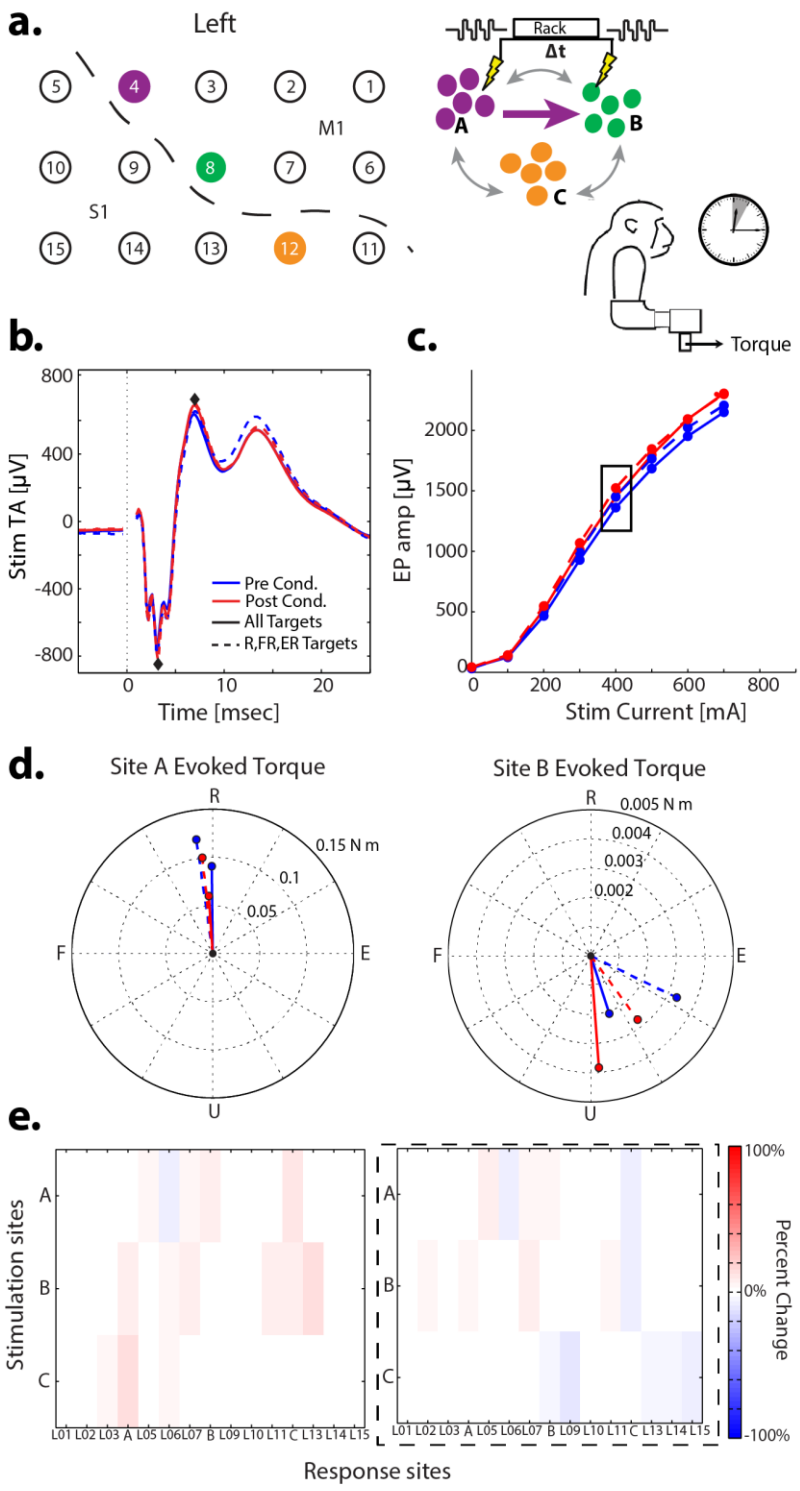

Figure 1.16 Conditioning session under different behavioral contexts.
a) Schematic of recording grid with A (purple), B (green), and C (orange) sites denoted for two conditioning sessions at a 20 ms delay in monkey U while in the recording booth for 1 hour. **b)** StTA of A→B EP before (blue) and after (red) conditioning for a session in which paired-stimulation was delivered continuously (solid lines) or only during presentation of particular targets in the behavioral task (dashed lines). Black diamonds mark the peak and trough used to calculate amplitudes in **c**. **c)** A→B stimulus-response curve before (blue) and after (red) conditioning during two conditioning sessions (solid vs. dashed lines) described in **b**. Black box denotes current for which responses in **b** were recorded. **d)** Direction and magnitude of ETs from site A (*left*) and site B (*right*) before and after conditioning in two sessions (colors and line-type follow **b** and **c**). **e)** Percent change in EP amplitude from A, B, and C to all other recording sites after conditioning. *Left* panel corresponds to the continuous paired-stimulation session while the *right* (dashed outline) panel corresponds to the conditioning session in which paired-stimulation was delivered in a task-dependent manner.

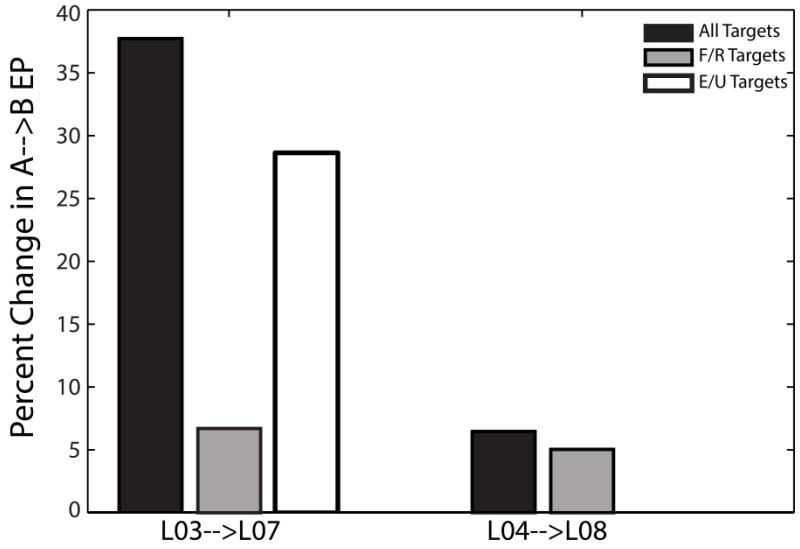

Figure 1.17 Effects of paired-stimulation under different behavioral conditions.
Percent change in A→B EP in 5 conditioning sessions between two site pairs. Black bars denote sessions in which paired-stimulation was delivered continuously while monkey U was performing a behavioral task. Grey bars denote sessions in which paired-stimulation was delivered only during acquisition of flexion or radial movement targets, while the white bar denotes a session in which paired-stimulation was delivered only during acquisition of extension or ulnar movement targets.

1.3.5 **Paired-stimulation effects on behavioral output**

Previous STDP studies in monkeys have shown effects on motor outputs such as stimulus-evoked wrist torque trajectories and individual muscle responses (Jackson et al., 2006; Lucas and Fetz, 2013; Nishimura et al., 2013). In two site pairs tested we observed ETs in the A and B site, including sites L03→L07 illustrated in Figure 1.9. In this session we saw a significant increase in the amplitude of ETs from both site A (+88.7%, $p = 2.96 \times 10^{-10}$) and B (+462%, $p = 1.16 \times 10^{-11}$) after conditioning at a delay of 20 ms (Figure 1.9e). There was also a significant shift in the direction of site A's ET (median ± s.e: 104 ± 0.5º to 83.4 ± 0.5º, p = 0.002). While these results suggest an effect of paired-stimulation conditioning on motor outputs, this was not consistently seen within or across site pairs. Sites L04→L08 did not show a shift in site A's ETs in either the full behavioral paradigm or the target-restricted paradigm (All targets: +3.36º, p = 0.84; Target-restricted: -2.01º, p = 0.65, Figure 1.16d). Overall we saw no change in the angular

separation of the ETs from site A and B before and after paired-stimulation conditioning ($p = 0.24$ $n = 13$), unlike the results from Jackson et al (2006), where the direction of the torque evoked from site A shifted towards that of site B after a STDP protocol. Though the amplitude of site B's ET after conditioning tended to increase this was not significant (mean ± s.e.: +100.7 ± 9.2%, paired *t*-test, $p = 0.42$, $n = 14$). Similarly, ETs from site A showed no significant increase in amplitude after conditioning (mean ± s.e.: +11.64 ± 11.56%, paired *t*-test, $p = 0.94$, $n = 17$). This is consistent with previous results showing inconsistent changes in ET amplitude (Jackson et al., 2006).

Table 1. Conditioning sessions for monkey Q

Exp	Session	A site	B site	C site	Pulses	Current (μA)	Frequency (Hz)	Delay (ms)	Duration (Hrs)	A-B % change	B-A % change	A-C % change	
1	20140917	R07	R11	R10	3@330 Hz	330	2	20	3	87.41*	3.13	3.91	Figure 1.6 Figure 1.8
	20141006							10		-42.13*	-62.80*	2.43	
	20141027							30		70.79*	13.78	14.30	
	20150119							20		34.70*	-53.50*	-25.0	
	20150316							200		-20.96	2.21	-0.21	
	20150330							50		-45.07*	-1.42	15.24	
	20150403							20		250.65*	7.50	8.45	
	20150403†							20		-3.45	-10.66	9.37	
	20150406							100		-10.39	-1.45	22.6	
	20150422							30		-17.77	6.94	31.43*	
	20150427							10		52.96*	-10.30	19.74	
	20150720					----	----	----		-7.92	29.42*	9.10	
2	20150216	L07	L11	L10	3@300 Hz	330	2	20	3	34.18*	-34.70*	-44.49*	
	20150608							20		-1.93	52.24*	-16.66	
	20150804							20		-19.18	28.47*	-25.7	
3	20150128	R11	R07	R10	3@300 Hz	330	2	20	3	-14.14	19.97	6.68	
4	20150126	L03	L04	L08	3@300 Hz	330	2	20	3	-17.82	-13.14	3.71	
5	20150615	L04	L03	L02	3@300 Hz	330	2	20	3	5.22	-29.65*	-10.61	
6	20150608	L08	L04	L06	3@300 Hz	330	2	20	3	-17.51	8.86	12.77	

Table 1.1 All conditioning sessions for monkey Q.
Experiments (Exp) are grouped by site pair and sessions are listed chronologically. Parameters were consistent for each experiment, and thus listed only in the first session entry (unless otherwise noted). In Session 20150403 two conditioning blocks were performed with a 3 hour gap in between. The first entry includes results of the first conditioning block while 20150403† is the second conditioning block (see Results). Asterisks denote $p < 0.05$ based on control distributions.

Table 2. Conditioning sessions for monkey U

Exp	Session	A site	B site	C site	Pulses	Current (µA)	Frequency (Hz)	Delay (ms)	Duration (Hrs)	A-B % change	B-A % change	A-C % change	
1	20150528	L03	L07	L02	3@330 Hz	80	2	20	1	51.37*	8.4	-12.4	
	20150529							B only stim		17.6	157.22*	2.5	
	20150603							20		43.27*	7.1	-16.0	Figure 1.9
	20150604					----	----	---		20.0	0.5	0.3	
	20150608							10		27.15*	5.4	-0.5	
	20150609							30		23.5	4.1	4.8	
	21050611							100		6.2	1.5	4.5	
	20150612							200		7.5	-3.8	0.9	
	20150806†							20		28.64*	5.2	12.2	
	20150807‡							20		6.7	-1.1	8.3	
	20150928							20		18.5	2.9	36.19*	
	20151001				1	200		6		11.7	5.3	13.9	
	20160108				3@300 Hz	80		50		11.1	17.2	29.10*	
2	20150707	L13	L12	L09	3@330 Hz	100	2	20	1	5.2	-1.1	0.2	
	20150708					200				-3.5	-0.4	-3.3	Figure 1.15
3	20150922‡	L04	L08	L12	3@330 Hz	80	2	20	1	5.0	3.3	-9.2	Figure 1.16
	20150924							20		6.5	9.0	11.1	Figure 1.16
4	20150521	L07	L03	L02	3@330 Hz	80	2	20	1	5.6	53.75*	-11.6	
5	20150522	L08	L06	L12	3@330 Hz	100	2	20	1	3.2	3.4	3.8	
6	20150527	L10	L15	L14	3@330 Hz	120	2	20	1	17.2	-7.3	27.45*	
7	20150702	L08	L09	L03	3@330 Hz	120	2	20	1	7.3	4.1	6.6	
8	20150709	L06	L02	L07	3@330 Hz	140	2	20	1	-4.1	2.9	4.7	
9	20150710	L12	L08	L13	3@330 Hz	140	2	20	1	1.2	4.8	-1.8	

Table 1.2 All conditioning sessions for monkey U.
Experiments (Exp) are grouped by site pair and sessions are listed chronologically. Parameters were consistent for each experiment, and thus listed only in the first session entry (unless otherwise noted). Restricted target paradigms are denoted by (†) in which paired-stimulation was delivered during E/U targets and (‡) in which paired-stimulation was delivered during F/R targets. Asterisks denote $p < 0.05$ based on control distributions.

1.4 Discussion

The present study aimed to induce cortico-cortical plasticity between sensorimotor populations in awake, behaving non-human primates utilizing a paired-stimulation conditioning protocol. Regions of primary motor or sensory cortex were deemed functionally connected if stimulation of one site evoked a response in LFP at another site, indicating a highly interconnected network. Paired-stimulation between two connected sites at a fixed delay, over a prolonged period of time, resulted in STDP as evidenced by increased EP amplitude at short delays but not long ones (Figure 1.10). Further, plasticity effects in the targeted A→B connection surpassed the global increase in connectivity seen throughout the network (Figure 1.13). Surprisingly, this effect was only produced in 2 out of 15 site pairs (13%). Effects in the other 13 site pairs predominantly showed global increases in network connectivity (50% of pairs) or depression of the targeted site pair (44% of pairs). The varied effects shown here beg the question of whether paired-stimulation to promote STDP with electrical stimulation is site-independent *in vivo*.

1.4.1 STDP between cortical populations may be induced via paired-stimulation

Typical STDP studies document changes in connectivity via a direct measure of excitatory post-synaptic potentials (Markram et al., 1997; Bi and Poo, 1998; Sjostrom et al., 2001; Froemke and Dan, 2002). Evidence of STDP has also been shown using more indirect measures such as evoked movements (Jackson et al., 2006; Lucas and Fetz, 2013) or electromyographic activity (Nishimura et al., 2013), motor evoked potentials (Wolters et al., 2003), spike modeling (Rebesco et al., 2010; Rebesco and Miller, 2011), and others (Feldman, 2012). This study is one of the first to show long-lasting STDP in evoked LFPs between large cortical populations. Though only two site pairs showed STDP, this effect was robust,

repeatable, and displayed a classic STDP curve (Figure 1.10). Targeted STDP effects far exceeded global increases in the A_{cont} and B_{cont} populations (Figure 1.13). The small global changes we observed likely result from stimulation at the A and B site which would promote untargeted long-term potentiation (LTP) (Teyler, 1989). We believe cortico-cortical EPs are evidence of the many mono and polysynaptic connections between two sites as evidenced by the multi-phasic nature of EPs. It is worth noting that effects of paired-stimulation were evident in multiple EP phases (Figure 1.6c) suggesting that many pathways between the two sites were enhanced by paired-stimulation. Taken together, these results indicate that paired-stimulation between two areas is a viable approach to inducing targeted plasticity. That a majority of sites did not show STDP could be the confluence of many factors, some of which will be discussed below.

1.4.2 **STDP is a multi-faceted phenomenon**

Paired-stimulation of a source population, A, and a target population, B, was modeled after pre→post pairing utilized in *in vitro* studies of STDP (Bi and Poo, 1998; Feldman, 2000; Froemke and Dan, 2002). Pre→post pairing induces STDP by eliciting a spike in a pre-synaptic neuron followed closely in time by intracellular depolarization of a post-synaptic neuron. In principle, paired electrical stimulation *in vivo* will also induce action potentials at the pre- and post-synaptic sites in an appropriately timed manner to promote plasticity. However, as has been demonstrated *in vitro*, timing is one of many factors governing plasticity at a given synapse (Feldman 2012) . Background firing rate, cooperativity of multiple synapses, and location of inputs all play a crucial role in STDP. Sjöström and colleagues (Sjostrom et al., 2001) showed that the efficacy of plasticity in primary visual cortex (V1) pyramidal neurons could be modified by varying the rate of stimulation or the number of recruited pre-synaptic inputs, all while

maintaining a pre→post pairing of +10 ms (in the window for conventional STDP). Others have also demonstrated that some form of spatiotemporal integration is critical for reaching sufficient depolarization in the post-synaptic neuron on top of which a well-timed back-propagating action potential will promote STDP (Lisman and Spruston 2005). Timing of pre- and post-synaptic activation is one of the few parameters we could control, along with rate of stimulation. For two pairs of sites, a sufficient combination of these other factors aligned such that the rate and timing of paired-stimulation delivered was effective at producing STDP. For the remaining 13 site pairs, any number of parameters could have been inappropriate for conditioning. We tested other stimulation protocols varying the rate, number of pulses, or duration of conditioning in order to optimize the parameter space (see Methods). That these did not produce conditioning effects does not say that plasticity could not be induced at those sites, but rather that these were not the optimal protocols for doing so. Therefore, it is possible that each site pair will need to be tuned just so in order to align the multi-faceted nature of STDP.

The intrinsic connectivity of neural networks is another key factor in determining whether plasticity may be induced just as the number, strength, and location of inputs (Sjostrom et al., 2001; Froemke et al., 2005) all play a role. By recording LFPs from large populations we have only a loose measure of the connectivity of the network, as evidenced by the presence of EPs between sites, and no information about what specific connectivity underlies the EP that is the target of conditioning. While there are general themes in connectivity patterns between areas of sensorimotor cortex, this ambiguity in specific pathways giving rise to EPs could explain the mixed results we saw in this study. Neuroanatomical studies have shown that major collaterals of layer 3 and 5 pyramidal neurons reach targets up to 6 mm from their branching point and stratify in multiple layers. Furthermore, branching off of the main collateral is relatively sparse,

sometimes with great distance (≥ 800 μm) in between branches (DeFelipe et al., 1986) suggesting that these collaterals are a major source of excitatory inter-areal input. These connections are almost surely prominent contributions to the EPs we measured between cortical sites, are the targets of cortico-cortical conditioning, and likely the site of plastic effects observed in other *in vivo* STDP studies (Jackson et al., 2006; Rebesco et al., 2010; Rebesco and Miller, 2011). However, as LFPs incorporates all nearby current sources (Buzsáki et al., 2012), significantly different pathways could give rise to similar EPs (Figure 1.18), some of which are more amenable to STDP than others. As spatial integration is one of the factors contributing to STDP (Sjostrom et al., 2001), pathways in which there is high convergence would have a higher likelihood of showing plasticity. There is anatomical evidence that projections from different branches converge at a common target (DeFelipe et al., 1986) suggesting that some horizontal connections may be more influential than others on the output of the target site. It is possible then, that site pairs in our study that produced a conditioned effect have a higher rate of convergence than those site pairs which did not show an effect (Figure 1.18, green pathway).

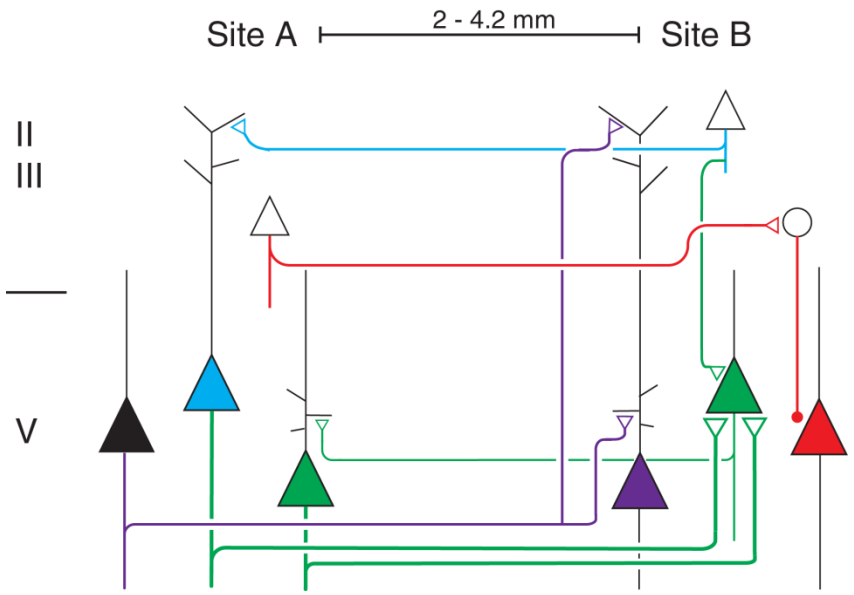

Figure 1.18 Diagram of potential interareal connections and STDP effects.
Four potential pathways connecting an A and B site are shown. Upper layer 2/3 and layer 5 are the likely targets of the dual electrodes for each site and thus only these layers are shown. The *green pathway* from A→B highlights successful potentiation due to convergent excitatory input between layer 5 pyramidal cells. Similarly the *green pathway* from B→A shows successful depression. The other 3 pathways do not promote STDP for a variety of reasons. The *red pathway* results in inhibition between A and B via inhibitory interneurons (circles). In the *purple pathway*, while inputs to the proximal dendrites would promote potentiation, inputs on the distal dendrites would not. Similarly, depression in the *blue pathway* is unsuccessful as the primary connection from B→A is in the distal dendrites.

In addition to the influence of multiple factors on the efficacy of STDP, there are also multiple forms of STDP that occur in a regional and synapse-specific fashion (Feldman 2012). In traditional Hebbian STDP positive, pre→post, delays produce LTP while negative, post→pre, delays promote long-term depression (LTD). Conversely, in anti-Hebbian STDP LTD is produced at positive delays and moderate LTP at negative delays. Anti-Hebbian STDP occurs at a variety of synapses particularly those of layer 2/3 on distal layer 5 dendrites likely due to attenuation of the back-propagating action potential over long distances (Sjostrom and Hausser, 2006). As we are almost certainly invoking STDP at both proximal and distal dendrites, the resulting mixture of Hebbian and anti-Hebbian effects could be interfering with each other at a majority of sites preventing LTP from occurring (Figure 1.18, purple pathway). STDP involving

inhibitory interneurons can similarly show Hebbian or anti-Hebbian effects (Caporale and Dan, 2008; Feldman, 2012; D'amour and Froemke, 2015) further clouding the net plasticity produced in a mixed inhibitory-excitatory population (Figure 1.18, red pathway). The expectation from classical Hebbian STDP would predict depression in the B→A connection as this can be thought of as a negative delay. However, if B→A is dominated by distal layer 2/3-layer 5 inputs then anti-Hebbian STDP would result, consistent with the lack of B→A depression that we observed (Figure 1.18, blue pathway). Strong recurrence between sites in our grid could also be contributing to the lack of B→A depression. Paired-stimulation *in vivo* likely activates many direct and indirect pathways such that precise spike timing becomes unstable (Diesmann et al., 1999). Froemke and Dan (2002) showed, in rat visual cortical slice, that STDP effects incorporating multiple spike times do not add linearly. Therefore, while B→A may experience a negative delay from the initial paired-stimulation pulses, ongoing activation via recurrence may interfere with the simplistic Hebbian mechanism.

1.4.3 **Electrical stimulation is artificial**

Electrical stimulation is the best tool with which to rapidly activate the nervous system, yet it is inherently artificial and non-specific. Electrical stimulation primarily acts via activation of small diameter processes, mostly axons, which then triggers both an antidromic and orthodromic action potential. The distance of activated neurons as a function of current injected can be fit with logarithmic (Tehovnik, 1996), or parabolic functions (Stoney et al., 1968). However, recent studies suggest that the area of activation remains static and rather large, on the order of millimeters, but that higher currents simply activate more neurons within the volume (Histed et al., 2009). The fact that electrical stimulation recruits post-synaptic neurons through transynaptic mechanisms means that recruitment may be highly specific, such that neighboring

neurons may not both be activated by a given stimulation event (Histed et al., 2009), and different from effects of sensory stimulation (Millard et al., 2015). Many studies that utilize electrical stimulation to induce STDP record an empirical signal from the pre- and post-synaptic site (Markram et al., 1997; Bi and Poo, 1998), or trigger post-synaptic stimulation from a neural event (Jackson et al., 2006; Rebesco et al., 2010; Lucas and Fetz, 2013; Nishimura et al., 2013; Zanos, 2013) to ensure proper timing of action potentials and depolarization. We hypothesized that our paired-stimulation protocol would be sufficient to induce well-timed spiking both pre- and post-synaptically in a way that would promote plasticity. This hypothesis is substantiated by recent *in vivo* evidence that paired-stimulation can change the inferred connectivity of neural networks modeled by a generalized linear spiking model (Rebesco and Miller, 2011). Furthermore, studies in humans using transcranial magnetic stimulation to pair stimulation of the median nerve with associated cortical areas demonstrate classic Hebbian STDP (Wolters et al., 2003). Therefore it is feasible to use paired-stimulation protocols, however indirect, to promote targeted plasticity and we observed this as well in a subset of site pairs. However, in sites that did not show conditioning effects it is possible that electrical stimulation was ineffective at activating the proper connections necessary to promote plasticity. This is supported by unpublished evidence utilizing paired optogenentic stimulation (Yazdan-Shahmorad et al., 2016) targeting layer 5 pyramidal cells, which showed more consistent effects between site pairs (Silversmith et al., 2016)(Figure 1.18, green pathway). Thus, optogenetic stimulation could selectively stimulate pathways that promote STDP compared to electrical stimulation which may indiscriminately activate pathways giving rise to conflicting forms of Hebbian plasticity (Figure 1.18).

1.4.4 **Context specificity and brain state**

Cortical processing is known to be highly influenced by contextual cues that vary with attention and general brain state (Gilbert and Sigman, 2007). For instance, studies in primary visual (Li et al., 2006) and auditory (Fritz, 2005) cortex have shown that neurons modulate their response in a context-specific manner even though the behavioral task or stimulus is identical. Therefore, the brain does not operate as a simple fixed input-output function, but rather individual neurons and neural networks experience states that may be switched in a context-specific way. In previous STDP studies in awake, behaving monkeys (Jackson et al., 2006; Lucas and Fetz, 2013; Nishimura et al., 2013; Zanos, 2013), the post-synaptic stimulation was triggered by a physiological event in the pre-synaptic site, thus ensuring that the cortical region was in a similar state or context with each post-synaptic stimulation event. We hypothesized that paired-stimulation of focal regions of cortex would synchronize the neural populations and thus induce a stable "brain state" on top of which STDP could be produced. Network modeling of effective connectivity has demonstrated that perturbations, such as electrical stimulation, can induce a state-shift that is highly dependent on the phase of ongoing oscillations (Battaglia et al., 2012). Physiological data from multi-unit activity and LFPs have also shown that effective connectivity between sites is dependent on phase-locking (Womelsdorf et al., 2007) and that STDP is phase dependent (Zanos, 2013). Given the influence of ongoing cortical rhythms, we attempted to use behavior as a contextual cue for conditioning by only delivering paired-stimulation during certain parts of the behavioral task. We hypothesized that this would provide a more homogenous state for each successive paired-stimulation event. That this paradigm did not produce a STDP effect could suggest that the behavioral trigger was not sufficient to set an effective phase relationship or state. Additionally, this paradigm resulted in 50% fewer paired-

stimulation events. Thus, future experiments controlling for the total number of stimuli and testing across more site pairs would be needed to fully test this hypothesis.

Chapter 2. INTRINSIC FUNCTIONAL CONNECTIVITY OF NEURAL POPULATIONS IN FORELIMB SENSORIMOTOR CORTEX

2.1 **Introduction**

Neurons in the brain interact on a broad spatiotemporal scale that can be described by anatomical and functional connections. The precise definition of functional connectivity, as measured with electrophysiological tools, is more ambiguous than its structural counterpart for both technical and empirical reasons. Electrical recording methods cover a wide spatiotemporal range from recordings of single neurons to electroencephalograms (EEG) recorded from the surface of the scalp. The choice of recording method determines the resolution of the neural module under investigation, and the functional connectivity methods applied to these recordings have limitations and biases (Bastos and Schoffelen, 2016). As a result, an accurate description of the functional interactions of neurons in the brain requires exploration along the whole spatiotemporal spectrum.

Pioneering works by Cajal and Sherrington suggested that neurons were the basic unit of the nervous system motivating a century of research on the electrical activity of individual neurons. Single-unit recordings in awake, behaving animals have provided great insight into the input – output processing of neurons (Yuste, 2015). Much of what we know about cortical processing, particularly in the motor system, comes from this approach (Evarts, 1968; Humphrey and Corrie, 1978; Fetz and Cheney, 1980; Georgopoulos et al., 1982). Motor cortex (M1) pyramidal cells show a variety of coding strategies incorporating the dynamics, kinematics, or other features of movement across a flexible temporal scale (Kalaska et al., 1989; Todorov and Jordan, 2002; Overduin et al., 2008; Shenoy et al., 2013), thus clouding the interpretation of

these input – output properties as well as the connectivity that gives rise to coordinated movement. The synaptic interactions of neuronal pairs have been estimated from the recording of two units at once via correlative or modeling analysis. These studies showed correlation patterns consistent with a variety of connection types (Murphy et al., 1985; Fetz et al., 1994; Smith and Fetz, 2009a) some of which are related to shared motor output (Jackson et al., 2003; Smith and Fetz, 2009b). Thus, there is evidence that movement encoding partially arises from specific population connectivity. Progress in technology and computing memory now allows for the recording of many neurons simultaneously, allowing for experiments that can directly test encoding of movement by neuronal populations. Studies in primate M1 have shown that coordinated activity among a population of neurons can add a superlinear dimension to movement encoding beyond summation of individual neuron activity (Hatsopoulos et al., 1998; Churchland et al., 2012).

Given these technological and conceptual advances, there has been renewed interest in true population-level recording such as intracortical local field potentials (LFPs), surface electrocorticography (ECoG), and EEG (Bressler and Menon, 2010). Additionally, studies in primate M1 showing that individual neuron spiking was phase-locked to particular LFP oscillations (Murthy and Fetz, 1992, 1996; Baker et al., 1997; Donoghue et al., 1998) furthered the paradigm shift from single-unit to population recording. The source of the extracellular field potential is generally attributed to summation of transmembrane currents around the recording electrode (Buzsáki et al., 2012). However, the cellular and synaptic mechanisms that generate oscillations in population recordings and their role in cortical processing continues to be researched and debated (Turkheimer et al., 2015). Nevertheless, recording of LFPs and ECoG

signals over the last decades has enabled new investigations of the functional connectivity within neural networks (Bressler and Menon, 2010; Turkheimer et al., 2015; Yuste, 2015).

Yet, even these approaches examine a wide range of spatiotemporal scales from local micro-circuits, measured by multi-electrode arrays (MEAs) to whole-brain macro-circuits, such as the default mode network (Bressler and Menon, 2010; Turkheimer et al., 2015) measured by large ECoG arrays or functional magnetic resonance imaging (fMRI). Studies using micro-ECoG (μECoG) arrays, which have a footprint one order of magnitude smaller than traditional ECoG arrays, have begun to explore meso-scale connectivity (Wang et al., 2009; Watanabe et al., 2012; Kellis et al., 2016). In a comparison of ECoG, μECoG, and MEA recording, the gross spatiotemporal correlations scaled accordingly, yet each modality showed distinct fine-grain patterns likely because each recording scale examines a different dimension of network processing (Kellis et al., 2016). To further our understanding of meso-scale networks, we recorded stimulus-evoked potentials (EPs) and spontaneous LFPs from awake, behaving monkeys implanted with dual intracortical and surface electrodes over a 12 mm by 6 mm area in the hand region of sensorimotor cortex. EPs allowed us to assess direct anatomical connections (either mono- or polysynaptic) between recorded populations while coherence in spontaneous oscillations showed potential higher-dimensional binding among the network. Potential overlap in these connectivity measures may show common patterns in functional connectivity that are highly relevant to network processing.

2.2 Methods

2.2.1 Implant

Dual Electrodes

Three monkeys (*macaca nemestrina*), O, Q, and U, were implanted with custom-made dual electrodes (Figure 2.1) arranged in two 3x5 grids over bilateral sensorimotor cortex (Figure 2.1b). Dual electrodes were constructed using 0.005" bare PtIr wire rods cut to 3 mm (surface) and 5 mm (intracortical) and each soldered to independent, 32 gauge, insulated lead wire (Figure 2.1a). The PtIr rod-lead wire construct was further insulated with 10 μm of parylene by the UW Microfabrication Facility to insulate the solder joint and PtIr rod. The tips of each rod were then de-insulated by hand using a scalpel to an impedance of 9-90 kΩ (monkey O), 22-160 kΩ (monkey Q), and 4-60 kΩ (monkey U). For each dual electrode, a 3 mm and 5 mm PtIr rod were secured in a small piece of PTFE tubing with silicon glue. The tips of the 3 and 5 mm rods were placed approximately 0.5 and 2-2.5 mm, respectively, from the edge of the PTFE tube (Figure 2.1a). When implanted, the 5 mm rod penetrated to layer 5 of sensorimotor cortex, where output pyramidal cells reside, while the 3 mm rod rested on the surface of the brain. After each dual electrode was constructed, the back ends of the lead wires were soldered to connectors.

Surgery

All surgeries were performed under isoflurane anesthesia and aseptic conditions. An incision was made along the midline of the scalp, and muscle and connective tissue were resected to expose enough skull to place a 2.5 inch diameter titanium casing. Four to eight skull screws were placed in the skull around the edge of the exposure. At least four of the skull screws were used as grounds for the electrode implant. Holes were drilled with a 1.1 mm bit in a 3x5 grid with 2-3 mm center-to-center spacing using stereotaxic coordinates (Figure 2.1b). After all

of the holes were drilled, one dual electrode was placed with forceps into each hole until resistance was felt between the longer rod and the dura. The electrode was then pushed through the dura and into the brain until a second resistance was felt between the shorter rod and the dura. We use the term "surface," instead of epi- or subdural, to describe the location of the shorter rod because it was impossible to know whether the dura was punctured by the shorter

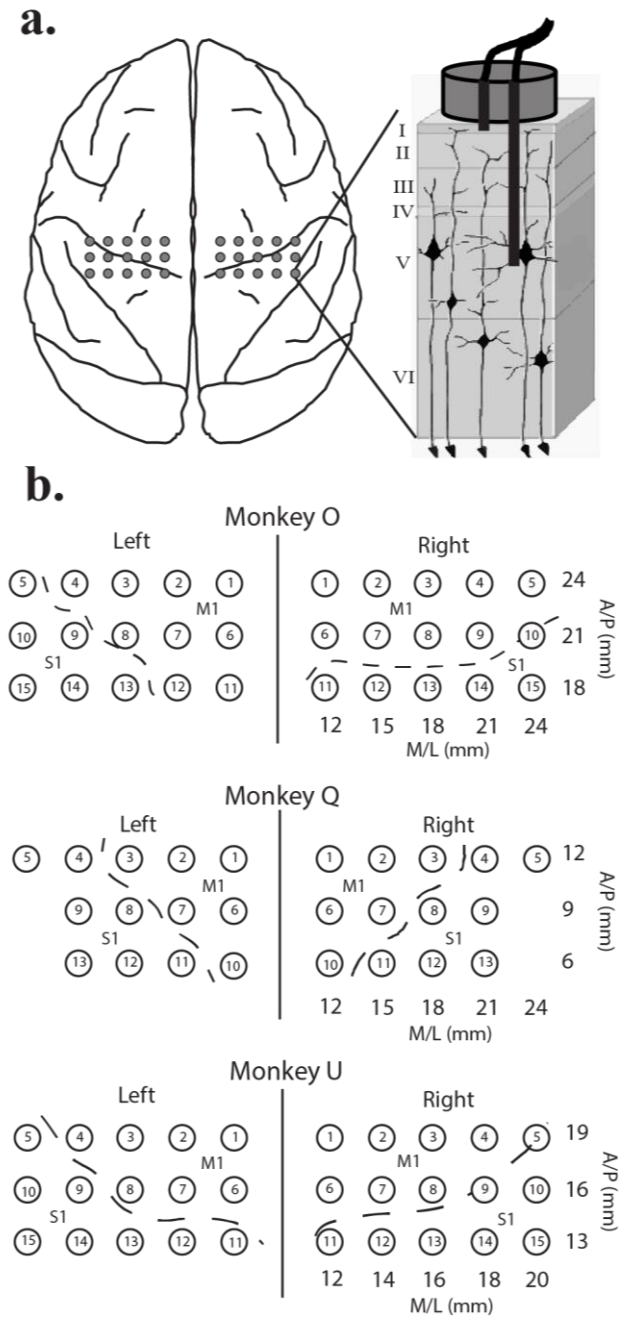

Figure 2.1 Cortical implant schematic.
a) Top-down view of macque brain. Grey circles indicate relative position of implanted dual electrode shown in cross-section to the right. Each dual electrode consisted of an intracortical lead which penetrated to ~ layer 5 and a surface lead. **b**) Electrode numbering and real-world stereotaxic coordinates for each animal. Dotted line marks the position of the central suclus as determined by median nerve stimulation.

rod. Once all of the dual electrodes for one hemisphere were implanted, a thin coat of dental acrylic (methyl methacrylate) was used to seal the holes and hold the implant in place. This process was repeated for the other hemisphere. The casing was then placed over the implant and secured to the skull screws with acrylic. The connectors for the dual electrodes were cemented to the skull within the casing. Animals received post-operative courses of analgesics and antibiotics.

2.2.2 **Recordings**

General Acquisition

LFP recordings were obtained using amplifiers from Guger Technologies (Graz, Austria) in monkey Q (4,800 Hz sampling rate) and the Grapevine Neural Interface System from Ripple (Salt Lake City, UT) in monkeys O and U (various sampling rates). Single-ended recordings from the intracortical and surface electrodes, referenced to a skull screw, were made simultaneously on up to 26 channels (13 dual electrodes) in monkey Q and up to 60 channels in monkeys O and U (30 dual electrodes). Post-hoc, recordings were re-referenced as a bipolar signal for each dual electrode (intracortical – surface) to acquire a more localized recording and filtered accordingly for different analyses (see Analysis).

During recording, monkeys O and U were engaged in a center-out target acquisition task in which torque about the right wrist moved a computer cursor towards a peripheral target in one of eight cardinal directions. The animal received an applesauce reward after the target was successfully acquired (holding the cursor for up to 2 seconds in the peripheral target) and had returned the cursor to the center of the screen. Monkey Q sat quietly in the recording booth.

Estimate of electrode location relative to the central sulcus

The stereotaxic coordinates at which the electrodes were implanted were determined prior to surgery using an atlas to target the hand area of sensorimotor cortex. As the atlas is only a rough guide, coordinates were sometimes amended in surgery such that the middle of the grid was ~18 mm lateral to Bregma, which is the approximate location of hand motor area (Fetz and Cheney, 1980). To more accurately determine the location of each dual electrode relative to M1 or primary sensory (S1) cortex, single-ended responses to stimulation of the contralateral median nerve were recorded with the monkey under ketamine sedation. The waveshape of the evoked potentials in stimulus triggered averages (StTA) of surface recordings indicated the position of the recoding site relative to the central sulcus (CS) (McCarthy et al., 1991). An evoked potential with a positive phase followed by a negative phase is generated in precentral cortex, while a negative phase followed by a positive phase indicates a site in postcentral cortex. Based on these recordings, a putative position of the CS was drawn onto the grid (Figure 2.1b, dotted lines).

2.2.3 **Analysis**

Stimulus-Evoked Potentials (EPs)

Stimulus evoked potentials (EPs) were used to establish connectivity between recording sites. Monkeys were seated in a primate chair in a recording booth while electrical stimulation was delivered to each dual electrode (Figure 2.2a). Stimulation was biphasic, with the negative phase leading on the intracortical wire and the positive phase leading on the surface wire of a given dual electrode. Stimuli were delivered in a series of increasing current intensities, termed stimulus ramps, ranging from 0 mA to 2.25 mA with 7-10 increments in the ramp and interstimulus intervals of 300-500 ms; each ramp was repeated 100 times (Figure 2.2a). Post-hoc, recordings from monkeys O and U, originally sampled at 30,000 Hz, were first down-sampled to

5,000 Hz to be comparable to monkey Q (sampled at 4,800 Hz). Recordings were then bipolar re-referenced and high-pass filtered over 10 Hz. EPs were measured at all ipsilateral sites (monkeys O and Q) as well as contralateral sites (monkey U) in response to stimulation at one site during testing. All sites underwent testing stimulation to build a map of connectivity across the implant for ipsilateral connections in monkeys O and Q. In monkey U, we were able to record both hemispheres simultaneously to explore ipsilateral and contralateral EP connections.

For StTAs, trials were aligned on stimulus onset and grouped for a given current intensity. All trials were inspected by eye and those with movement artifacts were removed. From the remaining trials, StTAs were calculated from 50 ms before to 300 ms after the time of stimulation for each current intensity (Figure 2.2b). In order to separate a physiological response from electrical artifact, a biphasic stimulation pulse was delivered directly into the Guger Technologies amplifiers to visualize the artifact. The artifact returned to baseline by 1 ms after stimulation and thus any response within the first millisecond was ignored. The Grapevine system has built-in artifact suppression, which grounded the recording channels for 1 ms at the time of stimulation. Each stimulus aligned trial was also examined by eye for evidence of a clean separation between the stimulus artifact and the response. Trials in which there was possible contamination by the artifact were discarded.

The amplitude of the average EP was quantified by subtracting the largest trough from the largest peak in a window 1.5 ms to 100 ms after stimulation for all current intensities (Figure 2.2c, red circles). This metric was chosen as a simple, unbiased way to capture the site-specific, often multi-phasic, shape of the EP. The slope of the stimulus-response curve for EP amplitude was used to assess the strength of cortico-cortical connectivity (Hess et al., 1996) and is referred to as ‘EP strength’ throughout the text and figures. Other EP metrics were calculated and

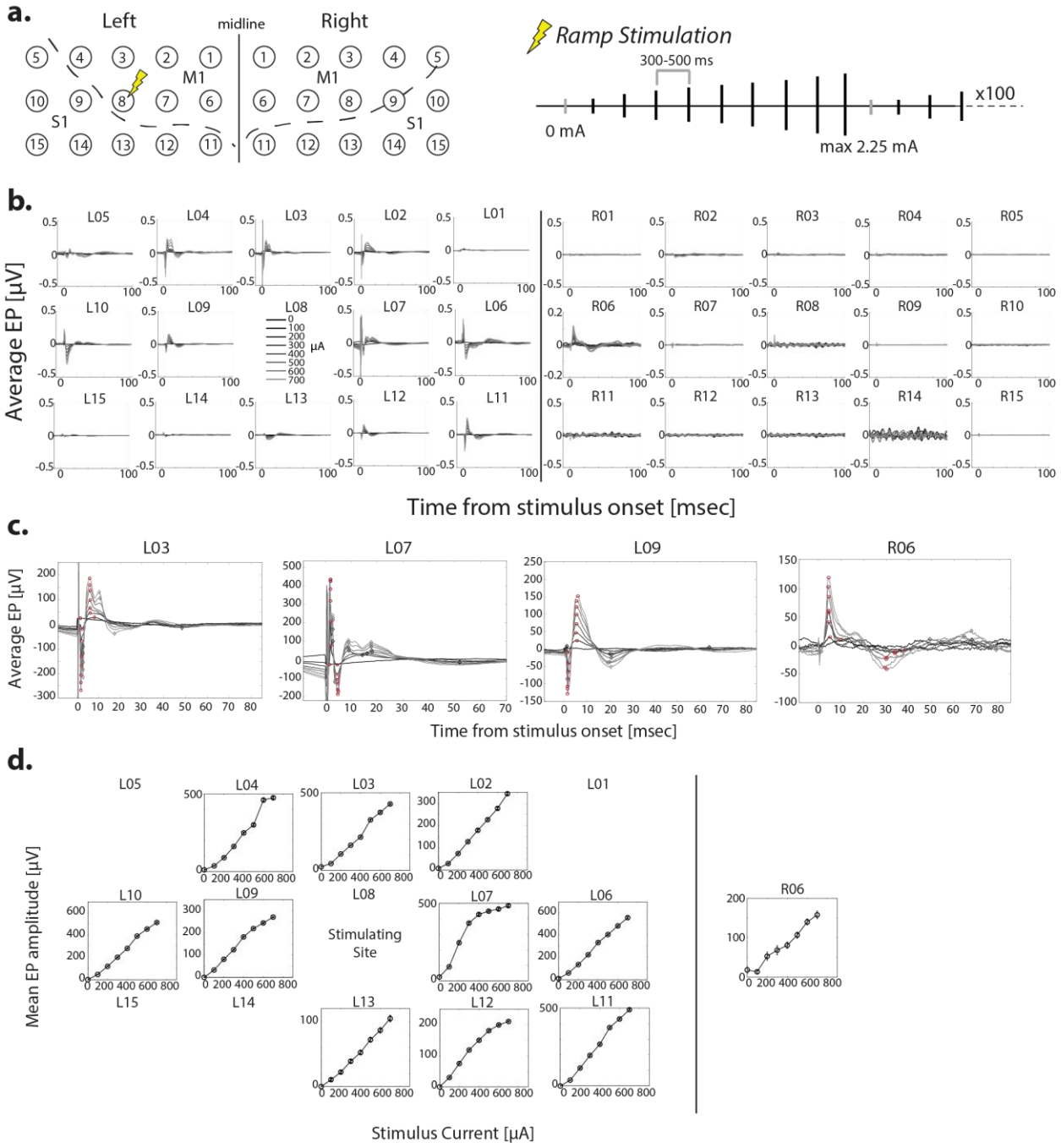

Figure 2.2 EP Characterization.

a) Ramp stimulation parameters used to test EP connections. In this example, site L08 in monkey U was stimulated. **b**) StTA EPs at each current intensity (n = 100) evoked from stimulation at L08. **c**) Selected StTAs showing results of peak-finding algorithm. Grey-scale diamonds denote all peaks and troughs. Red circles denote largest peak and trough used to calculate EP amplitude. **d**) Stimulus-response curve for each site in **b** that showed an EP.

analyzed to describe stimulus-evoked connectivity including: 1) binary presence of an EP between two sites, 2) latency to the first peak (or trough) of the EP from stimulus onset (referred to as peak latency), 3) the number of response phases, 4) reciprocal connections, 5) "out-degree," defined as the number of sites at which an EP was produced when a single site was stimulated (projections), 6) "in-degree," defined as the number of sites, that when stimulated, produced an EP at a single site, and 7) information flow (out-degree – in-degree). Out-degree, in-degree, and information flow are borrowed from graph theoretic methods which have previously been used to describe neural network processing (Keller et al., 2014). The number of phases were determined by a peak-finding algorithm (Yader, 2009), which captures the amplitude of the feature above a global baseline combined with a threshold separation from surrounding points ("peakiness"). The global baseline was two standard deviations above the pre-stimulation baseline and the peakiness was ±10 μV.

To assess regional differences between M1 and S1, each site was categorized as being in M1 or S1 based on the results of median nerve stimulation. The cross-sulcus probability was calculated as the number of projections from a particular site that crossed the CS divided by the total number of outputs. Connections were also labeled as being intra-M1 (M1-M1), intra-S1 (S1-S1), or inter-M1-S1 (M1-S1 or S1-M1) based on the cortical location of the two connected sites.

Spontaneous band-limited coherence

Spontaneous recording of LFPs from all ipsilateral (monkey Q) or all ipsilateral and contralateral (monkeys O and U) electrodes were acquired in 10-30 minute sessions while the animal was in the recording booth. Monkeys O and U were engaged in a behavioral task (see Recordings) while monkey Q sat quietly. Post-hoc, recordings were bipolar re-referenced and

down-sampled to 500 Hz. The Guger Technologies amplifiers applied a 0.1 Hz high-pass filter while the Grapevine amplifiers apply a 0.3 Hz high-pass filter during recording; no further filtering was done post-hoc as coherence analyses did not approach the Nyquist frequency. Recordings were inspected by eye for movement artifact, which was removed manually and the remaining data were concatenated for further analysis. A sliding, non-overlapping, 1-second Hanning window was used to calculate the fast Fourier transform (FFT) and power spectrum of the continuous recording up to 150 Hz. From this, the magnitude-squared coherence of LFPs between two cortical sites (Eq. 2.1) was calculated across the full spectrum where *P* is the power spectral density and *x* and *y* are two unique cortical sites.

$$C_{xy}(f) = \frac{|P_{xy}(f)|^2}{P_{xx}(f)P_{yy}(f)} \qquad \text{(Equation 2.1)}$$

An example coherence spectrum between sites R01 – R06 in monkey O is shown in Figure 2.3.

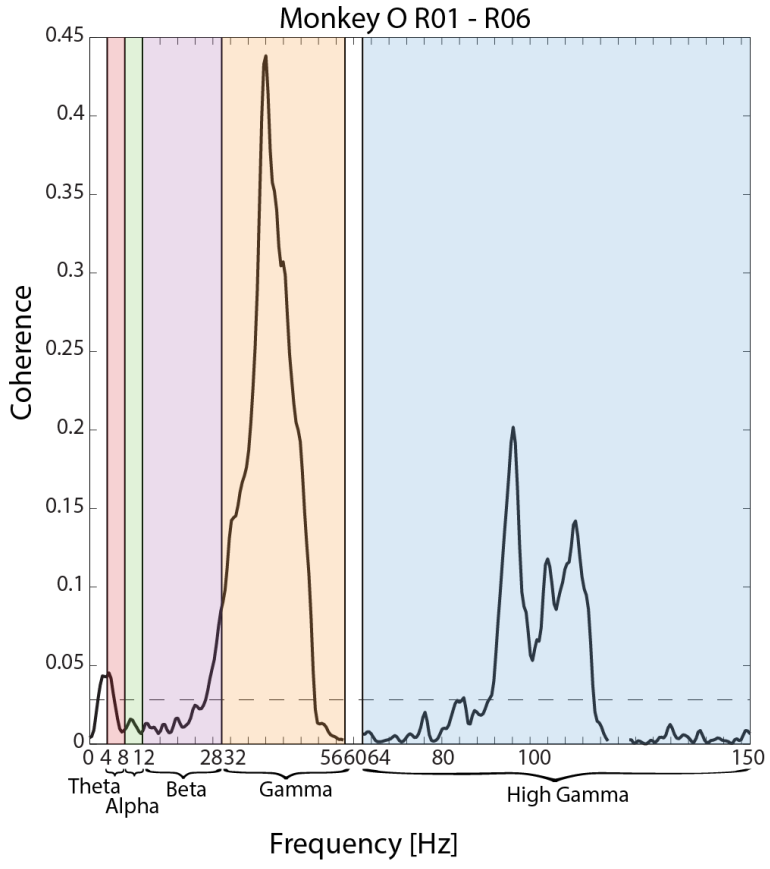

Figure 2.3 Coherence spectrum and band delimitations. Example coherence-frequency spectrum between R01 and R06 in monkey O. Frequency bands designated by colored shading.

The continuous frequency spectrum was binned into canonical frequency bands (Buzsáki and Draguhn, 2004), theta (4-8 Hz), alpha (8-12 Hz), beta (12-30 Hz), gamma (30-58 Hz), and high gamma (62-150 Hz) with notches at line noise (60 Hz) and its harmonics (Figure 2.3). The mean coherence in each of these five bands was used for further analysis to describe cortico-cortical coherence of spontaneous LFPs.

2.2.4 **Statistics**

Statistics were calculated with GraphPad Prism version 6 for Windows (GraphPad Software, La Jolla, CA) and MatLab (The MathWorks Inc., Natick, MA). For all figures statistical significance is reported as * $p < 0.05$, ** $p < 0.01$, *** $p < 0.001$, **** $p < 0.0001$.

EP connectivity

A linear regression was performed to quantify the dependence of EP probability, reciprocity, peak latency, and phase number on inter-electrode distance. Each animal and each hemisphere (for monkey U) were fit separately as the specific inter-electrode distances were slightly different between animals. The relationship between EP strength and inter-electrode distance was better fit with a one-phase decaying exponential compared to a linear regression as determined by R^2 values. For monkey U, ipsilateral and contralateral connections were combined.

An unpaired, two-sample *t*-test was used to assess differences in cross-sulcus probability for sites in M1 compared to S1 for monkeys O and Q reported as mean ± standard error. For monkey U, M1 and S1 sites were further separated into ipsilateral and contralateral connections, and for this case regional and hemispheric differences were assessed with a one-way ANOVA with Tukey correction for multiple comparisons. EP strength followed a lognormal distribution as has been shown for estimates of connection weights in anatomical studies of primate cortex

(Markov et al., 2014). EP strength was log-transformed by calculating the natural logarithm; log-transformed EP strength followed a Normal distribution as assessed with a chi-square test (monkey O: $p = 0.29$, monkey Q: $p = 0.34$, monkey U: $p = 0.38$; Figure 2.4). The strength of connections within and across regions (M1 and S1) was assessed via a one-way ANOVA on the log-transformed EP strength with Tukey correction for multiple comparisons. In monkey U, we were also able to assess regional differences across hemispheres with a two-way ANOVA with Tukey correction for multiple comparisons also on log-transformed EP strength. For ease of interpretation, non-transformed data are displayed in figures and text as median (IQR) where IQR is the inter-quartile range.

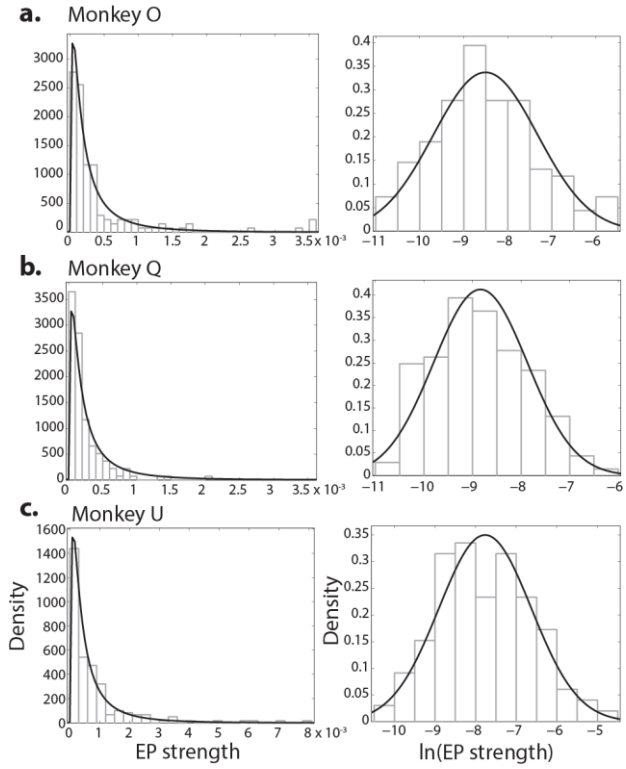

Figure 2.4 Log-normal distribution of EP strength. **a** – **c**) For each animal the left panels show distribution of EP strength fit with a log-normal function. Right panels show distribution of log-transformed EP strength fit with a normal Gaussian.

Spontaneous LFP coherence

Significant coherence across the full frequency spectrum was assessed via random shuffling of the time-series recording. The one-second data windows for one site were randomly re-ordered in time to disrupt any organization in the original data. Coherence between an un-

randomized site and the randomized site was calculated according to Equation 2.1 for all unique connection pairs and the absolute maximum value recorded. Random shuffling was repeated 100 times to create a distribution of maximum coherence values. The 95th percentile of this distribution served as an absolute significance level for all frequency bands and connection pairs (Figure 2.3, dotted grey line). Broadband LFP power has been shown to follow a $1/f^{x}$ ($x > 1$) distribution (Miller et al., 2009); coherence also seems to follow this function, with lower coherence in higher frequencies (Kajikawa and Schroeder, 2011). To account for this dependency, we also calculated significance cutoffs for each frequency band. During the randomization procedure, a distribution of maximum mean coherence across all connection pairs was created and the 95th percentile used as a cutoff for significance. For analysis and figures concerning band coherence, only significant connections were included. Banded coherence was also separated into ipsilateral and contralateral connections (monkeys O and U). Significant differences in coherence magnitude between bands were evaluated for ipsilateral and contralateral connections separately via a Kruskal-Wallis test with Dunn's correction for multiple comparisons. A Wilcoxon rank sum test with Bonferroni correction for multiple comparisons was used to assess coherence differences between ipsilateral and contralateral connections within a given frequency band.

The relationship between coherence magnitude in each frequency band and inter-electrode distance was fit with a one-phase decaying exponential in monkey O and U, with the exception of the theta band in monkey O which did not converge on an exponential fit and was fit with a linear regression. Data from monkey Q could not be significantly fit with linear or non-linear regressions. The magnitude of coherence within and across M1 and S1 (separately for ipsilateral and contralateral connections) was evaluated via a Kruskal-Wallis test with Dunn's

correction for multiple comparisons. All frequency bands were combined in order to assess regional differences in coherence. Additionally, since coherence is a symmetric measure, a connection which crosses the CS is the same regardless of direction. Thus M1→S1 and S1→M1 were combined into a "cross connection" group for comparison to intra-areal connections in M1 and S1. Values in the text are represented as median (IQR).

Comparison of EP and coherence connectivity

Spearman correlation coefficients and significance were calculated between EP strength and coherence magnitude in each frequency band with Bonferroni correction for multiple comparisons. Reciprocal EP connections have been shown to have a stronger LFP correlation (Keller et al., 2014), which we examined as well. Coherence between sites was separated based on whether a reciprocal EP existed between those sites or not. Median coherence in each band was calculated for these two groups and a Wilcoxon rank sum test with Bonferroni correction was used to test significance between reciprocal and unidirectional EP connections across frequency bands. Values in the text are represented as median (IQR).

2.3 **Results**

Sensorimotor connectivity was evaluated in three monkeys implanted with meso-scale dual electrode grids (see Methods). Data captured a reduced time span in each animal spanning roughly 1-2 months. Evidence from ongoing experiments suggests that these data are stable over a longer time period (at least 1 year), and thus, characterizing changes over time was beyond the scope of this analysis. Various connectivity metrics obtained from electrically stimulated EPs combined with coherence in spontaneous, continuous LFPs showed common connectivity patterns as well as highlighted clear differences. Metrics quantified from EPs were asymmetrical and included: 1) presence of EP between a stimulated site and recording sites (binary), 2)

strength of EP connection, 3) peak latency of EP, 4) number of phases in the EP, 5) in-degree, out-degree, and information flow, and 6) reciprocal connections. Spontaneous LFPs was analyzed in the frequency domain, quantifying the symmetrical coherence between recording sites in canonical frequency bands theta (4-8 Hz), alpha (8-12 Hz), beta (12-30 Hz), gamma (30-58 Hz), and high gamma (62-150 Hz). Similar to studies conducted in humans (Bickel et al., 2011; Keller et al., 2014), many of these metrics correlated with inter-electrode distance, however, regional differences between intra-areal M1and S1 connections and those that cross the CS were also found.

2.3.1 **Sensorimotor connectivity assessed via stimulus-evoked potentials**

Three monkeys, O, Q, and U were implanted with bilateral recording grids straddling the CS (Figure 2.1). Electrical stimulation ramps (see Methods) were delivered to a single electrode site while EPs were recorded at all other sites. An example from monkey U is shown in Figure 2.2 in which site L08 was stimulated (Figure 2.2a) while all other sites on both the ipsilateral (left) and contralateral (right) hemisphere were recorded. Many ipsilateral sites showed EPs in response to stimulation ramps, though not all. We also observed contralateral EPs at site R06. Several metrics were extracted from the EPs including peak-trough amplitude, peak latency, and number of response phases using a peak-finding algorithm (see Methods). Figure 2.2c shows the results of this algorithm in four example sites in which an EP was produced. Greyscale diamonds denote any peak or trough that was detected based on global and local thresholds. The red circles denote the largest peak and trough which were used to calculate the EP amplitude (peak-trough). The total number of peaks and troughs was counted as the number of phases for a particular EP produced at a particular current. For instance, the EP at site L03 evoked by the largest current (lightest grey) has 5 phases. Peak latency was measured as the time from stimulus onset to the

peak of the first phase of the EP. Site L03 also highlights the robustness of the algorithm to detect when new features appeared in the EP, as the second positive peak at ~10 ms only surpasses the local threshold for the two largest stimulus currents. The contralateral response at R06 also showcases the algorithm's resistance to noisy recordings. The peak-trough amplitude as a function of stimulus current is shown in Figure 2.2d. The slope of this stimulus-response curve is used as a proxy for connection strength throughout the rest of the text (see Methods)(Hess et al., 1996).

The procedure detailed above was conducted for all sites in the grid for all 3 monkeys to produce an EP connection matrix (Figure 2.5) where each row shows the outputs of a particular site and each column shows the inputs. These matrices highlight the connection strength between all combinations of sites, which ranged over several orders of magnitude (0.0185 – 7.97 μV/μA). EP strength followed a lognormal distribution (Figure 2.4)(Markov et al., 2014) and thus is shown on a log color scale. All 3 animals showed wide-spread EP connectivity including transcallosal projections in monkey U. Connectedness of the network (number of EP connections measured ÷ total number of possible connections) was ~40% for ipsilateral connections (monkey O: 137/420 (32.6%); monkey Q: 137/312 (43.9%); monkey U: 161/420 (38.3%)) and 8% for contralateral connections (monkey U: 36/500).

The connection matrices summarize all EP connections but the true spatial pattern is lost as adjacent matrix entries are not necessarily adjacent recording electrodes. Figure 2.6 showcases an example spatial output map from each nominal recording position sampled across all monkeys. A few qualitative features stand out from this representation. First, while many of the strongest connections (warm colors) are seen in close proximity to the stimulating site (open symbol), such as in positions 4 or 12, there are also examples of strong, distant connections such

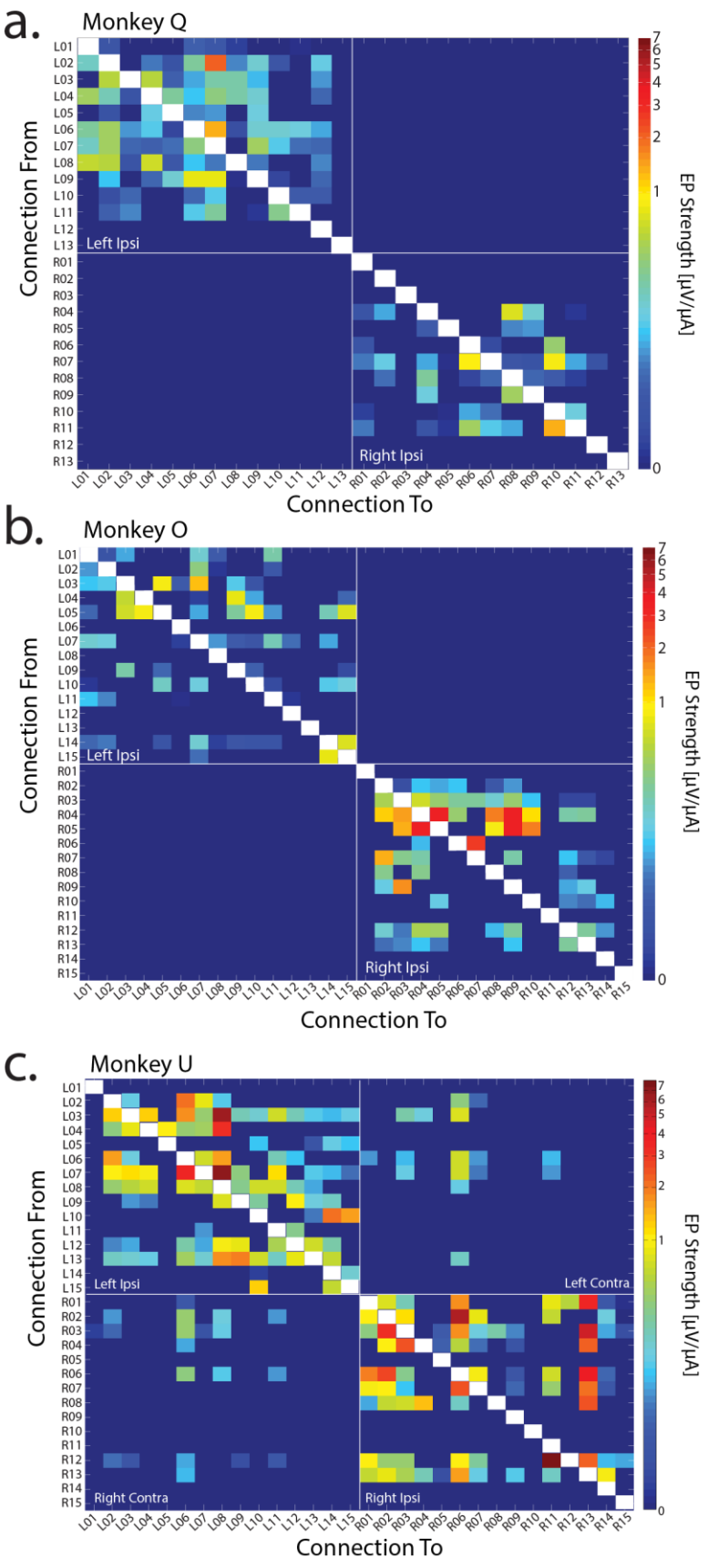

Figure 2.5 EP strength connection matrix.
a – **c**) Connection matrix for each animal in which the ordinate represents the site being stimulated and the abscissa all sites being recorded from. Thus, rows represent strength of an EP output and columns represent strength of an EP input. Contralateral EP connections were measured only in monkey U (**c**). EP strength is shown on a log color scale.

as in positions 6 or 9. Second, one might assume that sites located at the edge of the grid would show fewer connections simply due to edge effects (Keller et al., 2014). Again positions 4 and 12, along with position 3 show fairly extensive projections even though they are edge electrodes. However, corner positions 11 and 15 highlight cases in which we were likely under-sampling connections outside of the recording grid. Third, a majority of the sites depicted show connections that cross the CS and for monkey U connections that cross midline, highlighting inter-regional connectivity. In the remainder of this section, these observations will be expanded upon in an attempt to quantify EP connectivity within sensorimotor cortex.

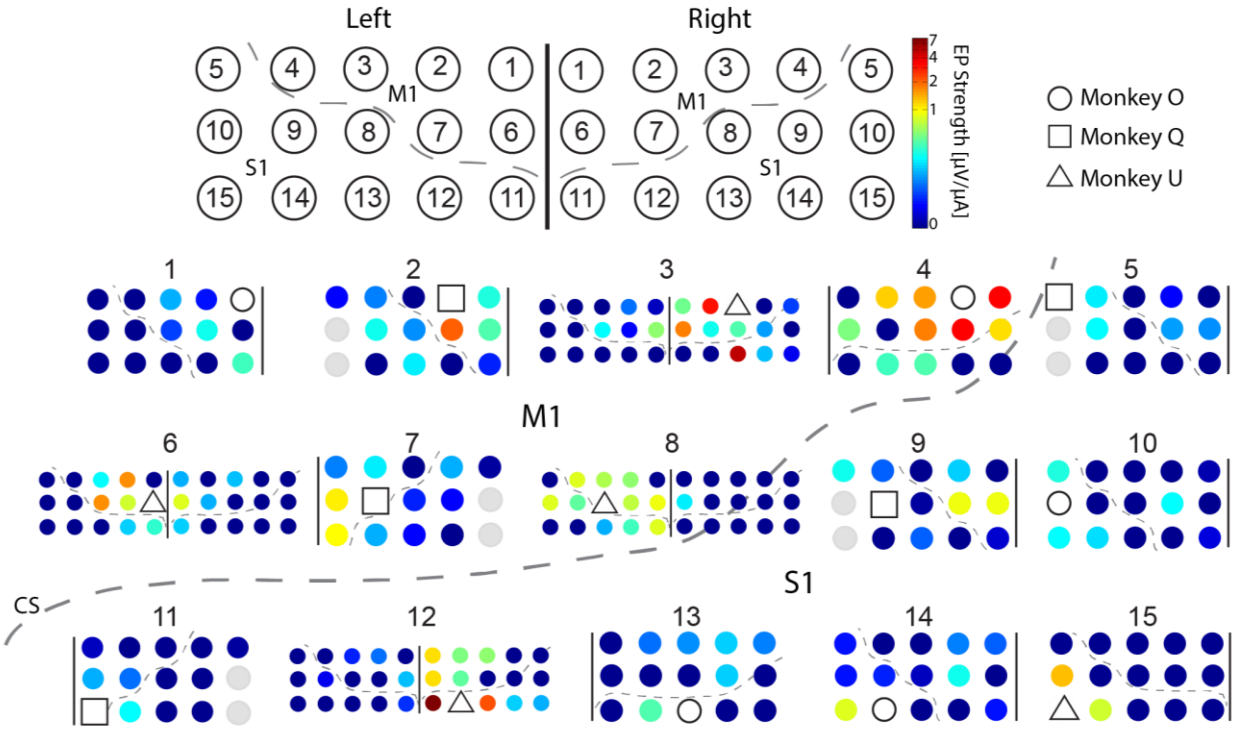

Figure 2.6 EP strength represented in true spatial arrangement.
The layout at the top shows each nominal position in the implant grid represented below by an example EP-projection map from a particular animal represented by the shape of the open symbol. In each EP-projection map, the solid line indicates midline and thus which hemisphere is represented, while the open symbols indicate the site being stimulated. Colored circles show the EP strength represented on a log scale. Five example sites are shown for each animal with at least one from each hemisphere as well as pre- and post-central sulcus. The dotted grey lines designate the CS. Only monkey U had bilateral recordings. Grey site positions in monkey Q were not implanted.

Inter-electrode distance captures some, but not all EP connectivity patterns

The Euclidian distance between the stimulating and recording sites is a considerable factor underlying connectivity. Five metrics of EP connectivity were quantified as a function of distance from the stimulation site: 1) probability of observing an EP, 2) probability of a reciprocal connection, 3) strength of the connection, 4) peak latency, and 5) number of phases in the response. The probability of observing an EP at distal sites was significantly lower than at proximal sites across all 3 animals (Figure 2.7). Ipsilateral connections in monkey U showed the

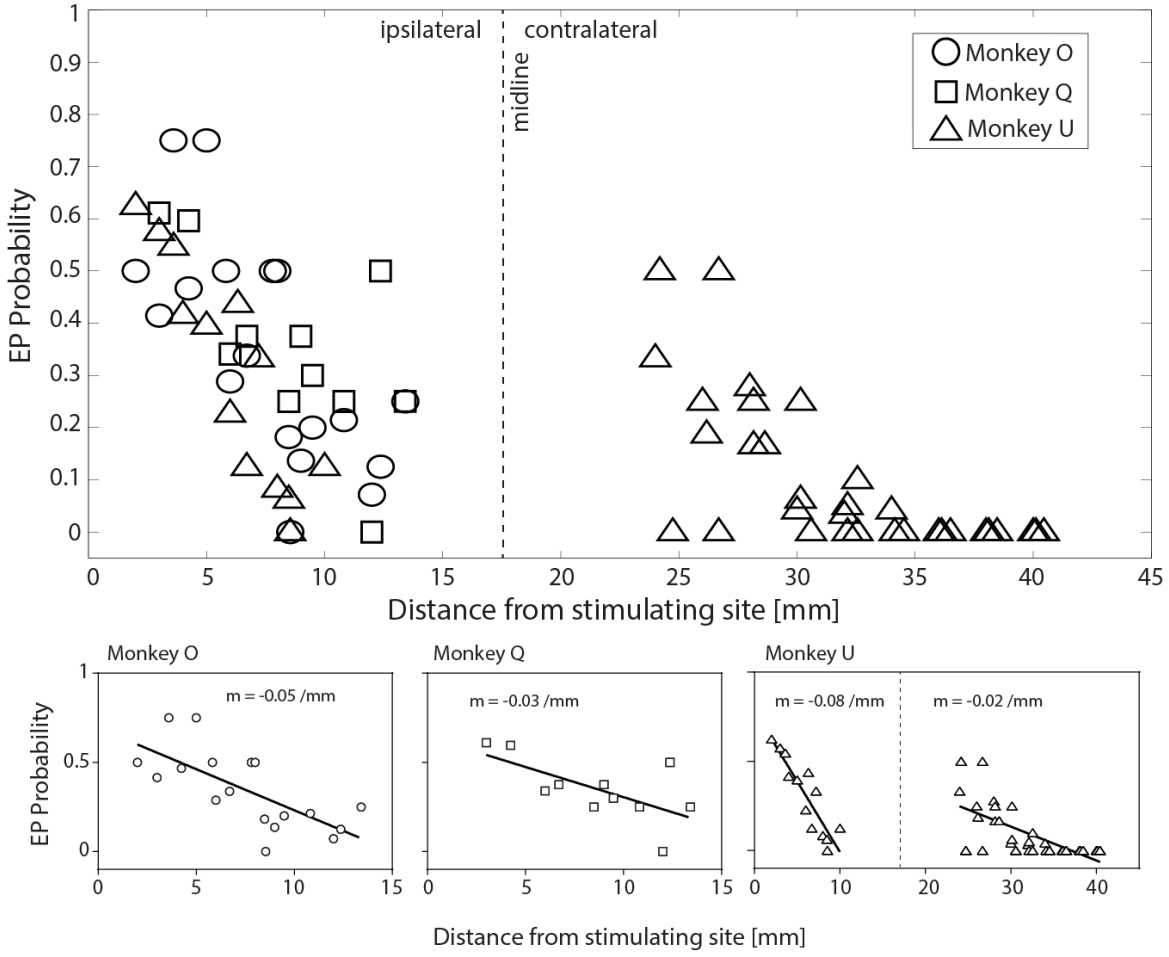

Figure 2.7 EP probability as a function of inter-electrode distance.
Top: Probability of an EP at each unique distance from the stimulating electrode across all 3 animals. *Bottom*: Probability of an EP as a function of distance for each animal individually fitted with a linear regression. Vertical dotted line shows the approximate location of midline.

steepest drop-off with a slope of -0.08/mm (R^2 = 0.81, p <0.0001), while contralateral connections showed a more gradual and bimodal decline with distance (m = -0.02/mm, R^2 = 0.45, p <0.001). EP probability in monkey O (m = -0.05/mm, R^2 = 0.49, p <0.01) and monkey Q (m = -0.03/mm, R^2 = 0.43, p <0.05) also showed a significant inverse relationship with inter-electrode distance.

The probability of reciprocal connections as a function of inter-electrode distance showed a very similar pattern to the probability of observing an EP at all (Figure 2.8). Again ipsilateral connections in monkey U showed the sharpest decline in reciprocity with distance (m = -0.06/mm, R^2 = 0.77, p < 0.0001) compared to contralateral connections (m = -0.007/mm, R^2 =

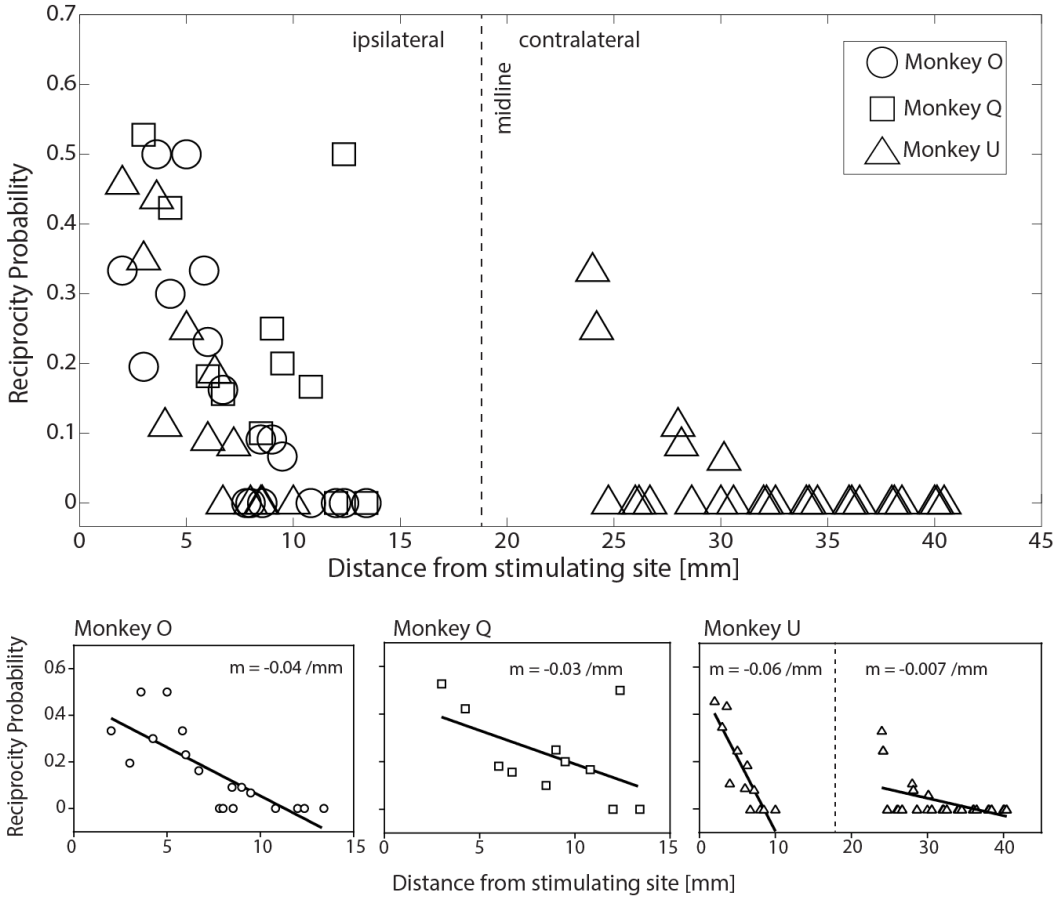

Figure 2.8 Probability of reciprocal EP as a function of inter-electrode distance.
Top: Probability of reciprocal EP connection at each unique distance from the stimulating electrode across all 3 animals. *Bottom*: Probability of reciprocal EP connection as a function of distance for each animal individually fitted with a linear regression. Vertical dotted line shows the approximate location of midline.

0.26, $p < 0.001$). However, only 6/30 sites (20%) showed reciprocal transcallosal connections compared to 22/30 sites (73%) which showed reciprocal ipsilateral connections. The probability of reciprocal connections in monkey O also significantly declined with inter-electrode distance (m = -0.04/mm, $R^2 = 0.63$, $p < 0.0001$) and showed a similar incidence of reciprocity (21/30 sites, 70%). Monkey Q showed an inverse relationship between reciprocity and inter-electrode distance (m = -0.03, $R^2 = 0.27$), but this was not significant ($p = 0.1$). Monkey Q did show a similar proportion of reciprocal sites (19/26, 73%) to the other two animals. The rate of reciprocity for an individual site covered a wide range compared to the rather consistent 70% reciprocity over the whole network for both ipsilateral (monkey O: 6-46%; monkey Q: 8-77%; monkey U: 6-50%) and contralateral (monkey U: 6-20%) sites.

The strength of EP connections showed an inverse exponential relationship with inter-electrode distance (Figure 2.9). The space constant for all three monkeys was ~3 mm (monkey O: 3.5 mm; monkey Q: 3.3 mm; monkey U: 2.7 mm), which was also the spacing of the implant (see Methods). Conversely, the peak latency to the first EP phase showed an increasing trend with distance from the stimulating electrode (Figure 2.11), but the slope of a linear regression was indistinguishable from zero in monkey O (m = 0.16, $R^2 = 0.02$, $p = 0.09$), monkey Q (m = 0.12, $R^2 = 0.01$, $p = 0.26$), and contralateral connections in monkey U (m = -0.001, $R^2 = 2x10^{-6}$, $p = 1.0$). The peak latency of ipsilateral connections in monkey U did show a significant relationship with inter-electrode distance (m = 0.38, $R^2 = 0.07$, $p < 0.001$).

Lastly, many EPs showed multiple phases (Figure 2.2b, c) which likely represent mono and polysynaptic connections. However, for ipsilateral connections across all animals we saw a rather homogenous distribution of phase number with distance from the stimulating electrode

(monkey O: m = 0.03 phases/mm, R^2 = 0.004, p = 0.5; monkey Q: m = -0.08 phases/mm, R^2 = 0.03, p = 0.06; monkey U: m = -0.05 phases/mm, R^2 = 0.004, p = 0.4; Figure 2.10). There was one exception for contralateral connections in monkey U which showed that the number of phases actually increased with distance (m = 0.15 phases/mm, R^2 = 0.11, $p < 0.05$).

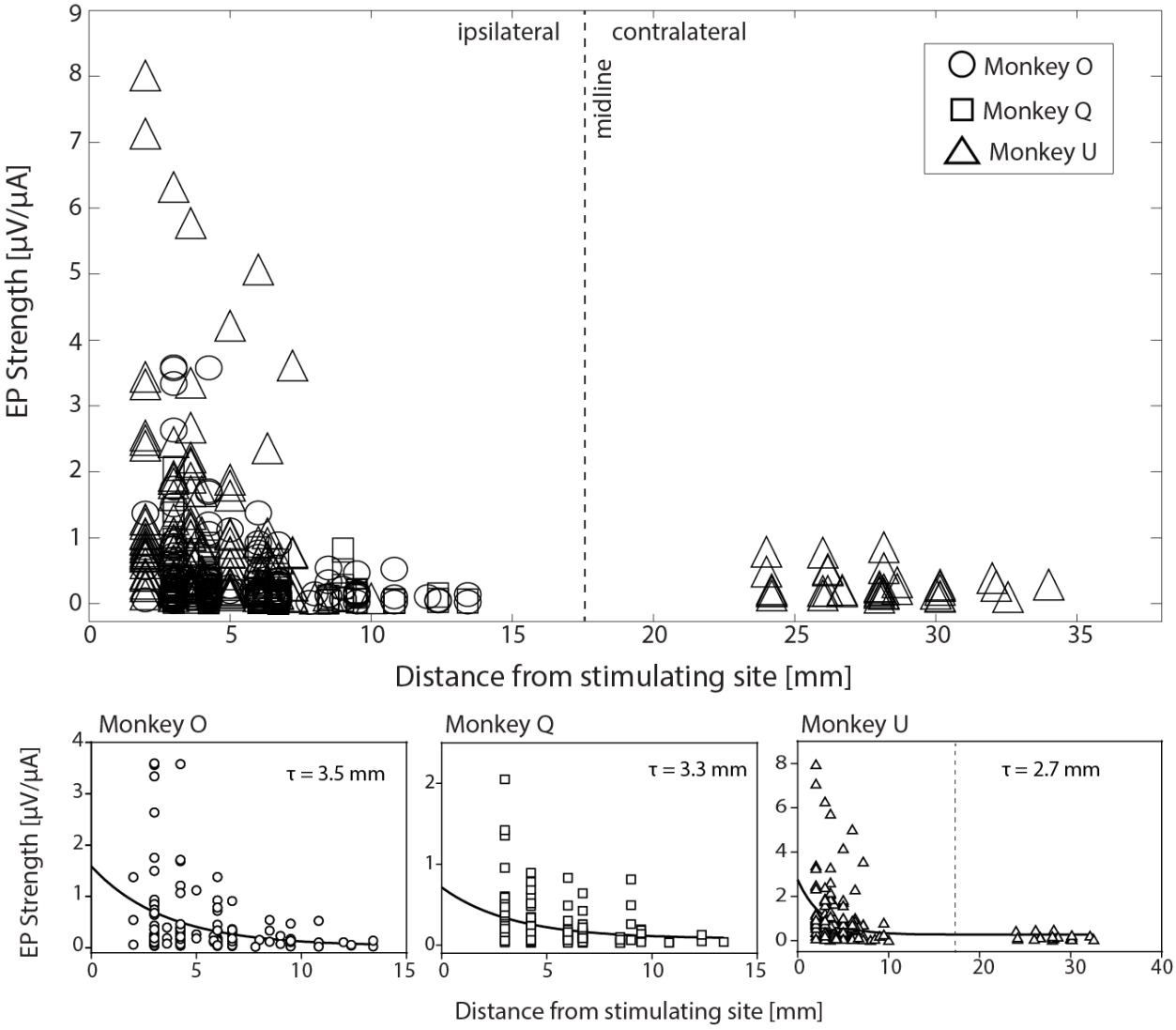

Figure 2.9 Strength of EP response as a function of inter-electrode distance.
Top: Strength of EP response at each unique distance from the stimulating electrode across all 3 animals. *Bottom*: Strength of EP response as a function of distance for each animal individually fitted with a one-phase decaying exponential. Vertical dotted line shows the approximate location of midline.

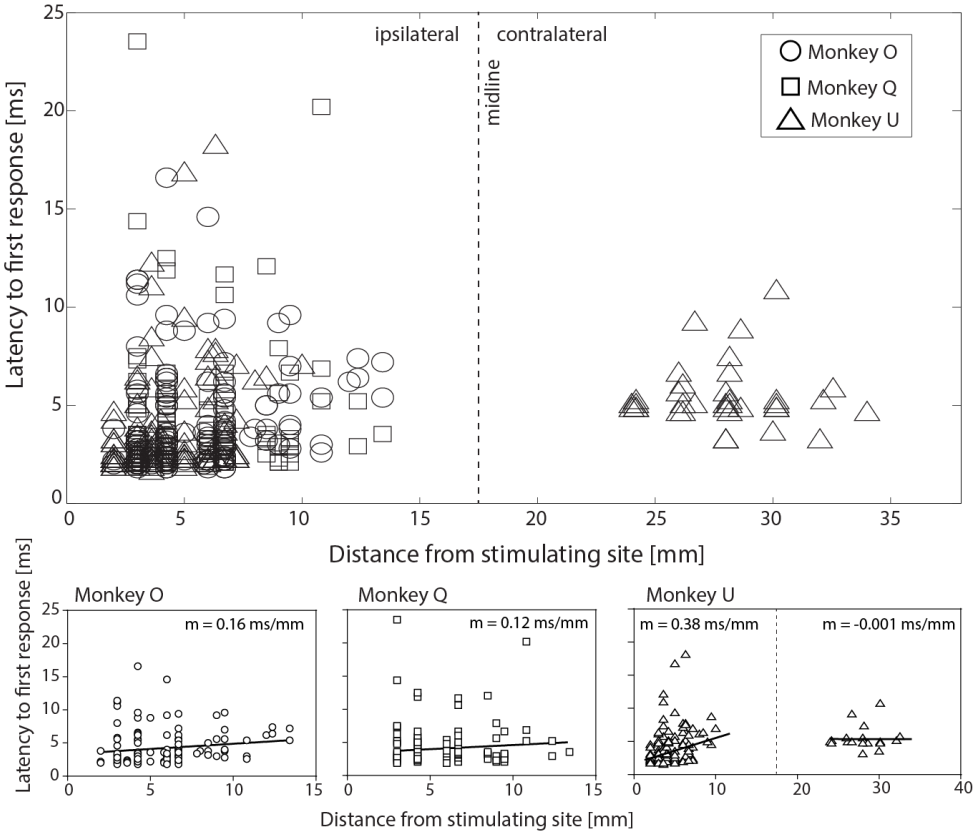

Figure 2.11 EP peak latency as a function of inter-electrode distance. *Top*: EP peak latency at each unique distance from the stimulating electrode across all 3 animals. *Bottom*: EP peak latency as a function of distance for each animal individually fitted with a linear regression. Vertical dotted line shows the approximate location of midline.

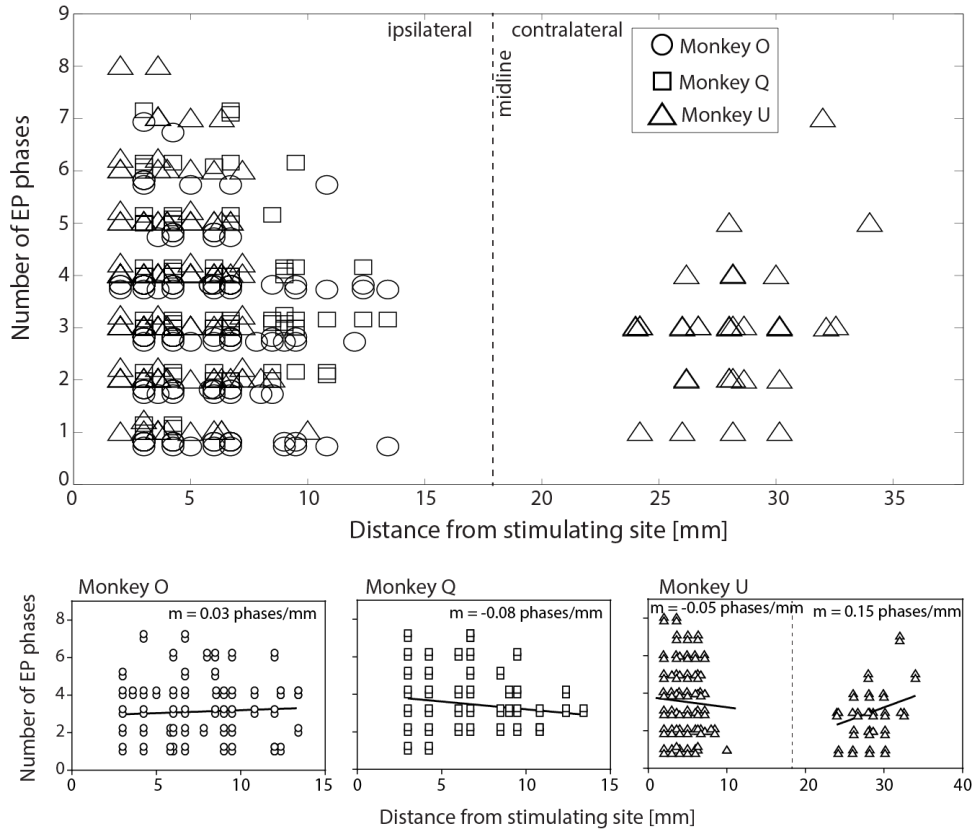

Figure 2.10 Number of EP phases as a function of inter-electrode distance. *Top*: Number of EP phases at each unique distance from the stimulating electrode across all 3 animals. *Bottom*: Number of EP phases as a function of distance for each animal individually fitted with a linear regression. Overlapping points were shifted in the vertical dimension; number of phases is expressed as a whole number. Vertical dotted line shows the approximate location of midline.

Information flow of EP connections

If inter-electrode distance were the only factor driving connectivity we would expect to see a high out-degree at the center of the recording grid that dissipates radially towards the edges. However, across all three monkeys we see a homogenous distribution of ipsilateral out-degree magnitudes with some of the highest projection sites on the edges and corners (Figure 2.12a). The same cannot be said for transcallosal projections (Figure 2.13a). Sites with the highest number of contralateral projections were located more medially, and no sites on the most lateral extent of the grid made transcallosal connections. In-degree showed a similar level of

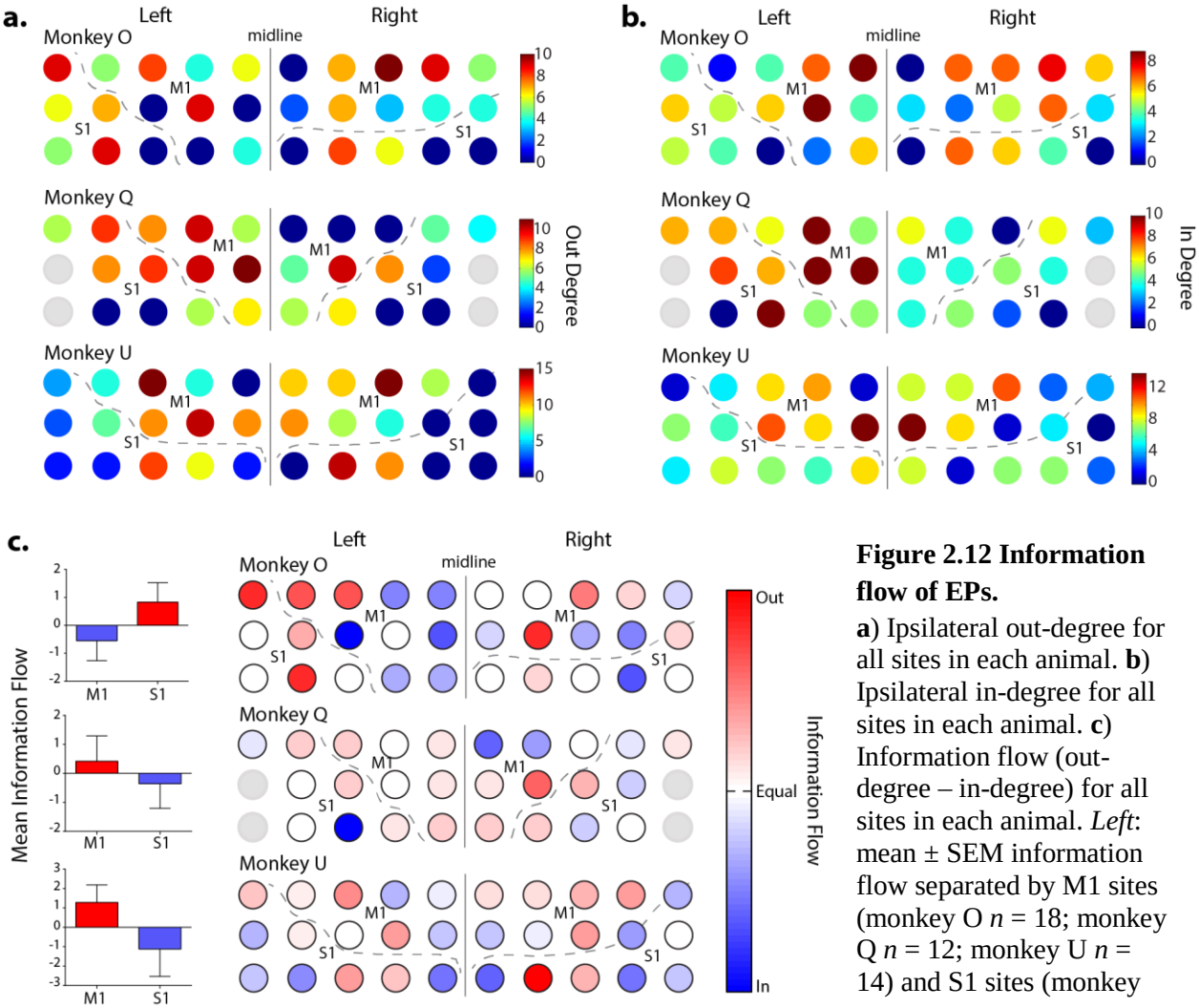

Figure 2.12 Information flow of EPs.
a) Ipsilateral out-degree for all sites in each animal. **b**) Ipsilateral in-degree for all sites in each animal. **c**) Information flow (out-degree – in-degree) for all sites in each animal. *Left*: mean ± SEM information flow separated by M1 sites (monkey O n = 18; monkey Q n = 12; monkey U n = 14) and S1 sites (monkey O n = 12; monkey Q n = 18; monkey U n = 16). A two-sample t-test showed no significant difference between M1 and S1. Grey sites in monkey Q were not implanted; grey dotted line designates CS.

homogeneity as out-degree (Figure 2.12b). One possible exception may be monkey U whose in-degree is qualitatively symmetric around the midline sites L06 and R06 (Figure 2.1b). Transcallosal inputs in monkey U also displayed this trend with the majority of contralateral inputs arriving to L06 or R06 (Figure 2.13b), suggesting that these two sites may be both local and hemispheric receiver nodes.

To assess whether a site was predominately a projector, having a high out-degree, or a receiver, having a high in-degree, the metric termed information flow was quantified as the difference between out-degree and in-degree. Figure 2.12c highlights the fact that many sites showed an equal amount of information flow in and out (white and pale colors), and in fact over all 86 sites recorded in the three animals there was no difference between out-degree (mean ± sem: 5.48 ± 0.46) and in-degree (mean ± sem: 5.48 ±0.35) (paired *t*-test, $p = 1$). However, there were a few sites in each animal which showed more outward or inward tendencies (more saturated colors). There does not seem to be a systematic pattern to these nodes with regard to whether they were an M1 or S1 site (Figure 2.12c, left panels), or whether they were a central or edge site. Thus, it is hard to draw firm conclusions about the role of these sites in the network; it is equally possible that they are true information hubs or the byproduct of our implant placement.

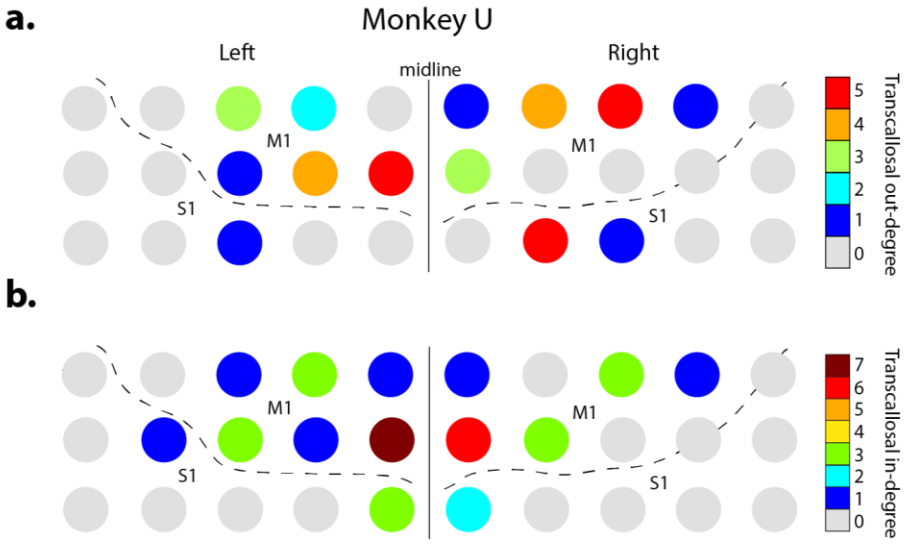

Figure 2.13 Contralateral EP connections. **a**) Number of contralateral outputs for each site. **b**) Number of contralateral inputs for each site. Data from monkey U; grey dotted line designates CS.

Connection patterns across the central sulcus

We recorded EPs from many sites showing projections across the CS (Figure 2.6). Across all three animals 62.8% (54/86) of recording sites had at least one output that crossed the CS. Between animals however, there was large variability in the patterns of sulcus crossing (Figure 2.14). Monkey O was the only animal to show a significant difference in cross-sulcus probability (see Methods) between sites originating in M1 or S1 (Figure 2.14a); S1 sites were significantly more likely to send projections to M1 than vice versa ($p < 0.001$). Monkeys Q ($p = 0.64$) and U ($p = 0.96$) showed no difference in ipsilateral cross-sulcus probability between M1 and S1 sites

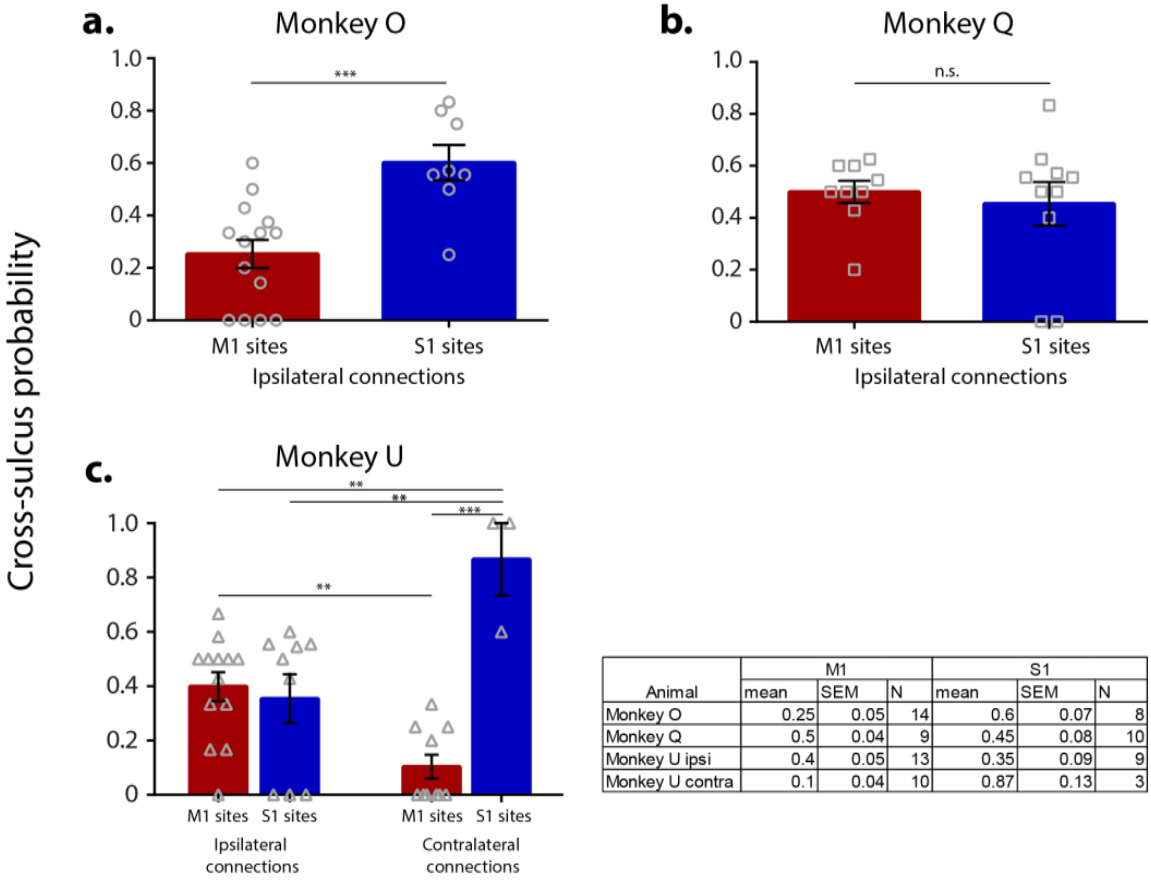

Animal	M1 mean	M1 SEM	M1 N	S1 mean	S1 SEM	S1 N
Monkey O	0.25	0.05	14	0.6	0.07	8
Monkey Q	0.5	0.04	9	0.45	0.08	10
Monkey U ipsi	0.4	0.05	13	0.35	0.09	9
Monkey U contra	0.1	0.04	10	0.87	0.13	3

Figure 2.14 Cross-sulcus EP probability.
a – **c**) Probability that an M1 or S1 site produced an EP which crossed the central sulcus. Colored bars show mean ± SEM while open grey symbols show individual sites. For **a** and **b** only ipsilateral connections are shown and a two-sample *t*-test used to test significance between M1 and S1 sites. For **c** ipsilateral and conralateral sites were separated and a one-way ANOVA used to test significance between groups. Table with full statistics in bottom right panel.

(Figure 2.14b, c; see figure table for full statistics). In monkey U we could also investigate the propensity for transcallosal connections to cross the CS. While many more M1 sites had contralateral outputs than S1sites (Figure 2.13a), the few contralateral connections from S1 were more likely to project to contralateral M1 sites than S1 sites ($p < 0.0001$; Figure 2.14c).

While there was no clear pattern in the distribution of intra- or inter-areal EP connections, the strength of these connections showed a trend for stronger M1→M1 connections compared to M1→S1, S1→M1, and S1→S1 (Figure 2.15). Across all animals, ipsilateral M1→M1

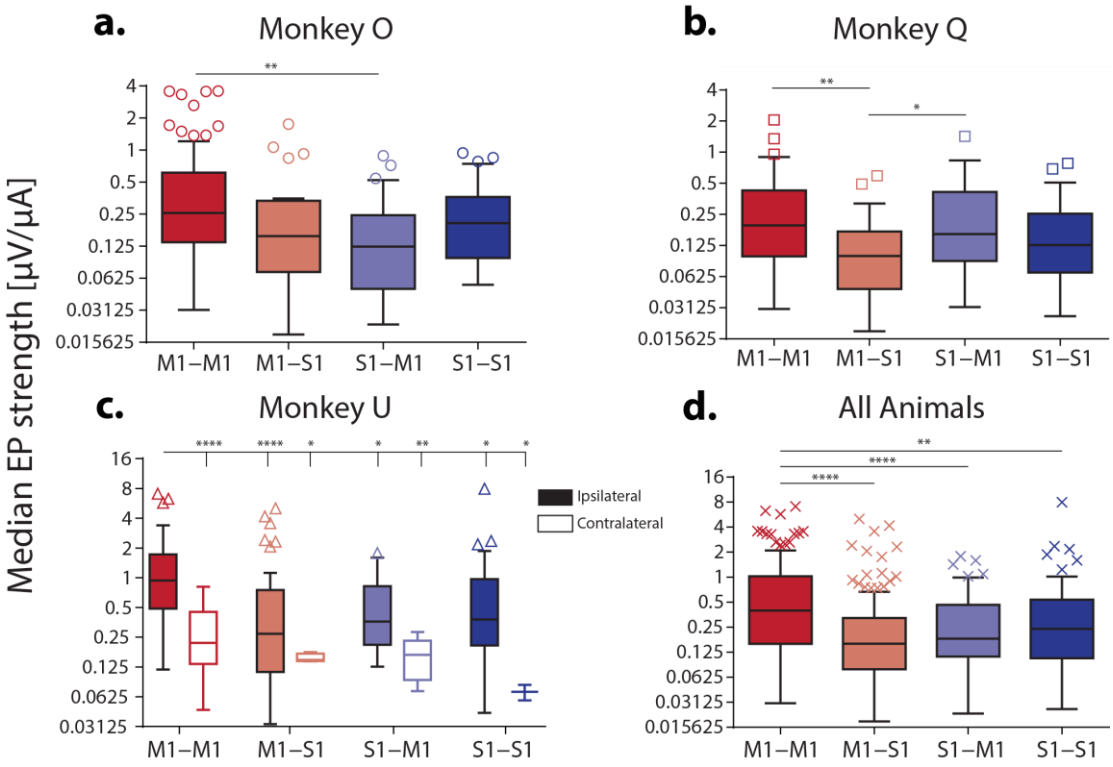

Animal	M1-M1			M1-S1			S1-M1			S1-S1		
	median	IQR	N	median	IQR	N	median	IQR	N	median	IQR	N
Monkey O	0.256	0.478	60	0.156	0.262	23	0.124	0.196	33	0.207	0.265	21
Monkey Q	0.196	0.329	35	0.099	0.123	38	0.162	0.324	33	0.127	0.186	31
Monkey U ipsi	0.937	1.238	56	0.272	0.64	45	0.362	0.611	26	0.379	0.759	33
Monkey U contra	0.219	0.317	25	0.148	0.027	4	0.166	0.138	5	0.07	0.025	2
All	0.397	0.872	152	0.159	0.245	106	0.182	0.355	92	0.239	0.433	85

Figure 2.15 EP strength separated by connection type.
a – **d**) Median EP strength separated for M1→M1, M1→S1, S1→M1, and S1→S1 connections. Box and whisker plotted on log scale with Tukey's method (upper and lower whiskers 75th and 25th percentiles plus 1.5xIQR). Solid filled plots indicate ipsilateral connections and open plots contralateral. For **a**, **b**, and **d** significance between connection types assessed with one-way ANOVA, and for **c** a two-way ANOVA on log-transformed data. Table with full statistics at the bottom.

connections were significantly stronger than all other connection types (M1-M1: 0.397(0.872); M1-S1: 0.159(0.245); S1-M1: 0.82(0.355); S1-S1: 0.239(0.433); $p < 0.0001$; Figure 2.15d). In all three animals, M1→M1 projections trended towards being the strongest connections even if not statistically significant than all other areal connection types (Figure 2.15a – c, see table for full statistics). Similarly for contralateral connections measured in monkey U, though none of the connection types were significantly different from one another, M1 to contralateral M1 connections showed the highest EP strength (Figure 2.15c, open box-plots).

Stimulus-evoked cortico-cortical EPs show extensive connections throughout sensorimotor cortex of primates both ipsilaterally and contralaterally. While inter-site distance is a large contributor to the patterns and strength of connectivity, there are clear examples of long-range projections that may serve as intra- and inter-areal hubs for the flow of information.

2.3.2 **Sensorimotor connectivity assessed via band-limited, spontaneous coherence**

During our recording sessions, 10-30 minutes of spontaneous LFPs was recorded while the monkey sat quietly or was engaged in a behavioral task (see Methods). Full spectrum coherence, up to 150 Hz, was calculated as a way to assess the synchrony of cortical activity and thus connectivity. While a majority of the spectrum showed low, insignificant (see Methods) coherence, there were also clear peaks in particular frequency bands (Figure 2.3). Figure 2.16, Figure 2.17, and Figure 2.18 show the raw frequency spectrum for each hemisphere (and interhemispheric where appropriate) as a matrix and heat map with unique connections on the ordinate and frequency on the abscissa. The heat maps show higher coherence in lower frequencies across many connections with some sparse coherence in the higher frequencies. In particular, all 3 monkeys showed a faint band of coherence between 10 – 30 Hz in ipsilateral

connections while contralateral connections mostly showed high coherence in frequencies less than 10 Hz.

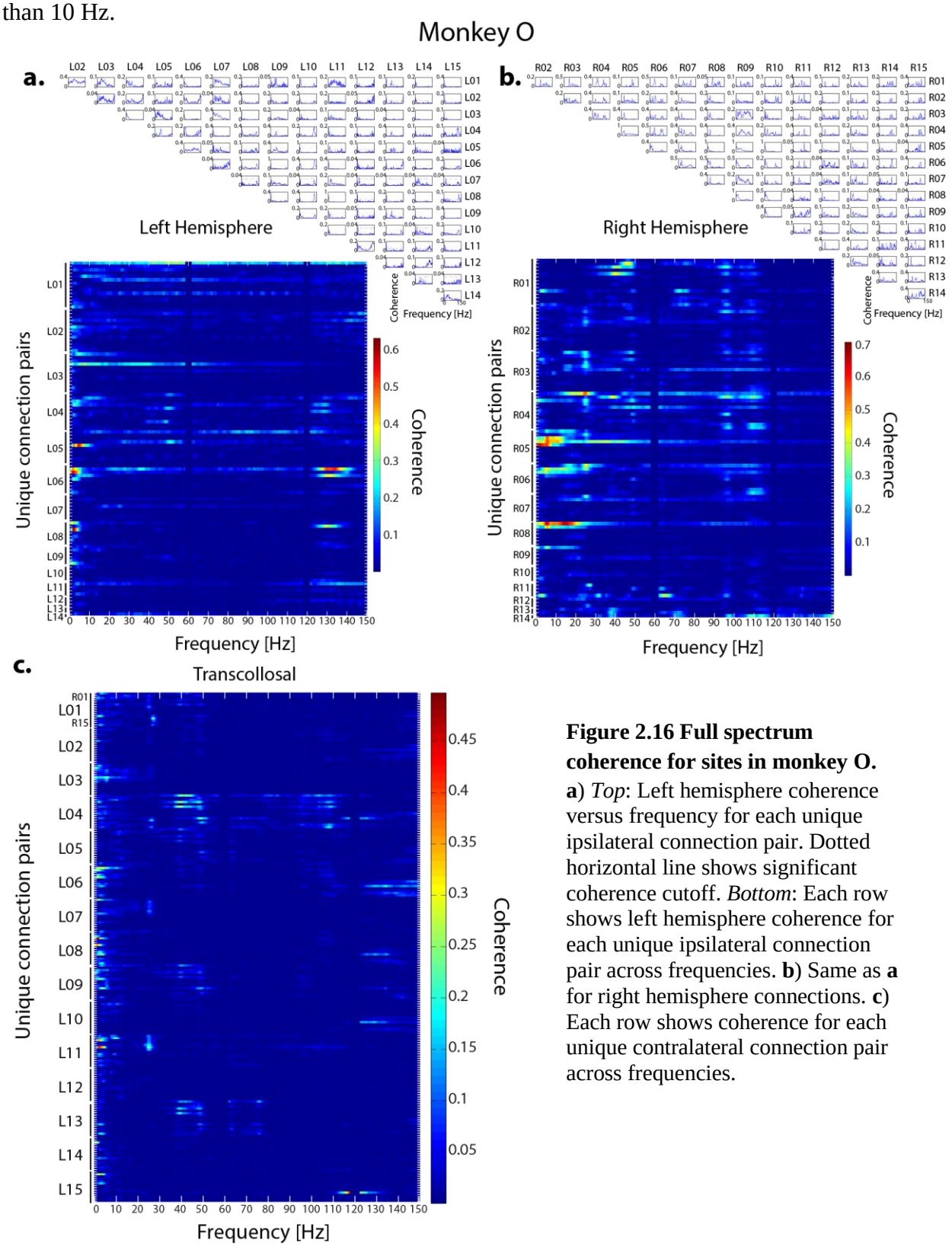

Figure 2.16 Full spectrum coherence for sites in monkey O. **a**) *Top*: Left hemisphere coherence versus frequency for each unique ipsilateral connection pair. Dotted horizontal line shows significant coherence cutoff. *Bottom*: Each row shows left hemisphere coherence for each unique ipsilateral connection pair across frequencies. **b**) Same as **a** for right hemisphere connections. **c**) Each row shows coherence for each unique contralateral connection pair across frequencies.

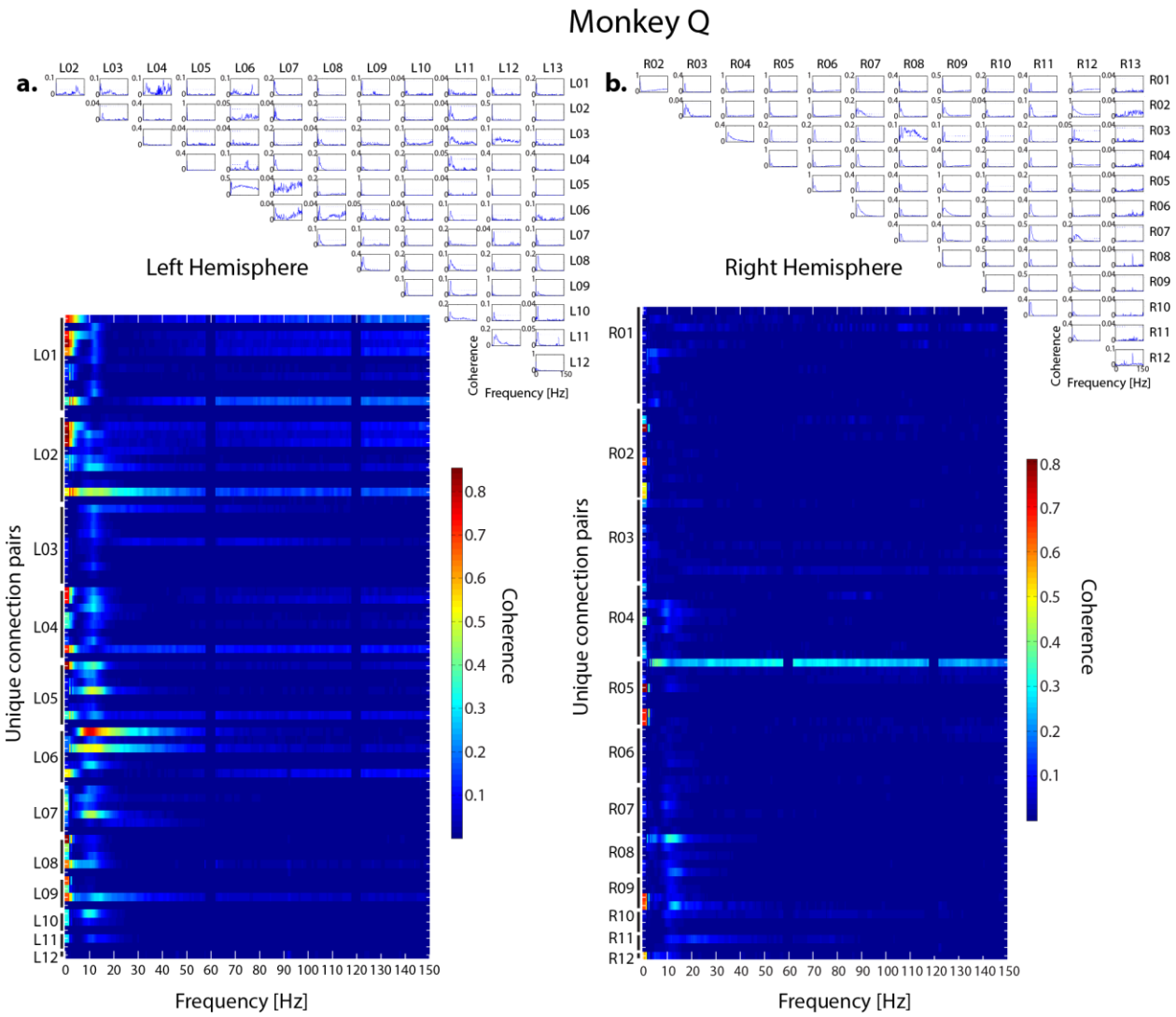

Figure 2.17 Full spectrum coherence for sites in monkey Q.
Top: Left hemisphere coherence versus frequency for each unique ipsilateral connection pair. Dotted horizontal line shows significant coherence cutoff. *Bottom*: Each row shows left hemisphere coherence for each unique ipsilateral connection pair across frequencies. **b**) Same as **a** for right hemisphere connections.

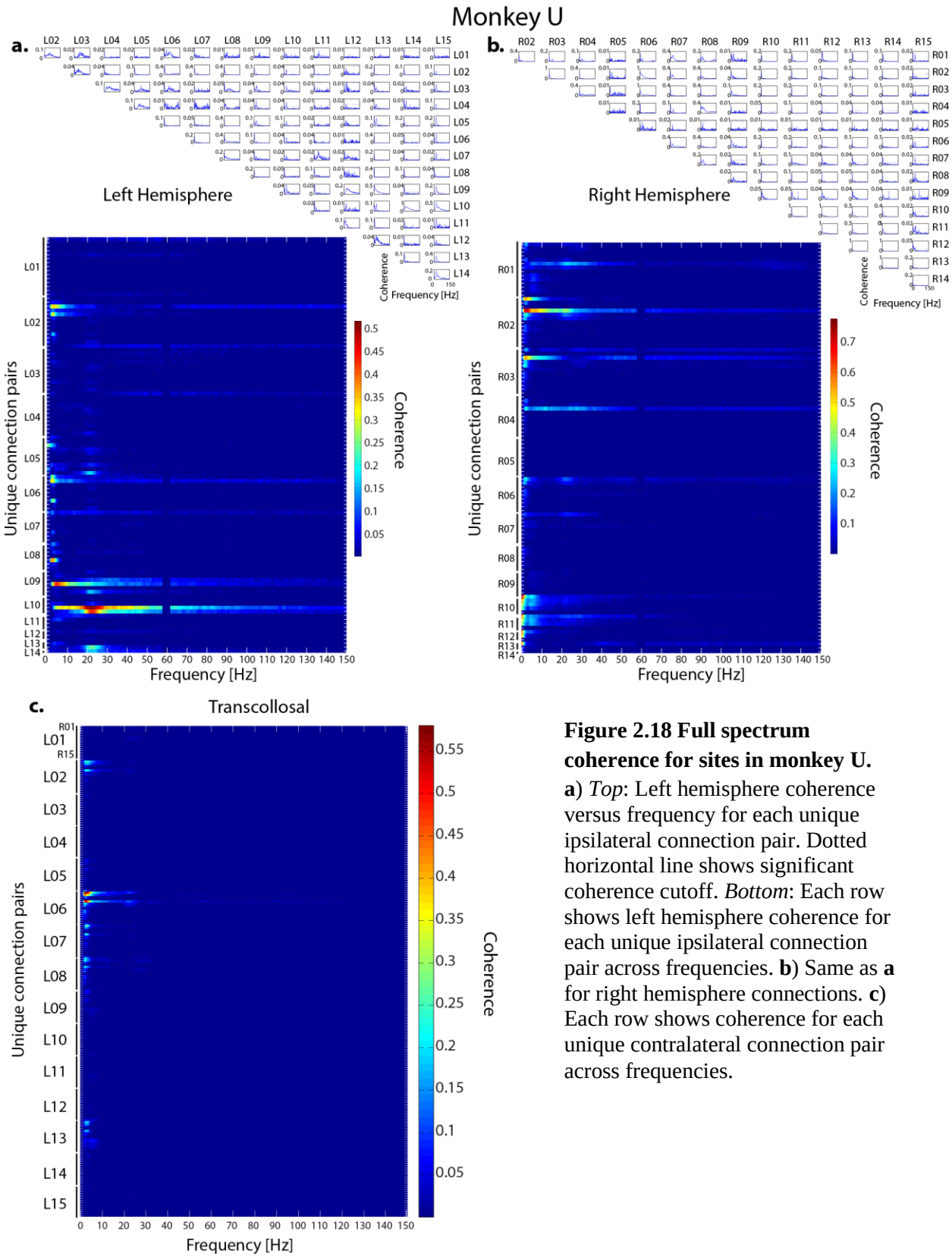

Figure 2.18 Full spectrum coherence for sites in monkey U. **a**) *Top*: Left hemisphere coherence versus frequency for each unique ipsilateral connection pair. Dotted horizontal line shows significant coherence cutoff. *Bottom*: Each row shows left hemisphere coherence for each unique ipsilateral connection pair across frequencies. **b**) Same as **a** for right hemisphere connections. **c**) Each row shows coherence for each unique contralateral connection pair across frequencies.

Figure 2.19, Figure 2.20, and Figure 2.21show the mean coherence in each of five frequency bands, theta, alpha, beta, gamma, and high gamma (see Methods) as a symmetric connectivity matrix. For each animal a few gross patterns emerged. Monkey O (Figure 2.19) showed a cluster of sites in the right hemisphere for which coherence was high across all frequency bands, but more so in beta (Figure 2.19c). In addition, the alpha band had a sparse distribution of coherence (Figure 2.19b) but had the highest total coherence of all the bands (Figure 2.19f). Monkey O also displayed many transcallosal connections with significant coherence across bands; however, contralateral coherence was significantly lower than ipsilateral coherence for most frequency bands (Figure 2.19f). Similar to monkey O, monkey U showed clusters of sites with high coherence in multiple bands, in particular sites R10 through R14. Overall coherence across frequency bands in monkey U had the characteristic $1/f^x$ trend (Figure 2.21f), and a propensity for significant coherence to concentrate around the identity of the matrix. This suggests that coherence in higher frequencies has a smaller spatial spread as has been noted by others (Buzsáki and Draguhn, 2004). Again, ipsilateral coherence was significantly greater than contralateral coherence for a majority of frequency bands (Figure 2.21f). In monkey Q we were only able to evaluate ipsilateral coherence (Figure 2.20). Interestingly, while the coherence magnitude was low (Figure 2.20f), monkey Q showed a large spread of statistically significant coherence at the highest frequencies (Figure 2.20d, e). The total mean coherence across frequency bands in monkey Q also showed a $1/f^x$ trend (Figure 2.20f).

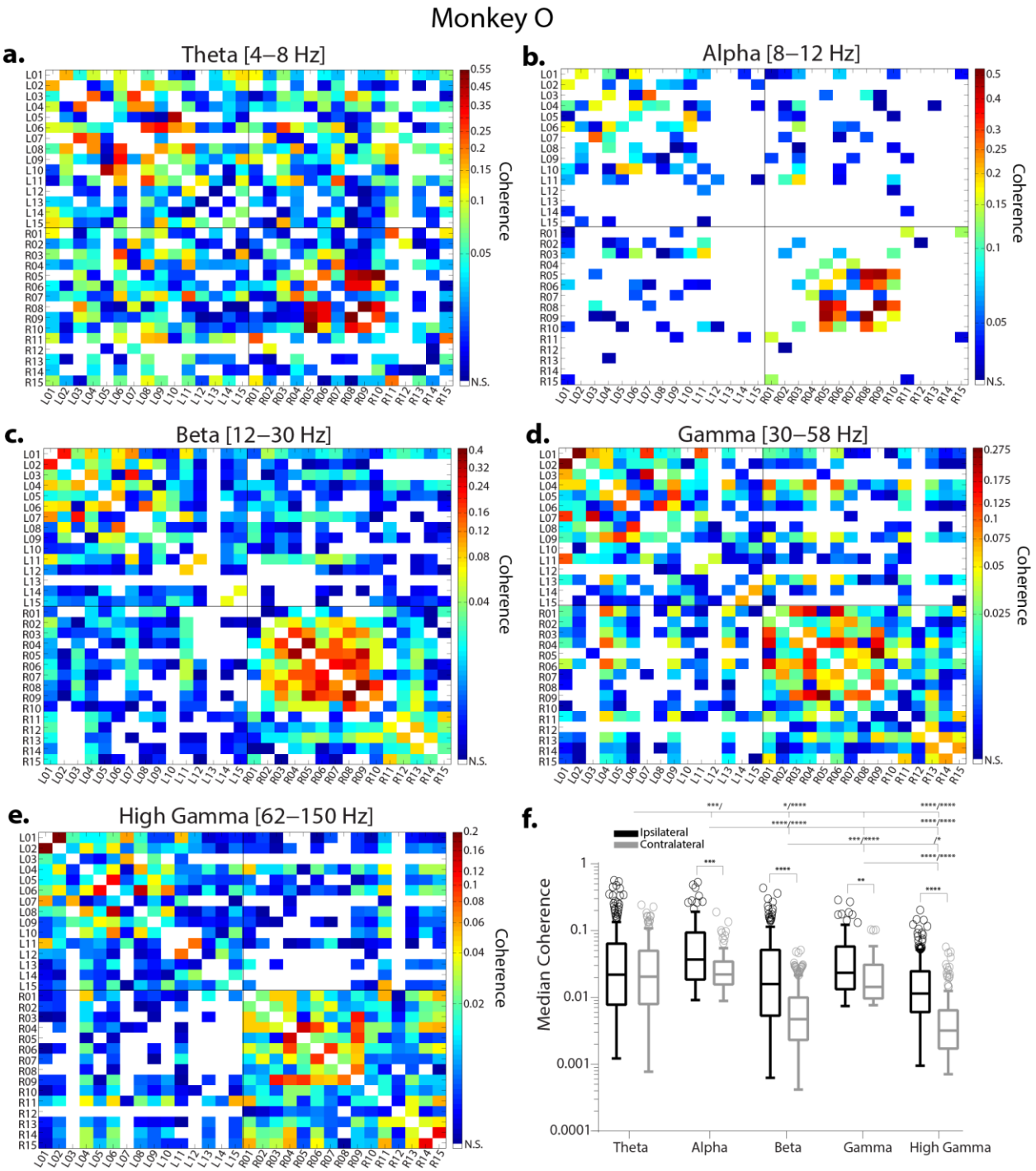

Figure 2.19 Band-limited coherence for monkey O.

a – **e**) Coherence connection matrix for five frequency bands shown on a log color scale. Columns and rows are symmetrical. Empty (white) entries did not reach significance cutoff based on permutation test. **f**) Median coherence in each frequency band for ipsilateral and contralateral connections. Box and whisker plotted on log scale with Tukey's method (upper and lower whiskers 75th and 25th percentiles plus 1.5xIQR). Within each frequency band, a Wilcoxon rank sum test assessed the difference between ipsilateral and contralateral connections. Across frequencies, a Kruskal-Wallis test assessed coherence differences for ipsilateral and conralateral connections separately (asterisks: ipsilateral/contralateral).

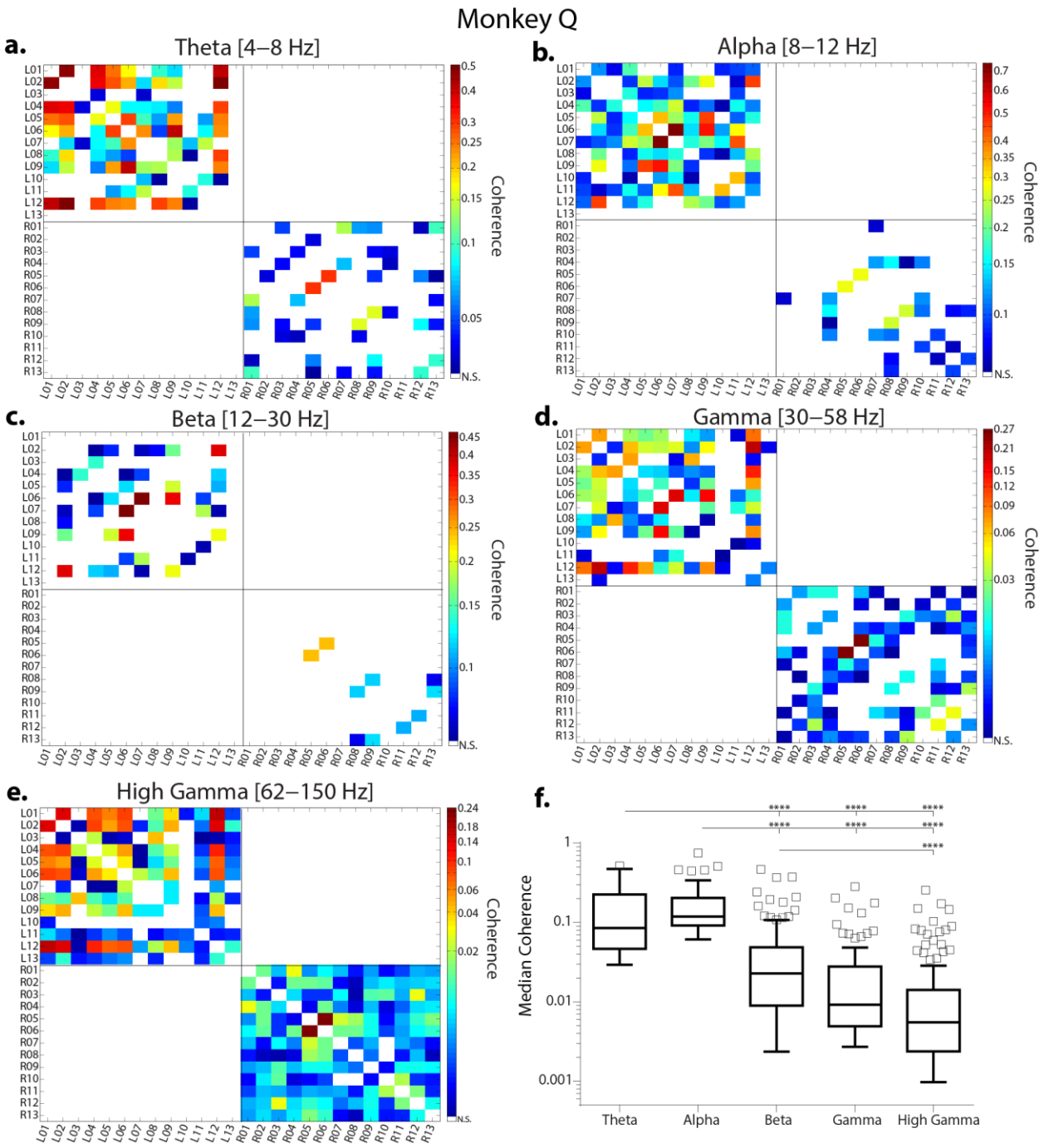

Figure 2.20 Band-limited coherence for monkey Q.

a – **e**) Coherence connection matrix for five frequency bands shown on a log color scale. Columns and rows are symmetrical. Empty (white) entries did not reach significance cutoff based on permutation test. Contralateral connections were not measured. **f**) Median coherence in each frequency band for ipsilateral connections. Box and whisker plotted on log scale with Tukey's method (upper and lower whiskers 75th and 25th percentiles plus 1.5xIQR). A Kruskal-Wallis test assessed significant coherence across frequencies.

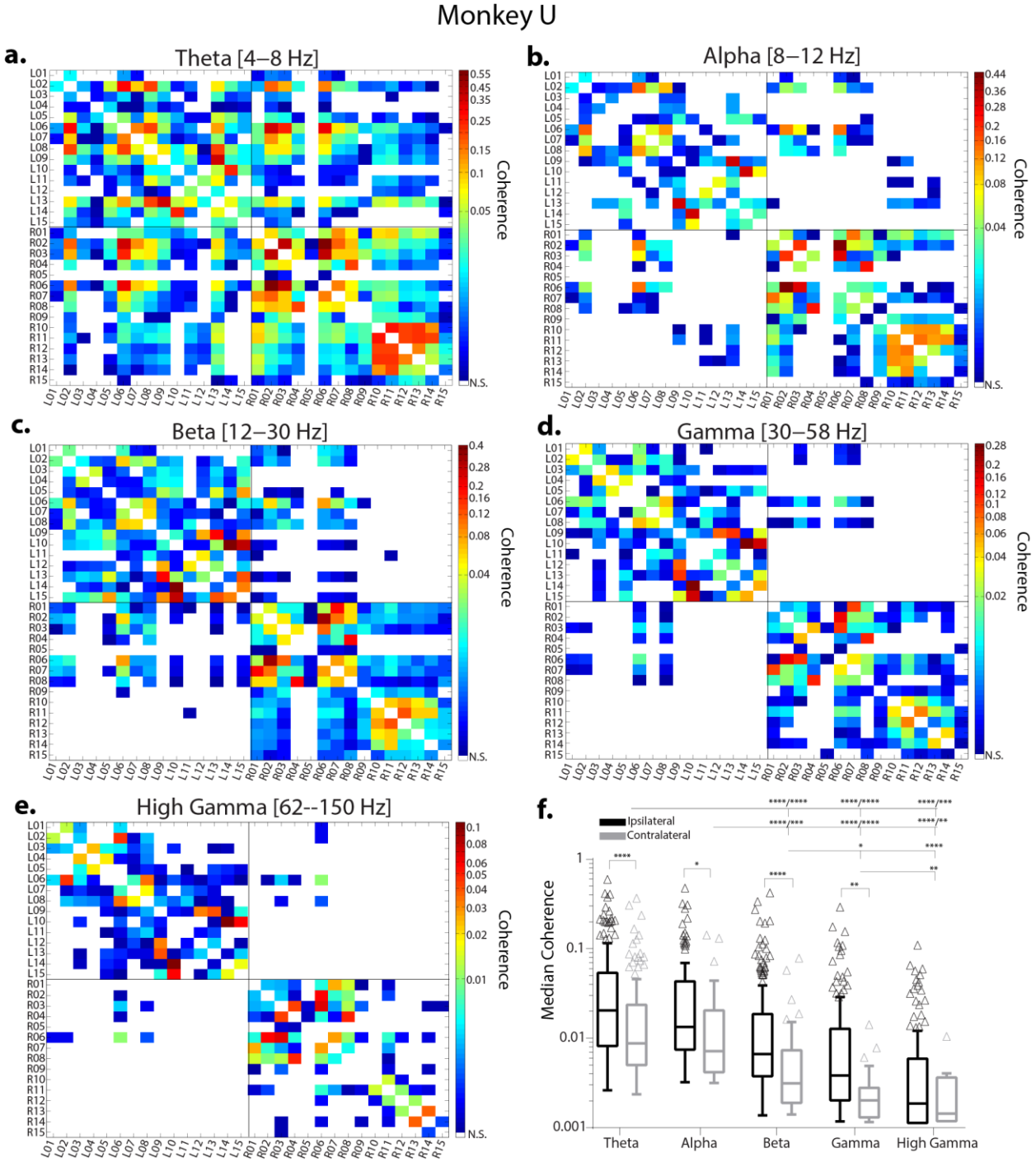

Figure 2.21 Band-limited coherence for monkey U.

a – **e**) Coherence connection matrix for five frequency bands shown on a log color scale. Columns and rows are symmetrical. Empty (white) entries did not reach significance cutoff based on permutation test. **f**) Median coherence in each frequency band for ipsilateral and contralateral connections. Box and whisker plotted on log scale with Tukey's method (upper and lower whiskers 75th and 25th percentiles plus 1.5xIQR). Within each frequency band, a Wilcoxon rank sum test assessed the difference between ipsilateral and contralateral connections. Across frequencies, a Kruskal-Wallis test assessed coherence differences for ipsilateral and conralateral connections separately (asterisks: ipsilateral/contralateral).

Similar to the EP connectivity matrices (Figure 2.5), these coherence matrices cannot resolve the real spatial patterns of coherence. Figure 2.22 shows gamma-band coherence in a manner similar to Figure 2.6 using the same sites for comparison. The first feature apparent from this view is that connectivity assessed via gamma coherence was fairly widespread. This was quantified by fitting the coherence magnitude in each band as a function of inter-electrode

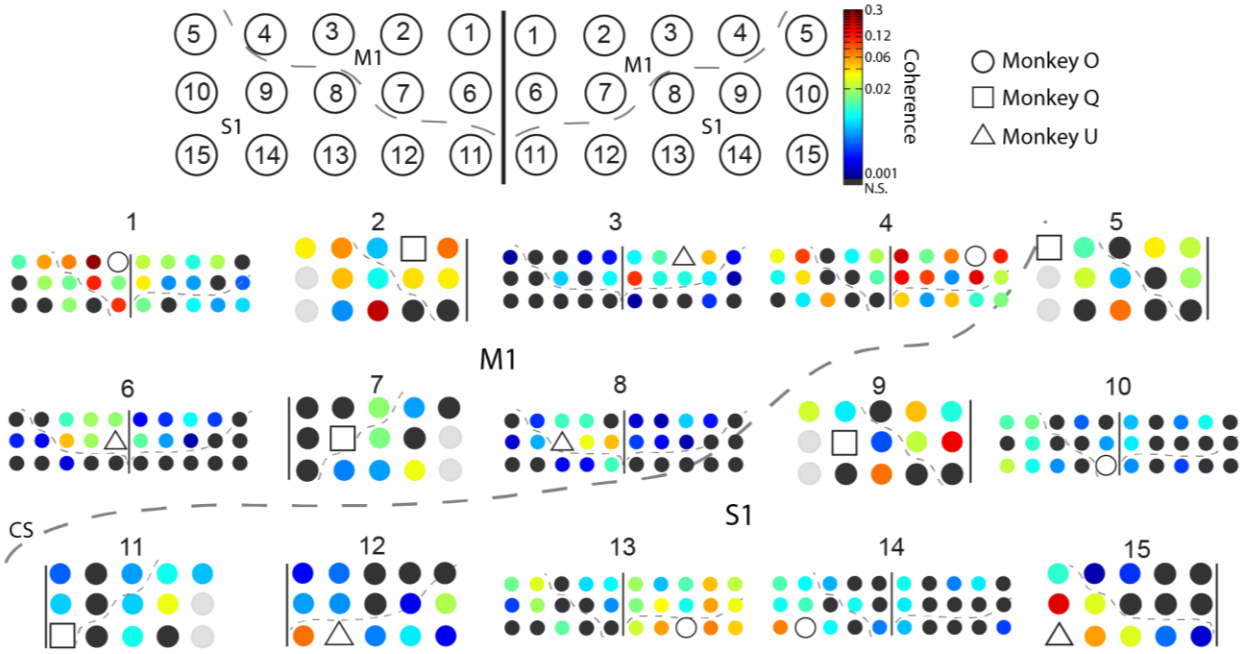

Figure 2.22 Coherence represented in true spatial arrangement.
The layout at the top shows each nominal position in the implant grid represented below by an example coherence map from a particular animal represented by the shape of the open symbol. In each coherence map, the solid line indicates midline and thus which hemisphere is represented while the open symbol indicates the site being stimulated. Colored circles show the coherence represented on a log scale; dark grey circles indicate no significant coherence. Five example sites are shown for each animal with at least one from each hemisphere as well as pre- and post-central sulcus and were the same as in Figure 2.6. The dotted grey lines designate the CS. Monkeys O and U had bilateral recordings. Light grey site positions in monkey Q were not implanted.

distance (see Methods; Figure 2.23). Similar to EP strength (Figure 2.9), the relationship between coherence and connection distance was exponential in monkeys O and U. The alpha band showed the longest distance constant (monkey O: 25.4 mm, $R^2 = 0.11$; monkey U: 8.1 mm, $R^2 = 0.06$), while beta had one of the shortest distance constants (monkey O: 4.6 mm, $R^2 = 0.17$; monkey U: 3.7 mm, $R^2 = 0.08$). The distance constants increased again in the gamma (monkey

O: 5.2 mm, R^2 = 0.07; monkey U: 4.0 mm, R^2 = 0.06) and high gamma (monkey O: 10.8 mm, R^2 = 0.15; monkey U: 4.3 mm, R^2 = 0.05) bands.

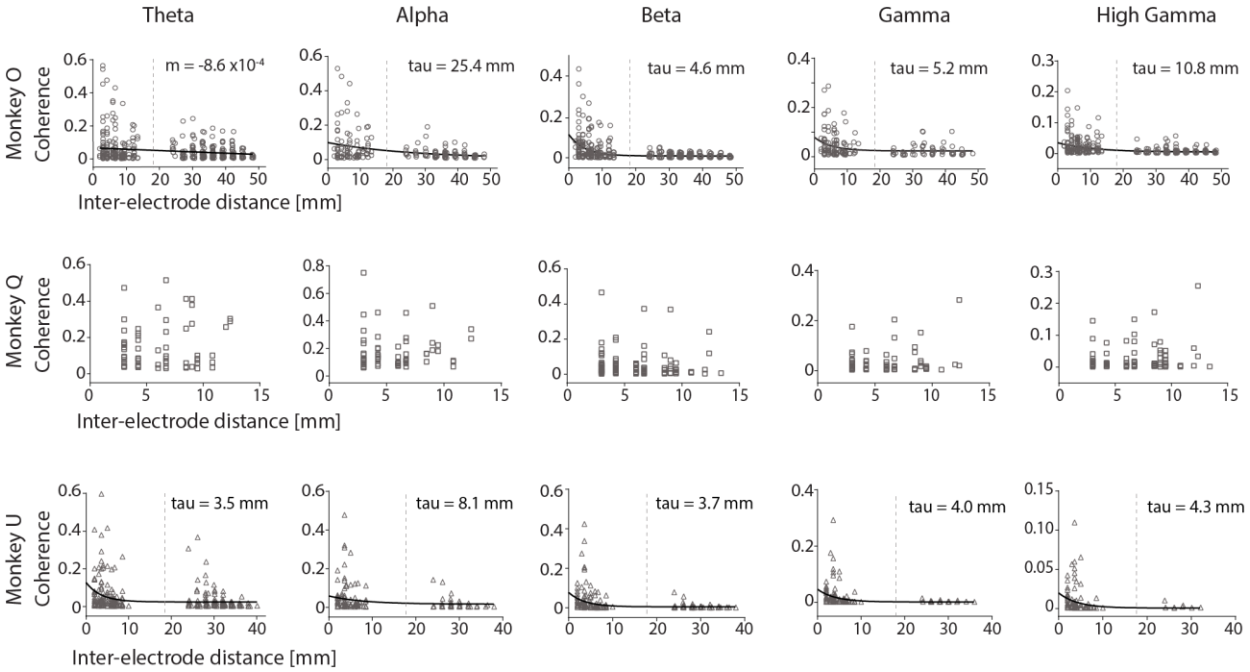

Figure 2.23 Coherence as a function of inter-electrode distance.
Coherence in each frequency band as a function of inter-electrode distance for each animal fitted with a one-phase decaying exponential. Vertical dotted line indicates approximate position of midline

Coherence across all frequency bands showed distinct patterns between intra-regional M1 or S1 connections and connections that crossed the CS (Figure 2.24). Overall, M1-M1 and S1-S1 connections showed higher coherence than inter-regional connections (Ipsilateral: $p < 0.0001$; Contralateral: $p < 0.0001$; Figure 2.24d, see figure table for full statistics). There was some variance across animals, notably that monkey Q showed no difference in coherence between intra- and inter-regional connections (Figure 2.24b). Monkey O (Figure 2.24a) showed higher coherence in M1-M1 connections above S1-S1 and cross CS connections in both ipsilateral ($p < 0.0001$) and contralateral ($p < 0.0001$) connections. Ipsilateral connections in monkey U (Figure 2.24c) showed significant differences between both intra- and inter-regional coherence ($p < 0.0001$) while in contralateral connections only M1-M1connections showed significantly higher

coherence ($p < 0.05$). Overall, regional patterns of coherence were qualitatively similar for ipsilateral and contralateral coherence suggesting that coherence may serve to bind similar interhemispheric areas.

Similar to EP connectivity, patterns of coherence across sensorimotor cortex were driven by inter-site distance as well as regionality. These patterns were consistent across frequency bands which tended to show a $1/f^x$ relationship.

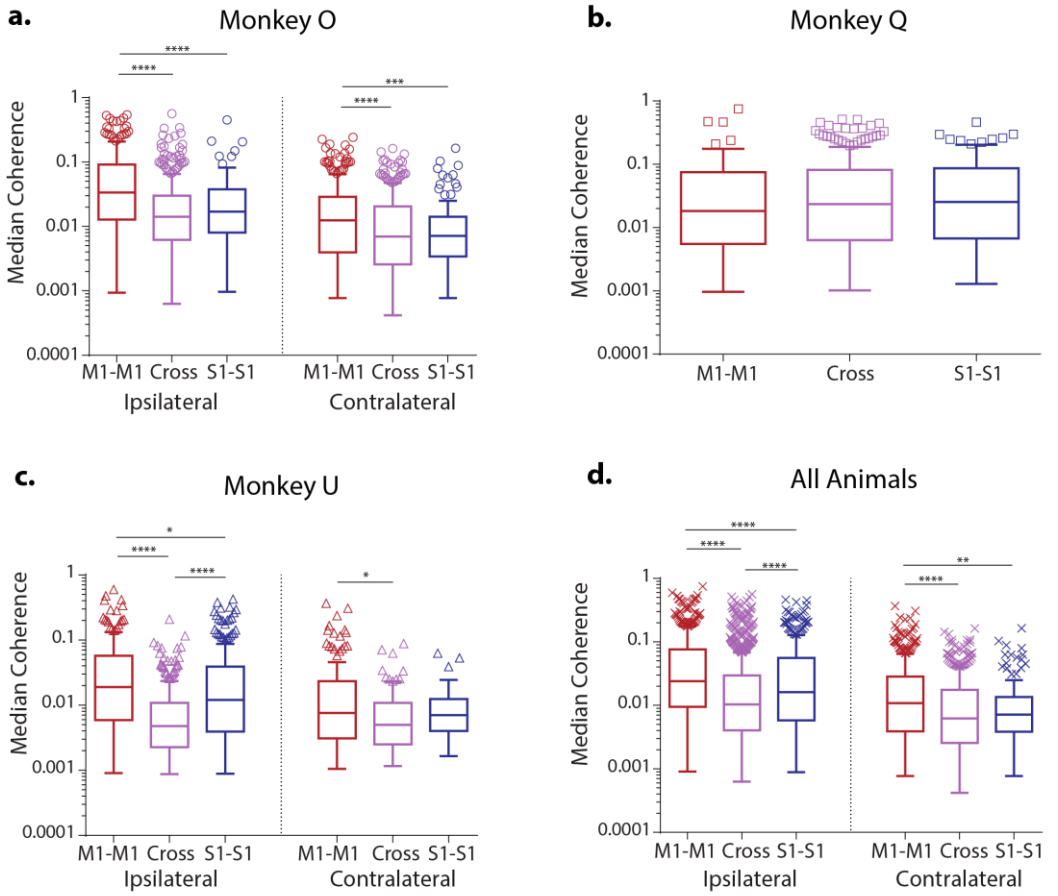

	Ipsilateral									Contralateral								
	M1-M1			Cross			S1-S1			M1-M1			Cross			S1-S1		
Animal	median	IQR	N	median	IQR	N	median	IQR	N	median	IQR	N	median	IQR	N	median	IQR	N
Monkey O	0.0336	0.0789	319	0.0141	0.0239	418	0.0171	0.0298	123	0.0124	0.025	313	0.007	0.0179	404	0.0072	0.0107	134
Monkey Q	0.0183	0.07	93	0.0235	0.0752	265	0.0255	0.08	143									
Monkey U	0.019	0.0512	190	0.0048	0.0082	333	0.0121	0.0351	211	0.0076	0.0203	126	0.005	0.0083	103	0.007	0.0084	40
All	0.0241	0.0669	602	0.0103	0.0255	1016	0.0161	0.0502	477	0.0108	0.0247	439	0.0062	0.015	507	0.0072	0.0097	174

Figure 2.24 Coherence separated by connection type.
a – **d**) Median coherence separated for M1→M1, S1→S1, and cross-sulcus connections separated by ipsilateral and contralateral connections (**a**, **c**, and **d)**. Box and whisker plotted on log scale with Tukey's method (upper and lower whiskers 75th and 25th percentiles plus 1.5xIQR). Significance between connection types assessed with Kruskal-Wallis test separately for ipsilateral and contralateral connections. Table with full statistics at the bottom.

2.3.3 **Relationship between EP and spontaneous connectivity**

Both stimulus-evoked potentials and band-limited coherence showed connectivity patterns across sensorimotor cortex of three monkeys. We were curious whether there was overlap in these two connectivity maps that might elucidate a third dimension of connectivity. Upon first examination of a few example sites there were clear similarities as well as differences in connections quantified by EP strength (Figure 2.6) compared to gamma coherence (Figure 2.22). For instance, positions 12, 14, and 15, while having broader connections in gamma coherence, the strongest connections were the most proximal ones in both coherence and EPs. Conversely, there were also instances in which EP strength and gamma coherence were in opposition such as at positions 4, 7, and 13. There was no EP connection from R04→R01 or R07 in monkey O (Figure 2.1b & Figure 2.6); however, the gamma coherence between those sites was quite high (Figure 2.22). Alternatively, the EP connection from R07→ R06 and R10 in monkey Q (Figure 2.1b & Figure 2.6) were the strongest connections, however, there was not significant gamma coherence between them (Figure 2.22).

In order to quantify the potential overlap in EP and coherence connectivity maps, the Spearman correlation between EP strength and band-limited coherence was calculated (Figure 2.25). For monkeys O and Q, each hemisphere was treated separately since contralateral EPs were not measured, unlike monkey U in which simultaneous recordings of both hemispheres were available for both metrics. Similar to the examples highlighted above, there was variability in the relationship between these two connectivity metrics both within the same animal (across hemispheres) and between animals. Monkeys O and Q both showed generally higher correlation in the right hemisphere than the left while also showing varied patterns across bands. For instance in monkey O, theta was weakly anti-correlated with EP strength in the left hemisphere (r

= -0.15) while significantly positively correlated in the right hemisphere (r = 0.4, $p < 0.01$). One trend that was marginally consistent across animals was a significant correlation between beta coherence and EP strength (monkey O: right hemisphere r = 0.64, $p < 0.0001$; monkey Q: left hemisphere r = 0.27, $p < 0.05$, right hemisphere r = 0.46, $p < 0.05$; monkey U: both hemispheres r = 0.35, $p < 0.0001$). While no coherence band showed significant correlation with EPs in the left hemisphere of monkey O (Figure 2.25a), the beta band trended towards significance (r = 0.27, $p = 0.021$, $\alpha = 0.01$ Bonferroni adjusted).

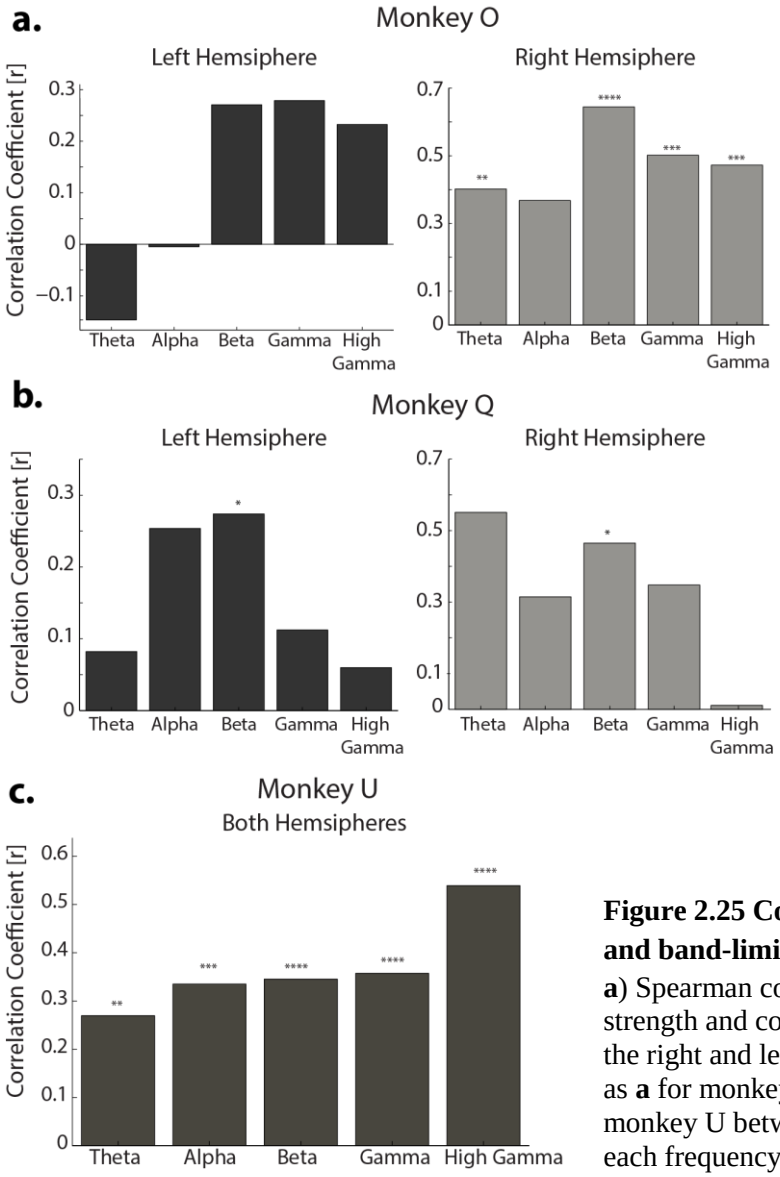

Figure 2.25 Correlation between EP strength and band-limited coherence.
a) Spearman correlation for monkey O between EP strength and coherence in each frequency band for the right and left hemispheres separately. **b**) Same as **a** for monkey Q. **c**) Spearman correlation for monkey U between EP strength and coherence in each frequency band combined across hemispheres.

Due to the wide variability in correlation between EP and spontaneous LFP connectivity and the large range over which both EP strength (Figure 2.4) and coherence magnitude varied, we examined the relationship just in the tail of these distributions as defined by the 95th percentile. The number of connections that exceeded the 95th percentile for either EP strength or banded coherence ranged from 3 to 22 (2 – 16%) with an average of 10. Thus, we examined the top 10 connections with highest EP strength and coherence magnitude in each band to see if the intersection of these "outlier" connections was more consistent than the rest of the network. However, the overlap in the top 10 connections for EP strength and at least one coherence band was low. Monkey O had the highest overlap with 5/10 connections shown as blue arrows in Figure 2.26. Furthermore, a majority of these connections were concentrated in the most anterolateral corner of the right hemisphere. Monkeys Q and U, on the other hand, only showed one overlapping connection in the top 10 highlighted as a solid arrow in Figure 2.26. When we examined the next 10 strongest connections 3 more common connections emerged between EP strength and coherence (Figure 2.26, dashed arrows). Of the 4 connections in monkey Q, 3 of

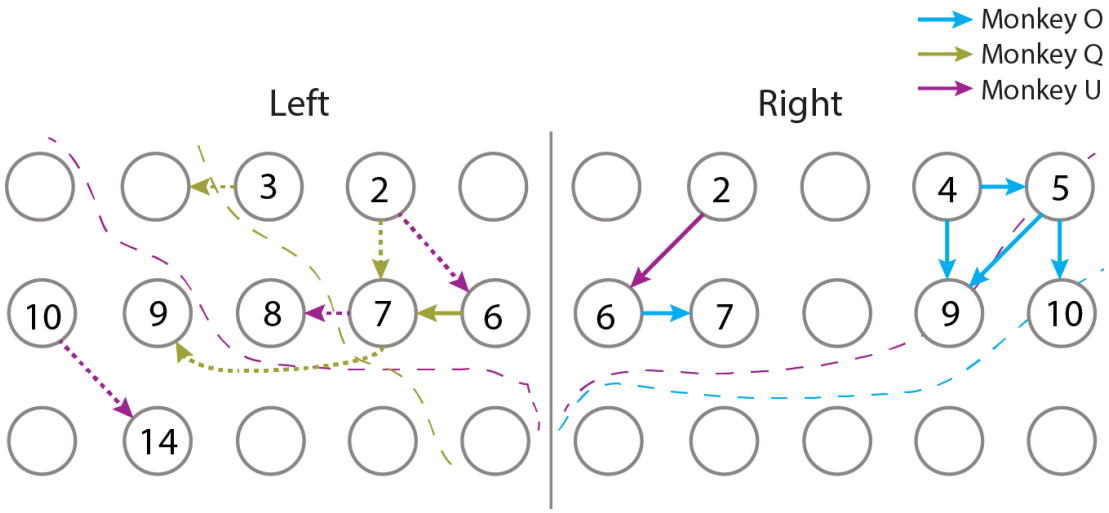

Figure 2.26 Profile of strongest connections.
Solid colored arrows indicate connections that showed overlap in the top 10 strongest EP and coherence connections for each animal. Dotted colored arrows indicate connections that showed overlap in the top 11-20 strongest EP and coherence connections for monkeys Q and U. Dashed lines are CS for each animal and the solid line indicates midline.

them included site L07 (Figure 2.1b), while connections in monkey U showed no common sites. These results coupled with the network-wide correlations suggests that while on the whole there is variability between the EP and coherence connectivity maps, on a finer scale individual sites or connections may show a strong and consistent relationship between connectivity metrics.

Others have shown that sites with reciprocal EPs also have high correlation in spontaneous LFP (Keller et al., 2014). We separated connections that had reciprocal EPs or unidirectional EPs and saw a significant difference in coherence across all frequency bands for monkey U (Figure 2.27c). Similar to the correlation between EP strength and coherence, the beta band showed one of the stronger effects when reciprocity was accounted for (monkey U: reciprocal 0.018(0.053), unidirectional 0.005(0.007), $p < 0.0001$) and was one of the only band in which monkeys O (Figure 2.27a) and Q (Figure 2.27b) showed a significant difference in coherence between reciprocal and unidirectional connections (monkey O: reciprocal 0.045(0.055), unidirectional 0.01(0.016), $p < 0.0001$; monkey Q: reciprocal 0.051(0.051), unidirectional 0.013(0.02), $p < 0.0001$). While not statistically significant, monkey Q also showed a trend for stronger reciprocal connections in all of the bands (theta: $p = 0.017$; alpha: $p = 0.021$; gamma: $p = 0.014$; high gamma: $p = 0.044$; Bonferroni corrected $\alpha = 0.01$). This relationship between EP reciprocity and coherence is reasonable considering that coherence is non-directional.

In summary, though both EP connectivity and coherence connectivity showed similar patterns with inter-electrode distance and position relative to the CS, this was not sufficient to promote consistent correlations between the two metrics. However, upon comparing individual sites, there are commonalities that may serve to link these two modes of information transfer.

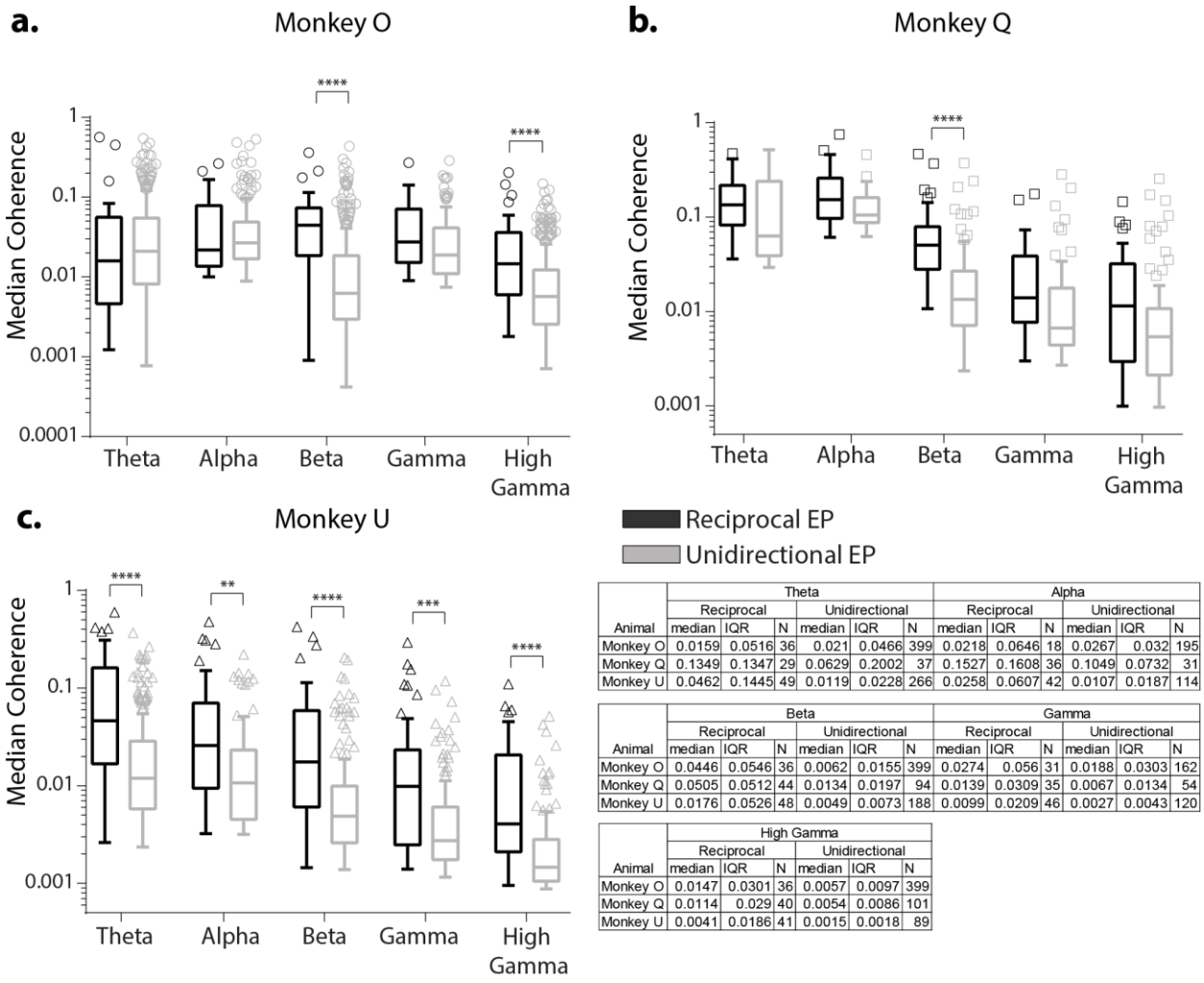

	Theta						Alpha					
	Reciprocal			Unidirectional			Reciprocal			Unidirectional		
Animal	median	IQR	N	median	IQR	N	median	IQR	N	median	IQR	N
Monkey O	0.0159	0.0516	36	0.021	0.0466	399	0.0218	0.0646	18	0.0267	0.032	195
Monkey Q	0.1349	0.1347	29	0.0629	0.2002	37	0.1527	0.1608	36	0.1049	0.0732	31
Monkey U	0.0462	0.1445	49	0.0119	0.0228	266	0.0258	0.0607	42	0.0107	0.0187	114

	Beta						Gamma					
	Reciprocal			Unidirectional			Reciprocal			Unidirectional		
Animal	median	IQR	N	median	IQR	N	median	IQR	N	median	IQR	N
Monkey O	0.0446	0.0546	36	0.0062	0.0155	399	0.0274	0.056	31	0.0188	0.0303	162
Monkey Q	0.0505	0.0512	44	0.0134	0.0197	94	0.0139	0.0309	35	0.0067	0.0134	54
Monkey U	0.0176	0.0526	48	0.0049	0.0073	188	0.0099	0.0209	46	0.0027	0.0043	120

	High Gamma					
	Reciprocal			Unidirectional		
Animal	median	IQR	N	median	IQR	N
Monkey O	0.0147	0.0301	36	0.0057	0.0097	399
Monkey Q	0.0114	0.029	40	0.0054	0.0086	101
Monkey U	0.0041	0.0186	41	0.0015	0.0018	89

Figure 2.27 Coherence relationship with reciprocal EPs.

a – **c**) Median coherence in each frequency band separated between reciprocal and unidirectional EPs for each animal. Box and whisker plotted on log scale with Tukey's method (upper and lower whiskers 75th and 25th percentiles plus 1.5xIQR). A Wilcoxon rank sum test was used to test significance between reciprocal and unidirectional coherence for each band separately. Table with full statistics at the right.

2.4 Discussion

Cortical connectivity and processing exist along a large spatiotemporal spectrum. Exploration of functional connectivity within sensorimotor cortex of primates has been conducted predominantly at two extremes of this scale: single-unit recording and whole-brain techniques such as ECoG, EEG, or fMRI. Here we described cortico-cortical connectivity within the hand area of sensorimotor cortex in monkeys at the meso-scale via stimulus -evoked potentials and coherence in spontaneous LFP. Similar to other metrics, inter-electrode distance was a large factor in the extent of functional connectivity for both EPs and coherence, however more nuanced patterns also emerged.

2.4.1 Meso-scale EP connectivity consistent with other functional connectivity estimates

We measured a variety of characteristics pertaining to EP cortico-cortical connectivity including observation of an EP connection, the strength of EP connections, and reciprocity. These metrics showed an inverse relationship with distance from the stimulating electrode that is consistent with previous anatomical and functional studies on intrinsic sensorimotor connections (Lund et al., 1993; Schieber, 2001; Matsumoto et al., 2007; Bickel et al., 2011; Keller et al., 2014). Anatomical tracer studies have shown lateral connections in motor and sensory cortices of monkeys which extend densely from 0.5 – 1 mm, moderately from 1 – 2 mm, and taper off after 3 mm (Schieber, 2001), but may extend up to 6 mm (DeFelipe et al., 1986). Furthermore, physiological evidence from intracellular recordings of primate M1 revealed that the strongest monosynaptic connections occurred within 2.5 mm (Matsumura et al., 1996). Our results showed that the strength of EP connections falls off with a space constant of ~3 mm, which is consistent with these previous studies. Further, this relationship with distance seems more monotonic for ipsilateral connections compared to contralateral ones, suggesting that transcallosal tracts may

have clustered terminations, as has been shown for some long-distance connections (Lund et al., 1993).

Peak latency showed an increasing trend with distance, which is reasonable for monosynaptic connections simply due to increased conduction distance. Alternatively, it could also be that distant connections are polysynaptic (Asanuma and Rosen, 1973), which would also increase peak latency. We interpret the multi-phasic nature of EPs as potential monosynaptic connections at the earliest latencies and polysynaptic connections at later latencies. Given the relationship of mono and polysynaptic connections with distance (Asanuma and Rosen, 1973; Matsumoto et al., 2007), it is possible that the number of phases in a given EP also relates to distance. That we did not observe a distance effect on phase number suggests: 1) the high likelihood that our interpretation of the synaptic content of EP phases is oversimplified and 2) combined with the peak latency results, that inter-electrode distance is not the only factor driving connectivity patterns. The second observation is consistent with cortico-corical EP studies in humans in which significant intrinsic connectivity remained even when effects of distance were accounted for (Bickel et al., 2011; Keller et al., 2014). Though EPs clearly showed multiple phases of different polarities, we are hesitant to ascribe excitatory or inhibitory sources to upward or downward deflecting potentials. Current source density (CSD) methods have been applied to similar EPs in order to identify current sources and sinks, however, the interpretation of which specific currents contribute to the CSD is complex (Mitzdorf, 1985). Knowledge of underlying anatomical structure or a more densely sampled laminar recording can aid in CSD interpretation from which connectivity may be inferred. As we are only sampling at two points along the vertical extent, surface and depth, CSD analysis and interpretation is not possible.

Aside from linear distance, the composition of connections to and from individual sites contributes strongly to connectivity patterns within sensorimotor cortex. Studies of EP connectivity in humans showed 75-90% of network connections were reciprocal, whereas individual sites showed reciprocity rates ranging from 9-50% (Matsumoto et al., 2007; Keller et al., 2014). This suggests that for a given network, the number of sites that show reciprocal connections is consistent, whereas the number of reciprocal connections at an individual site is quite variable. We similarly saw ~70% reciprocity of the sensorimotor network across three monkeys while reciprocal connections of individual sites ranged from ~6-80%. In addition to reciprocal connections, the pattern of output projections and incoming connections across a network can reveal a more structured flow of information within the network as opposed to a pure distance relationship. Sites in which connections are predominately outward or inward may suggest that these sites are regional hubs. A study in which information flow was assessed via EPs across many cortical areas in humans found that sensorimotor cortex showed markedly higher out-degree than other areas (Keller et al., 2014). Our results also showed high out-degree (100% at some sites) across many sites but due to our meso-scale view we did not measure connections of other areas. This example highlights the necessity for analysis across many scales.

Finally, the regional identity of sites and intracortical connections, especially between pre- and post-central cortex has been studied extensively. The CS divides primary motor and sensory cortex, yet there are both anatomical (DeFelipe et al., 1986; Ghosh et al., 1987; Felleman and Van Essen, 1991; Keller, 1993; Lund et al., 1993; Markov et al., 2014) and functional (Matsumoto et al., 2007; Smith and Fetz, 2009a; Bickel et al., 2011) connections between these two cortices. Consistent with these previous results, we measured many EP connections between

M1 and S1 sites. There has been debate in the anatomical literature as to the extent of connections to M1, especially from areas 3a and 3b (DeFelipe et al., 1986; Ghosh et al., 1987; Geyer et al., 2000). Our arrays likely sample somatosensory areas 3b, 1, and 2 of which areas 1 and 2 show anatomical projections to M1 (DeFelipe et al., 1986). In two of the three animals there was no preference for trans-sulcal projections from M1 or S1; however one monkey showed that S1 sites were more likely to produce EPs in M1 sites than vice versa. Similarly, there was a trend for S1→M1 EP connections to be stronger than M1→S1. Our definition of the CS is based on functional responses to median nerve stimulation (McCarthy et al., 1991; Towle et al., 1998), which can provide a good estimate of electrode location, though we cannot know the exact positioning, especially in the bank of the CS.

2.4.2 **Connectivity via binding of cortical oscillations**

Stimulus-evoked potentials are mediated by anatomical connections (Keller et al., 2014), whereas spontaneous oscillations in LFPs are thought to synchronize neurons that may or may not be directly anatomically connected (Engel et al., 2001; Buzsáki and Draguhn, 2004). Correlated activity, especially in the gamma range, is due to intrinsic oscillations in inhibitory interneurons, which restricts the time window in which excitatory pyramidal neurons may fire (Cardin et al., 2009; Buzsáki and Wang, 2012). Thus, while a population of excitatory neurons may not be physically connected, coherent activity among common inhibitory inputs can drive cortical oscillations. Communication through coherence (CTC) is a current theory which hypothesizes that coherence in select frequency ranges between two cortical regions enhances communication or information transfer (Akam & Kullmann, 2014; Engel, Fries, & Singer, 2001). Different cortical regions are thought to employ different frequency ranges for CTC (Buzsáki and Draguhn, 2004) with sensorimotor cortex mainly showing desynchronization of beta

oscillations and synchronization of gamma and high gamma oscillations during voluntary movement (Pfurtscheller et al., 2003). Beta oscillations are also strongly implicated in the planning (Donoghue et al., 1998), execution (Murthy and Fetz, 1992), and imagination (Miller et al., 2010) of complex movements. The consistent relationship between beta coherence and EP connections in our results may be further evidence that the beta rhythm is supporting synaptic connectivity in sensorimotor cortex and promoting CTC.

Although coherence shows a dependence on inter-site distance (Towle et al., 1998), similar to EPs, it is likely due to a different mechanism. Whereas stimulus-evoked connectivity is limited by anatomical factors, oscillations are effectively limited by their wavelength such that lower frequency oscillations recruit larger networks compared to higher frequency oscillations which are more spatially confined (Buzsáki and Draguhn, 2004). We did not observe differences between frequency bands, other than a $1/f^{x}$ distribution, that suggests coherence in certain bands is important for different aspects of cortical processing even though this has been suggested for the beta and high gamma bands in movement-related activity (Pfurtscheller et al., 2003). While CTC is thought to potentially bind different cortical regions for communication, there is still evidence for separation of different functional centers. In humans, coherence in the delta band (1-4 Hz) is lower along the CS (Towle et al., 1998), consistent with our result that intra-regional coherence was higher than inter-regional coherence.

2.4.3 **Intersection of functional connectivity metrics**

In order to elucidate how connectivity gives rise to function, it is important to explore the relationship or intersection of various functional connectivity measures. Though both EP and coherence connectivity relied on inter-electrode distance and local regionality, this was not sufficient to show strong correlations between the two connectivity maps on a whole network

scale. However, for some individual sites or connections, the strength of EP connectivity and coherence was well matched. This result is consistent with a previous study in humans in which single site connectivity in ECoG and EPs showed strong positive correlations whereas global connectivity profiles were negatively correlated (Keller et al., 2014). This discrepancy may highlight a fundamental difference in the two connectivity metrics in that EPs are more anatomically based, whereas correlation of spontaneous LFPs can be highly dynamic and modulate with behavioral state (Akam and Kullmann, 2014). EP connectivity also incorporates directionality which is lost in the coherence measure. Thus, it is unsurprising that correlation between the two metrics was higher for reciprocal connections than non-reciprocal connections. Regardless of functional connectivity metric, we chose to quantify a bipolar-referenced signal in order to confine the spatial view of our recording. Interpretation and analyses for monopolar versus bipolar signals is debated (Zaveri et al., 2006; Bastos and Schoffelen, 2016) and could account for poor overlap between EP and coherence connectivity.

Stimulus-evoked potentials and coherence are just two ways to assess functional connectivity. There are many methods in both the time and frequency domains for characterizing directed and undirected connections between neuronal populations. The assumptions and relationships between these methods, while mathematically understood, become more ambiguous when applied to physiological data (Bastos and Schoffelen, 2016). We chose two methods, one in the directed time domain and another in the undirected frequency domain, which have been previously applied to descriptions of cortico-cortical connectivity. Granger causality, a directed measure showing causation between the activity of two sites, has been used to describe sensorimotor connectivity in behaving monkeys and showed a close correspondence to coherence in the beta band (Brovelli et al., 2004). Extending our results to Granger causality or

other such connectivity metrics may bring us closer to understanding complex spatiotemporal patterns of cortical connectivity.

CONCLUSIONS

This thesis explored the connectivity of cortical populations in hand area of sensorimotor cortex in awake, behaving monkeys and the potential to induce plasticity among these connections. Stimulus-evoked potentials were the primary metric used to quantify not only which sites were connected, but the strength of those connections. We found that EPs were stable, robust, and effective for determining intracortical connectivity on a meso-scale resolution. Further, we were able to repeatedly induce long-lasting, STDP between a subset of these sites using a paired-stimulation paradigm. Our inability to resolve the specific connections giving rise to EPs was likely why we observed such site-dependent STDP effects. We also assessed inter-site connections with band-limited, spontaneous coherence to gain additional insight into how the network was organized. We saw clear structure in inter-site coherence that was similar to EPs, namely an inverse relationship with distance and a propensity for weaker connections across the central sulcus. However, these similarities were insufficient to show strong correlations between these two connectivity metrics likely because they are measuring different network phenomena. EPs highlight anatomical connections between sites whereas coherence shows correlated activity that may or may not be the result of direct connections. For two site pairs, EPs showed clear and consistent amplitude changes with paired-stimulation, whereas consistent coherence changes were not observed. Exploring various metrics of EP and coherence connectivity was also ineffective at separating the two site pairs that showed STDP effects from other site pairs that did not show effects.

From the results of paired-stimulation conditioning and connectivity analysis we hypothesize that certain pathways will be more susceptible to STDP than others and that we are unable to resolve what those connections are with current methods. The use of optogenetic

stimulation (Yazdan-Shahmorad et al., 2016) or other means to target paired-stimulation to specific pathways is one way to test this hypothesis. Further, using different directed functional connectivity measures (Bastos and Schoffelen, 2016) such as Granger causality may yield more informative comparisons with EP connectivity to extract the composition of these connections. It is clear that cortical populations serve an important role in cortical processing, but exactly what that is, the mechanisms that generate it, and how it may be modulated are unclear. By combining several technological and analytical approaches we stand to elucidate important network structure and function at a level that has not been thoroughly explored.

The results described here also have potential application for targeted, rehabilitative therapies in injuries which disrupt connectivity such as stroke or spinal cord injury. The use of brain-computer interfaces has evolved to utilize single-unit, intracortical LFP, and ECoG recordings in order to restore function for motor impaired patients (Moran, 2010). Typical BCI algorithms are not intuitive and require a high degree of learning for the patient (Green and Kalaska, 2011). A better understanding of the connectivity and encoding of population activity driving BCIs could lead to algorithms that utilize this intrinsic functionality and are easier to use. Furthermore, BCIs could be leveraged to strengthen spared connections by using targeted plasticity paradigms (McPherson et al., 2015) similar to the paired-stimulation used here. The optimal case would be to target synaptic plasticity only within the injured area in a way that is minimally invasive, restores functional movement, and is long-lasting so as to reduce dependency on the BCI. The site-dependency of our paired-stimulation effects highlights important considerations towards this goal, yet they may be overcome with further exploration into network connectivity and mechanisms governing population plasticity.

BIBLIOGRAPHY

Akam T, Kullmann DM (2014) Oscillatory multiplexing of population codes for selective communication in the mammalian brain. Nat Rev Neurosci 15:111–122.

Arai N, Muller-Dahlhaus F, Murakami T, Bliem B, Lu M-K, Ugawa Y, Ziemann U (2011) State-dependent and timing-dependent bidirectional associative plasticity in the human SMA-M1 network. J Neurosci 31:15376–15383.

Asanuma H, Rosen I (1973) Spread of mono- and polysynaptic connections within cat's motor cortex. Exp Brain Res 16:507–520.

Baker SN, Olivier E, Lemon RN (1997) Coherent oscillations in monkey motor cortex and hand muscle EMG show task-dependent modulation. J Physiol 501:225–241.

Bastos AM, Schoffelen J-M (2016) A tutorial review of functional connectivity analysis methods and their interpretational pitfalls. Front Syst Neurosci 9:1–23.

Battaglia D, Witt A, Wolf F, Geisel T (2012) Dynamic effective connectivity of inter-areal brain circuits. PLoS Comput Biol 8.

Bi G, Poo M (1998) Synaptic modifications in cultured hippocampal neurons: dependence on spike timing, synaptic strength, and postsynaptic cell type. J Neurosci 18:10464–10472.

Bi G, Poo M (2001) Synaptic modification by correlated activity: Hebb's postulate revisited. Annu Rev Neurosci 24:139–166.

Bickel S, Entz L, Ulbert I, Milham MP, Keller CJ, Bickel S, Entz L, Ulbert I, Milham MP, Kelly C (2011) Intrinsic functional architecture predicts electrically evoked responses in the human brain. Proc Natl Acad Sci 108:17234–17234.

Bressler SL, Menon V (2010) Large-scale brain networks in cognition: Emerging methods and principles. Trends Cogn Sci 14:277–290.

Brovelli A, Ding M, Ledberg A, Chen Y, Nakamura R, Bressler SL (2004) Beta oscillations in a large-scale sensorimotor cortical network: directional influences revealed by Granger causality. Proc Natl Acad Sci 101:9849–9854.

Brown TH, Keenan CL, Kairiss EW, Keenan CL (1990) Hebbian synapses: Biophysical mechanisms and algorithms. Annu Rev Neurosci 13:475–511.

Buetefisch C, Heger R, Schicks W, Seitz R, Netz J (2011) Hebbian-type stimulation during robot-assisted training in patients with stroke. Neurorehabil Neural Repair 25:645–655.

Buzsáki G, Anastassiou CA, Koch C (2012) The origin of extracellular fields and currents--EEG, ECoG, LFP and spikes. Nat Rev Neurosci 13:407–420.

Buzsáki G, Draguhn A (2004) Neuronal oscillations in cortical networks. Science 304:1926–1929.

Buzsáki G, Wang X-J (2012) Mechanisms of gamma oscillations. Annu Rev Neurosci 35:203–225.

Caporale N, Dan Y (2008) Spike timing-dependent plasticity: a Hebbian learning rule. Annu Rev Neurosci 31:25–46.

Cardin J a., Carlén M, Meletis K, Knoblich U, Zhang F, Deisseroth K, Tsai L-H, Moore CI (2009) Driving fast-spiking cells induces gamma rhythm and controls sensory responses. Nature 459:663–667.

Churchland MM, Cunningham JP, Kaufman MT, Foster JD, Nuyujukian P, Ryu SI, Shenoy K V. (2012) Neural population dynamics during reaching. Nature 487:51–56.

D'amour JA, Froemke RC (2015) Inhibitory and excitatory spike-timing-dependent plasticity in the auditory cortex. Neuron 86:514–528.

DeFelipe J, Conley M, Jones EG (1986) Long-range focal collateralization of axons arising from corticocortical cells in monkey sensory-motor cortex. J Neurosci 6:3749–3766.

Diesmann M, Gewaltig MO, Aertsen A (1999) Stable propagation of synchronous spiking in cortical neural networks. Nature 402:529–533.

Donoghue JP, Sanes JN, Hatsopoulos NG, Gaál G (1998) Neural discharge and local field potential oscillations in primate motor cortex during voluntary movements. J Neurophysiol 1:159–173.

Einevoll GT, Kayser C, Logothetis NK, Panzeri S (2013) Modelling and analysis of local field potentials for studying the function of cortical circuits. Nat Rev Neurosci 14:770–785.

Engel AK, Fries P, Singer W (2001) Dynamic predictions: oscillations and synchrony in top-down processing. Nat Rev Neurosci 2:704–716.

Evarts E V (1968) Relation of pyramidal tract activity to force exerted during voluntary movement. J Neurophysiol 31:14–27.

Feldman DE (2000) Timing-based LTP and LTD at vertical inputs to layer II/III pyramidal cells in rat barrel cortex. Neuron 27:45–56.

Feldman DE (2012) The spike-timing dependence of plasticity. Neuron 75:556–571.

Felleman DJ, Van Essen DC (1991) Distributed hierarchical processing in the primate cerebral cortex. Cereb Cortex 1:1–47.

Fetz EE, Cheney PD (1980) Postspike facilitation of forelimb muscle activity by primate corticomotoneuronal cells. J Neurophysiol 44:751–772.

Fetz EE, Shupe LE, Georgopoulos AP, Taira M, Lukashin A V (1994) Measuring synaptic interactions. Science 263:1295–1297.

Fritz JB (2005) Differential dynamic plasticity of A1 receptive fields during multiple spectral tasks. J Neurosci 25:7623–7635.

Froemke RC, Dan Y (2002) Spike-timing-dependent synaptic modification induced by natural spike trains. Nature 416:433–438.

Froemke RC, Poo M, Dan Y (2005) Spike-timing-dependent synaptic plasticity depends on dendritic location. Nature 2033:2032–2033.

Georgopoulos AP, Kalaska JF, Caminiti R, Massey JT (1982) On the relations between the direction of two-dimensional arm movements and cell discharge in primate motor cortex. J Neurosci 2:1527–1537.

Geyer S, Matelli M, Luppino G, Zilles K (2000) Functional neuroanatomy of the primate isocortical motor system. Anat Embryol (Berl) 202:443–474.

Ghosh S, Brinkman C, Porter R (1987) A quantitative study of the distribution of neurons projecting to the precentral motor cortex in the monkey (M. fascicularis). J Comp Neurol 259:424–444.

Gilbert CD, Sigman M (2007) Brain states: top-down influences in sensory processing. Neuron 54:677–696.

Green AM, Kalaska JF (2011) Learning to move machines with the mind. Trends Neurosci 34:61–75.

Guggenmos DJ, Azin M, Barbay S, Mahnken JD, Dunham C, Mohseni P, Nudo RJ (2013) Restoration of function after brain damage using a neural prosthesis. Proc Natl Acad Sci 110:21177–21182.

Hatsopoulos NG, Ojakangas CL, Paninski L, Donoghue JP (1998) Information about movement direction obtained from synchronous activity of motor cortical neurons. Proc Natl Acad Sci 95:15706–15711.

Hebb DO (1949) The Organization of Behavior: A Neuropsychological Theory. New York, NY: Wiley.

Hess G, Aizenman CD, Donoghue JP (1996) Conditions for the induction of long-term potentiation in layer II/III horizontal connections of the rat motor cortex. J Neurophysiol 75:1765–1778.

Histed MH, Bonin V, Reid RC (2009) Direct activation of sparse, distributed populations of cortical neurons by electrical microstimulation. Neuron 63:508–522.

Humphrey DR, Corrie WS (1978) Properties of pyramidal tract neuron system within a functionally defined subregion of primate motor cortex. J Neurophysiol 41:216–243.

Jackson A, Gee VJ, Baker SN, Lemon RN (2003) Synchrony between neurons with similar muscle fields in monkey motor cortex. Neuron 38:115–125.

Jackson A, Mavoori J, Fetz EE (2006) Long-term motor cortex plasticity induced by an electronic neural implant. Nature 444:56–60.

Kajikawa Y, Schroeder CE (2011) How local is the local field potential? Neuron 72:847–858.

Kalaska JF, Cohen DAD, Hyde L (1989) A comparison of movement direction-related versus load activity in primate motor cortex , using a two- dimensional reaching task. J Neurosci 9:2080–2102.

Keller A (1993) Intrinsic synaptic organization of the motor cortex. Cereb Cortex 3:430–441.

Keller CJ, Honey CJ, Entz L, Bickel S, Groppe DM, Toth E, Ulbert I, Lado FA, Mehta AD (2014) Corticocortical evoked potentials reveal projectors and integrators in human brain networks. J Neurosci 34:9152–9163.

Kellis S, Sorensen L, Darvas F, Sayres C, O'Neill K, Brown R, House P, Ojemann J, Greger B (2016) Multi-scale analysis of neural activity in humans: implications for micro-scale electrocorticography. Clin Neurophysiol 127:1–11.

Koch G, Ponzo V, Di Lorenzo F, Caltagirone C, Veniero D (2013) Hebbian and anti-Hebbian spike-timing-dependent plasticity of human cortico-cortical connections. J Neurosci 33:9725–9733.

Li W, Piech V, Gilbert CD (2006) Contour saliency in primary visual cortex. Neuron 50:951–962.

Lisman J, Spruston N (2005) Postsynaptic depolarization requirements for LTP and LTD: a critique of spike timing-dependent plasticity. Nat Neurosci 8:839–841.

Lu J, Li C, Zhao J-P, Poo M, Zhang X (2007) Spike-timing-dependent plasticity of neocortical excitatory synapses on inhibitory interneurons depends on target cell type. J Neurosci 27:9711–9720.

Lucas TH, Fetz EE (2013) Myo-cortical crossed feedback reorganizes primate motor cortex output. J Neurosci 33:5261–5274.

Lund JS, Yoshioka T, Levitt JB (1993) Comparison of intrinsic connectivity in different areas of macaque monkey cerebral cortex. Cereb Cortex 3:148–162.

Markov NT et al. (2014) A weighted and directed interareal connectivity matrix for macaque cerebral cortex. Cereb Cortex 24:17–36.

Markram H, Lübke J, Frotscher M, Sakmann B (1997) Regulation of synaptic efficacy by coincidence of postsynaptic APs and EPSPs. Science 275:213–215.

Matsumoto R, Nair DR, Lapresto E, Bingaman W, Shibasaki H, Lu HO (2007) Functional connectivity in human cortical motor system : a cortico-cortical evoked potential study. Brain 130:181–197.

Matsumura M, Chen D, Sawaguchi T, Kubota K, Fetz EE (1996) Synaptic interactions between primate precentral cortex neurons revealed by spike-triggered averaging of intracellular membrane potentials in vivo. J Neurosci 16:7757–7767.

McCarthy G, Wood CC, Allison T (1991) Cortical somatosensory evoked potentials. I. Recordings in the monkey Macaca fascicularis. J Neurophysiol 66:53–63.

McCreery DB, Bullara LA, Agnew WF (1986) Neuronal activity evoked by chronically implanted intracortical microelectrodes. Exp Neurol 92:147–161.

McPherson JG, Miller RR, Perlmutter SI (2015) Targeted, activity-dependent spinal stimulation produces long-lasting motor recovery in chronic cervical spinal cord injury. Proc Natl Acad Sci 112:201505383.

Millard DC, Whitmire CJ, Gollnick CA, Rozell CJ, Stanley GB (2015) Electrical and optical activation of mesoscale neural circuits with implications for coding. J Neurosci 35:15702–15715.

Miller KJ, Schalk G, Fetz EE, den Nijs M, Ojemann JG, Rao RPN (2010) Cortical activity during motor execution, motor imagery, and imagery-based online feedback. Proc Natl Acad Sci 107:4430–4435.

Miller KJ, Sorensen LB, Ojemann JG, Den Nijs M (2009) Power-law scaling in the brain surface electric potential. PLoS Comput Biol 5.

Mitzdorf U (1985) Current source-density method and application in cat cerebral cortex: investigation of evoked potentials and EEG phenomena. Physiol Rev 65:37–100.

Moran D (2010) Evolution of brain-computer interface: Action potentials, local field potentials and electrocorticograms. Curr Opin Neurobiol 20:741–745.

Murphy JT, Kwan HC, Wong YT (1985) Cross correlation studies in primate motor cortex: synaptic interaction and shared input. Can J Neurol Sci 12:11–23.

Murthy VN, Fetz EE (1992) Coherent 25- to 35-Hz oscillations in the sensorimotor cortex of awake behaving monkeys. Proc Natl Acad Sci 89:5670–5674.

Murthy VN, Fetz EE (1996) Oscillatory activity in sensorimotor cortex of awake monkeys: synchronization of local field potentials and relation to behavior. J Neurophysiol 76:3949–3967.

Nishimura Y, Perlmutter SI, Eaton RW, Fetz EE (2013) Spike-timing-dependent plasticity in primate corticospinal connections induced during free behavior. Neuron 80:1301–1309.

Overduin SA, D'Avella A, Roh J, Bizzi E (2008) Modulation of muscle synergy recruitment in primate grasping. J Neurosci 28:880–892.

Pfurtscheller G, Graimann B, Huggins JE, Levine SP, Schuh LA (2003) Spatiotemporal patterns of beta desynchronization and gamma synchronization in corticographic data during self-paced movement. Clin Neurophysiol 114:1226–1236.

Rebesco JM, Miller LE (2011) Enhanced detection threshold for in vivo cortical stimulation produced by Hebbian conditioning. J Neural Eng 8:016011.

Rebesco JM, Stevenson IH, Körding KP, Solla SA, Miller LE (2010) Rewiring neural interactions by micro-stimulation. Front Syst Neurosci 4:1–15.

Richardson AG, Fetz EE (2012) Brain state-dependence of electrically evoked potentials monitored with head-mounted electronics. IEEE Trans Neural Syst Rehabil Eng 20:756–761.

Sanes JN, Donoghue JP (2000) Plasticity and primary motor cortex. Annu Rev Neurosci 23:393–415.

Schalk G, Leuthardt EC (2011) Brain-computer interfaces using electrocorticographic signals. IEEE Rev Biomed Eng 4:140–154.

Schieber MH (2001) Constraints on somatotopic organization in the primary motor cortex. J Neurophysiol 86:2125–2143.

Shenoy K V, Sahani M, Churchland MM (2013) Cortical control of arm movements: a dynamical systems perspective. Annu Rev Neurosci 36:337–359.

Silversmith DB, Yazadahn-Shamorad A, Sabes PN (2016) Targeted cortical reorganization using optogenetics in non-human primates. Soc Neurosci Abstr.

Sjostrom PJ, Hausser M (2006) A cooperative switch determines the sign of synaptic plasticity in distal dendrites of neocortical pyramidal neurons. Neuron 51:227–238.

Sjostrom PJ, Turrigiano GG, Nelson SB (2001) Rate, timing, and cooperativity jointly determine cortical synaptic plasticity. Neuron 32:1149–1164.

Smith WS, Fetz EE (2009a) Synaptic interactions between forelimb-related motor cortex neurons in behaving primates. J Neurophysiol 102:1026–1039.

Smith WS, Fetz EE (2009b) Synaptic linkages between corticomotoneuronal cells affecting forelimb muscles in behaving primates. J Neurophysiol 102:1040–1048.

Stoney SD, Thompson WD, Asanuma H (1968) Excitation of pyramidal tract cells by intracortical microstimulation: effective extent of stimulating current. J Neurophysiol 31:659–669.

Stuchlik A (2014) Dynamic learning and memory, synaptic plasticity and neurogenesis: an update. Front Behav Neurosci 8:1–6.

Tehovnik EJ (1996) Electrical stimulation of neural tissue to evoke behavioral responses. J Neurosci Methods 65:1–17.

Teyler TJ (1989) Comparative aspects of hippocampal and neocortical long-term potentiation. J Neurosci Methods 28:101–108.

Todorov E, Jordan MI (2002) Optimal feedback control as a theory of motor coordination. Nat Neurosci 5:1226–1235.

Towle VL, Syed I, Berger C, Grzesczcuk R, Milton J, Erickson RK, Cogen P, Berkson E, Spire JP (1998) Identification of the sensory/motor area and pathologic regions using ECoG coherence. Electroencephalogr Clin Neurophysiol 106:30–39.

Turkheimer FE, Leech R, Expert P, Lord LD, Vernon AC (2015) The brain's code and its canonical computational motifs. From sensory cortex to the default mode network: A multi-scale model of brain function in health and disease. Neurosci Biobehav Rev 55:211–222.

Wang W, Degenhart AD, Collinger JL, Vinjamuri R, Sudre GP, Adelson PD, Holder DL, Leuthardt EC, Moran DW, Boninger ML, Schwartz AB, Crammond DJ, Tyler-Kabara EC, Weber DJ (2009) Human motor cortical activity recorded with micro-ECoG electrodes during individual finger movements. Proc 31st Annu Int Conf IEEE Eng Med Biol Soc Eng Futur Biomed EMBC 2009:586–589.

Watanabe H, Sato M-A, Suzuki T, Nambu A, Nishimura Y, Kawato M, Isa T (2012) Reconstruction of movement-related intracortical activity from micro-electrocorticogram array signals in monkey primary motor cortex. J Neural Eng 9.

Wolters A, Sandbrink F, Schlottmann A, Kunesch E, Stefan K, Cohen LG, Benecke R, Classen J (2003) A temporally asymmetric Hebbian rule governing plasticity in the human motor cortex. J Neurophysiol 89:2339–2345.

Womelsdorf T, Schoffelen J-M, Oostenveld R, Singer W, Desimone R, Engel AK, Fries P (2007) Modulation of neuronal interactions through neuronal synchronization. Science 316:1609–1612.

Yazdan-Shahmorad A, Diaz-Botia C, Hanson TL, Kharazia V, Ledochowitsch P, Maharbiz MM, Sabes PN (2016) A large-scale interface for optogenetic stimulation and recording in nonhuman primates. Neuron 89:1–13.

Yuste R (2015) From the neuron doctrine to neural networks. Nat Rev Neurosci 16:487–497.

Zanos S (2013) Cortical surface recurrent brain-computer interfaces (Doctoral Dissertation).

Zanos S, Richardson AG, Shupe L, Miles FP, Fetz EE (2011) The Neurochip-2: an autonomous head-fixed computer for recording and stimulating in freely behaving monkeys. IEEE Trans Neural Syst Rehabil Eng 19:427–435.

Zaveri HP, Duckrow RB, Spencer SS (2006) On the use of bipolar montages for time-series analysis of intracranial electroencephalograms. Clin Neurophysiol 117:2102–2108.